INVESTIGATION OF FATIGUE RESISTANCE OF

FILLET-WELDED TUBE CONNECTION DETAILS FOR

SIGN SUPPORT STRUCTURES

by
HYUNGJOO CHOI

A dissertation submitted to the

School of Graduate Studies

Rutgers, the State University of New Jersey

in partial fulfillment of the requirements

For the degree of

Doctor of Philosophy

Graduate Program in Civil and Environmental Engineering

written under the direction of

Dr. Husam S. Najm,

And approved by

_____

_____

_____

_____

New Brunswick, New Jersey,
October 2018

ABSTRACT OF THE DISSERTATION

INVESTIGATION OF FATIGUE RESISTANCE OF FILLET-WELDED TUBE CONNECTION DETAILS FOR SIGN SUPPORT STRUCTURES

By HYUNGJOO CHOI

Dissertation Director:

Dr. Husam S. Najm

Stiffened and unstiffened fillet-welded tube-to-transverse plate connection details are widely used for mast-arm and base-plate connection in highway support structures in New Jersey and many other states. However, repetitive wind loads which induce cyclic fatigue stresses are the primary source of failure at fatigue critical locations such as tube-to-stiffener and tube-to-base plate welded connection. The resistance of fatigue critical connections details has been an on-going research topic due to limited experimental work and the variability in existing fatigue testing results.

The main objective of this dissertation is to evaluate fatigue resistance of both unstiffened and stiffened fillet-welded tube connection details. Synthetic data analysis, Finite Element (FE), strain-life corrosion fatigue resistance model, fatigue reliability analysis were performed to determine the fatigue performance of fillet-welded connections.

Existing fatigue test data was collected to perform a synthetic data analysis and then analysis results were used to as fatigue input data in ANSYS Workbench platform and for the proposed SWT corrosion model. The fatigue resistance obtained from the FE analysis is expressed in terms of fatigue life, fatigue damage, and fatigue safety factor. The local stress level at fatigue critical locations was evaluated using a static FE model for different

number of stiffeners and boundary conditions.

The effect of corrosion on the fatigue resistance on stiffened fillet-welded tube connection was studied using a modified Strain-Life Smith-Watson-Toper (SWT) corrosion model. Chemical components and material properties of ASTM steels were also investigated for corrosion-resistant weathering steel and low-carbon steel. Corrosion Index, I, was obtained to estimate the corrosion resistance by following the equations from ASTM G101 Standards (ASTM G101, 2004). Under various corrosion categories, the proposed Constant Amplitude Fatigue Thresholds (CAFT) were obtained for weathering steel, low-carbon steel, hot-dip galvanized steel, and fillet-welded connection details.

This dissertation also includes a reliability-based fatigue assessment for the potential crack initiation at the tip of stiffeners at the tube-base plate connection. A synthetic analysis of 1-hour averaged wind data from two New Jersey weather stations was performed. The wind data was transformed to the transient domain to represent the turbulent natural wind phenomena and effective stress ranges and number of cycles were obtained using the Rainflow counting technique. A statistical analysis for existing test data was conducted to obtain stress-life (S-N) fatigue coefficients. Results from the reliability-based assessment and the probabilities of crack initiation can provide needed information to state officials for establishing inspection frequencies of tube-to-transverse plate connections of sign structures.

ACKNOWLEDGEMENTS

Foremost, I would like to thank my advisor, Dr. Husam S. Najm. I am deeply grateful for his guidance, encouragement and financial supports. He has been always fully supportive and willing to provide me warm advice. Without his guidance, this research work would not have been possible.

I also deeply thank my committee members, Dr. Perumalsamy N. Balaguru, Dr. Yook-Kong Yong, and Dr. Thomas Tsakalakos. I am grateful for their guidance, consideration and encouragement.

I am also very grateful to our department chair, Dr. Nenad Gucunski. He provided me an opportunity to work as Graduate Research Fellow and MATLAB Teaching Assistant. I always enjoyed working with Dr. Philip Brown and other TA members. I also thanks to research staffs at CAIT, Shane Mott and Hooman Parvardeh.

My sincere thanks are extended to all of my colleagues at Rutgers University. Dr. Howard Klinger provided me great insights and guidance on my future engineering career. I am also grateful to Civil Engineering department staffs, Linda Sazary and Gina Cullari.

Acknowledgement would not be completed without mentioning my parents (Jin Choi and Hyangsim Kim) and my family who always love and support me. The unconditional love from them was the greatest source to complete this work.

I also would like to express my gratitude to my wife, Jungeun Huh. Without your support and love, I would not able to complete my journey at Rutgers University. I love you, Woojin Choi, and you are the most precious blessing to us.

TABLE OF CONTENTS

LIST OF FIGURES

LIST OF TABLES

CHAPTER I

INTRODUCTION

1.1 General Overview

Recent failure investigations and published reports concluded that fatigue is the main cause of failure in sign structures (Fisher et al. 1991; John and Dexter, 1998; Kaczinski et al. 1998; Gilani and Whittaker 2000; Foley et al. 2004). Due to repetitive wind loads which induce cyclic fatigue stresses, localized fatigue failure have occurred around fatigue critical locations such as at the toe of fillet welds and at the tip of stiffeners in stiffened tube-to-transverse plate connections. Connections, anchorages, and splices are critical locations that should be carefully designed and detailed to provide infinite fatigue life for sign structures according to the AASHTO Specifications.

A recent study (Roy et al. 2001) concluded that the fillet-weld tube-to-transverse plate connection is the most fatigue critical detail as compared to groove-weld connection with a back ring. However, due to the easiness of fabrication and cost-effectiveness, fillet-weld connection details have been widely used for mast-arm connection and base-plate connection. Stiffened fillet-welded connection were initially developed to achieve a lower stress level at the fillet weld toe at the base by decreasing out-of-plane distortion at the pole wall (Roy et al. 2009).

However, the termination of the stiffeners on tube wall and the fillet welds at the tip of stiffener locations became more critical location for potential fatigue cracking (AASHTO 2015). In the State of New Jersey, tube-to-transverse plate connection details with longitudinal stiffeners are designed following standard drawings [New Jersey Department of Transportation (NJDOT) 2007]. These type of connections are extensively used for cantilevered and overhead sign structures.

To investigate the fatigue resistance of this detail several experimental studies were conducted in past several decades. However, the specimen and the test matrix were designed following the state's own design specification and the interest of the study. The standard drawings of each state are different with regard to the geometry and the treatment type of specimen. Moreover, the details which includes the specification do not represent all state's connection details. The fatigue provision of AASHTO specifications (AASHTO, 2001; AASHTO, 2009; AASHTO, 2015; AASHTO, 2017) has been modified and updated following findings from the recent fatigue testing and research work.

In addition, recent fatigue tests on galvanized unstiffened specimens under Federal Highway Administration (FHWA) research program (Ocel, 2014) found that there are significant influences in the workmanship which causes scatters in testing results due to the quality of welding and inherent defects in welding from manufactures. Thus, fatigue resistance for both analysis and design needs to be determined by minimizing risks from an unknown effects or parameters. Further, the variation in crack length was attributed to the difficulty in observing the initial crack while cyclic loadings are applied in fatigue testing and many experimental studies provide no information for the first crack length. Additional variation can be observed in the light of considering the fatigue failure criteria

defined as a 305 mm (12 inch) long crack (Ocel, 2014) and ten percent loss in overall stiffness (Stam et al., 2011).

Because of those facts, fatigue resistance of unstiffened and stiffened fillet-welded tube-to-transverse connection detail is on-going research topic including fatigue failure criteria and determining the connection details that can achieve the infinite fatigue life is a still challenging task for the State DOT's.

1.2 Research Objectives

The main objective of this study is to evaluate the fatigue resistance of fillet-welded connection details for sign supports structures. This includes the collecting and analyzing of existing fatigue test data, development of FE (Finite Element) model for fatigue analysis, development of a modified strain-life Smith-Watson-Topper (SWT) model, and a fatigue reliability assessment and probabilities of potential crack initiation.

1.3 Research Plan

The research plan for this dissertation will follow the flowchart shown in Figure 1.1.
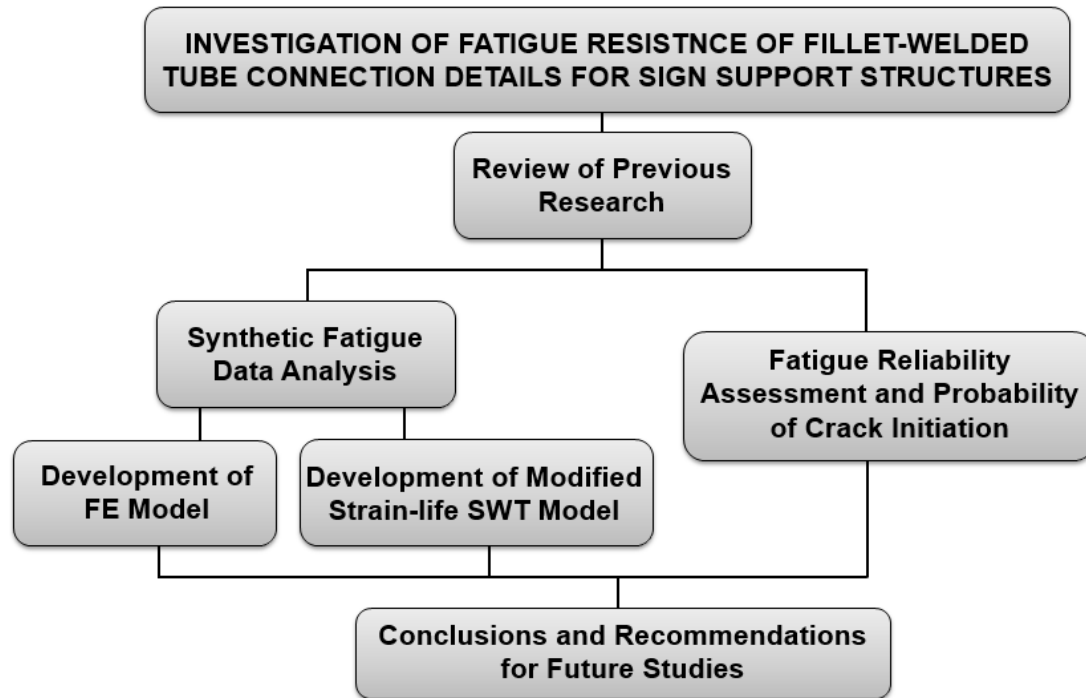
Figure 1.1 Framework for the dissertation

From the review of previous research, existing fatigue test data was collected to perform a synthetic data analysis. The results from the analysis results were used to as fatigue input data in the FE model developed using the ANSYS Workbench platform as well as the in the developed modified SWT corrosion model. From the static FE analysis, the local stress level at fatigue critical locations was evaluated with respect to different number of stiffeners and boundary conditions. By utilizing data analysis results, the fatigue resistance of these connections is expressed in terms of fatigue life, fatigue damage, and fatigue safety factor.

The fatigue resistance will also be investigated under corrosion effects using modified Strain-Life Smith-Watson-Toper (SWT) corrosion model. Under various corrosion categories, Constant Amplitude Fatigue Thresholds (CAFT) will be proposed in a form of range for weathering steel, low-carbon steel, hot-dip galvanized steel.

A reliability-based fatigue assessment will be investigated for the probabilities of potential crack initiation at the tip of stiffeners at the tube-base plate connection. This reliability-based assessment and the probabilities of potential fatigue cracking will be performed using synthetic analysis of 1-hour averaged wind data from two New Jersey weather stations. The analysis will transform collected wind data to the transient domain to represent the turbulent natural wind phenomena and use Rainflow counting for effective stress ranges and number of cycles. Results from the reliability-based assessment and the probabilities of crack initiation can provide needed information to state officials for establishing inspection frequencies of tube-to-transverse plate connections of sign structures.

1.4 Outline of the Dissertation

This dissertation is organized into six chapters. A brief description of each chapter will be addressed herein:

- Chapter I presents an introduction and an overview of this study, research objectives, research plan, and an outline of the dissertation.

- Chapter II summarizes the literature review which includes the problem statement, cases of structural failure due to fatigue, fatigue theoretical background, history of the AASHTO specifications for Luminaires and Traffic Signals (LTS) Specification, previous experimental and analytical research on fatigue failure, and the fatigue module in ANSYS Workbench.

- Chapter III presents synthetic fatigue data analysis of fillet-welded connection details to evaluate fatigue resistance of both unstiffened and

stiffened fillet-welded connections. The fatigue test data are grouped based on significant parameters such as geometry or the surface treatment. A statistical analysis was then performed to establish the Constant Amplitude Fatigue Threshold (CAFT) that achieves infinite fatigue life. Analysis results will be utilized as input parameters of fatigue module in ANSYS Workbench and to evaluate a modified SWT fatigue corrosion model.

- Chapter IV presents three dimensional FE model development that includes material properties, contact regions, mesh generation and boundary condition. The validation of FE model is also addressed.

- Chapter V covers a modified Strain-Life Smith-Watson-Topper (SWT) corrosion model. Chemical components and material properties of corrosion-resistant weathering steel and low-carbon steel are investigated using ASTM specifications. Under various corrosion categories, a range of the Constant Amplitude Fatigue Thresholds (CAFT) are proposed for infinite fatigue life design.

- Chapter VI presents fatigue reliability assessment methodology for the potential crack initiation at the tip of stiffeners at the tube-base plate connection. The analysis includes synthetic wind data analysis, data transformation to the transient domain to represent the turbulent natural wind phenomena, Rainflow counting technique, and a statistical analysis for existing test data. Results from the reliability-based assessment are addressed in the probabilities of crack initiation.

- Chapter VII summarize the conclusions from this dissertation and recommendation for future work.

CHAPTER II

LITERATURE REVIEW

2.1 Problem Statement

In highway transportation systems, structural supports play an important role in providing useful information to the public. However, the unexpected fatigue failure at a critical connection detail can cause severe injuries, property damage, disruption to traffic and accidents (Hosseini, 2013). The damage raises the safety concern with respect to the highway system and can cost up to thousands of dollars per occurrence. Across the United States, several support structures can be found in every single mile along a major highway.

Structural supports for overhead signs, luminaires, and traffic signal supports are typically long span structures with a small cross section and with its own mass (i.e. sign panel). Those facts induce unique structural characteristics such as low natural frequency and low damping, approximately one percent of critical damping (Kaczinski et al. 1998). Thus, there is no significant reduction in wind-induced amplitudes of vibration. Excessive vibrations and rapid damage accumulation of stress cycles make these structures susceptible to fatigue failure.

In 1996, along Route 147 in New Jersey, a sign failure resulted from fatigue loading at the aluminum shoe base socket connection. Failure reports (John and Dexter, 1998)

indicated that the poles experienced repeated stress cycles exceeding 12 ksi during the night of the failure. However, the socket connection shoe base was designed as category E' which has a Constant Amplitude Fatigue Threshold (CAFT) equal to 1.0 ksi for aluminum structures. In 2003, a 140 ft high-mast lighting towers along I-29 near Sioux City, IA collapsed due to fatigue loads. A forensic study by Connor et al. (2006) revealed that fatigue is the main cause of the failures at the base plate-to-column weld, at the handhole detail, or of anchor rods. At the time of collapse, the pole experienced large number of cyclic stress-range which was induced by vortex shedding phenomenon (John and Dexter, 1998). Corrosion of the tube wall was also identified as potential cause of failure. A more comprehensive review of fatigue failure of sign structures will be presented in this section.

2.1.1 The socket connection detail: Tube-to-transvers plate connection

A socket connection is an unequal leg fillet-welded socket connection or commonly referred as tube-to-transverse plate connection, was classified as Category E' having a Constant Amplitude Fatigue Limit (CAFL) of 2.6 ksi for steel and of 1 ksi for aluminum (AASHTO 2001). A typical fillet-welded socket connection is shown in Figure 2.1. According to previous research (Azzam, 2006), the term "socket" refers "to the way the baseplate is cutout to allow the pole to fit inside". There are two fillet welds in this connection detail: The first weld is applied at the top of the base plate and the second fillet weld is applied inside the cut-out inside the base plate, between the bottom surface of the pole and the sides of the base plate. The first fillet weld is more structurally significant than the second one as it resists shear and tensile stresses versus tensile stresses alone. For infinite life design requirement where no crack is anticipated, the stress range must be

below than CAFL.

<div align="center">(a)   (b)</div>
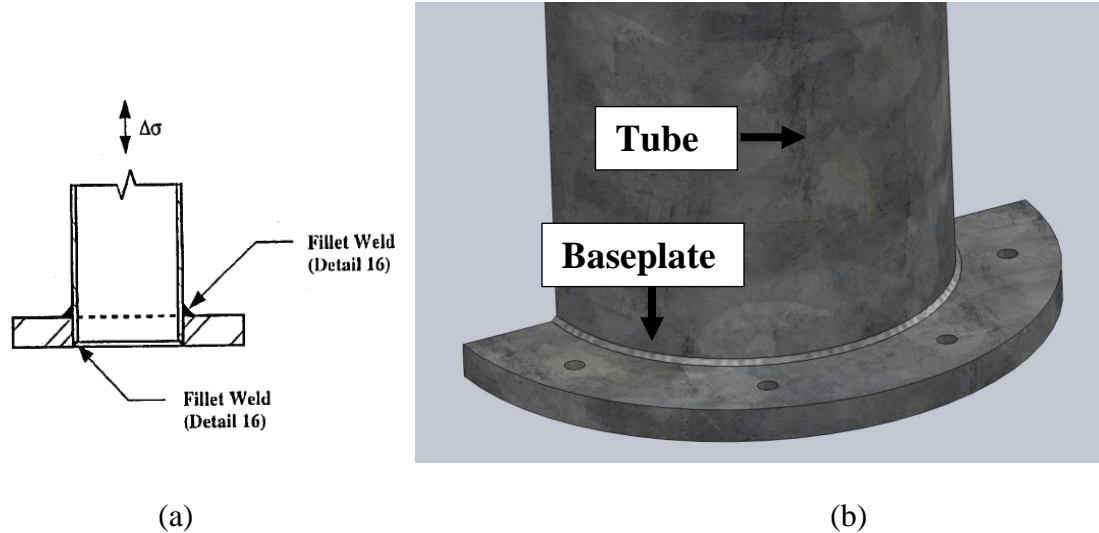
Figure 2.1 (a) Fillet-welded socket connection (AASHTO, 2001) and (b) SolidWork

Model for Tube-to-transvers plate connection

In 2001, Valmont Industries performed fatigue testing to evaluate the fatigue resistance of unstiffened welded socket connections using unequal leg fillet welds (Machietto, 2002). This detail was the same as Detail #16 in the 2001 AASHTO Specifications with fatigue category E'. However, in spite of the scatter in the test data, the fillet-welded sockets showed a better fatigue resistance than Category E. The 2001 AASHTO specification were inconsistent as unstiffened socket connection was classified as either Category E or E'. In addition, with respect to comparing unstiffened and stiffened specimens, results have shown that the fatigue resistance of the socket connection without stiffeners was significantly greater than the stiffened details. This could not attributed to geometry of the stiffeners that failed to reduce the level of stress at the weld toe at base plate. In such a case, adding stiffeners likely has created stress concentration points that may have resulted in pre-mature fatigue failure.

In past decades, research at the University of Texas in Austin (Koenigs et al. 2003;

Hall 2004; Hall and Connor, 2008) was conducted to examine the influence of fatigue resistance of mast arm socket connection due to the flexibility of the base plate. A total of fifty five full-size specimens were tested and the studies concluded that a 2 inch of base plate thickness showed an improvement of fatigue resistance compared to the 1.5 inch thick plates. Ultrasonic Impact treatment showed a significant improvement of the fatigue life of a fillet-welded socket connection (Koenigs et al. 2003).

At the University of Minnesota, full-scale 8-sided polygonal tube-to-transverse plate connection detail were tested using different tube diameters, tube thickness and base plate thickness (Ocel et al. 2006). Multi-sided connection demonstrated category K2 which is below the fatigue limit specified in 4th edition of the AASHTO specification. The hammer peening treatment improved the fatigue performance to category E'. The specimens with doubled base plate thickness reached Category E which is three categories improvement compared to the 1.25 inch think base plate.

To study the fatigue behavior of aluminum light pole structure, full-scale fatigue testing was performed on aluminum light pole structures to observe fatigue behavior for aluminum plate and shoe base socket connections and to determine lower bound fatigue resistance for infinite fatigue life design (Azzam, 2006). The plate socket connection was tested with a stress range of 0.9 ksi up to 4.5 ksi and the lower bound was much below the AASHTO category E' which has CAFL of 1.0 ksi for aluminum structure. This study found that the presence of compressive residual stresses at the surface of shoe base detail is the primary reason for shifting obtained fatigue data from this study above AASHTO category E'. At failure, a developed fatigue crack was observed at the weld toe area as expected. Experimental results also showed that relatively low strengths for the through plate socket

connection as compared to the shoe base details. The difference in strength between two details was a factor of 3.5.

To study cost-effective fatigue resistant connection details for cantilevered highway sign, luminaire and traffic signal support, an experimental and analytical research work was conducted at Lehigh University (Roy et al., 2011). The study demonstrated that galvanized tube-to-transverse plate connections are the most fatigue critical details with a thin plate with a few discrete fasteners at a larger bolt circle. Most of the reported fatigue cracking in service has been at unstiffened fillet-welded tube-to-transverse plate connections (Roy et al. 2011). According to the findings from previous studies (Koenigs 2003, Ocel et al. 2006, Hall and Connor, 2008), a minimum plate thickness of 2 inch was recommended and with larger diameter tubes, a groove-welded tube-to-transverse plate connection or a stiffened connection were recommended. With regard to welding, fillet-welds for unstiffened connection were specified as unequal leg welds, with the long leg at approximately 30 degree to the tube. To avoid significant scatter due to the variation in the fabricated weld profile, the weld geometry was carefully controlled to reduce the scatter in fatigue performance of tube-to-transverse plate connections.

An additional extensive experimental and analytical study of the fatigue behavior of the welded end connection for the use of high-mast lighting structures and traffic signal masts was conducted by Stam et al. (2011). Fatigue performance is a function of several parameters such as base plate thickness or stiffness, weld type and geometry, and number of anchor bolts. Their study pointed out that the classification the fatigue performance of the connection detail in term of category is no longer feasible due to the interaction of the overall connection geometry. The research indicates the variables that can affect the fatigue

strength are 1) end/base plate stiffness, 2) weld profile, 3) relative stiffness of mast or pole to the stiffness of base plate and 4) galvanizing.

To address the premature failure caused by cracking in the zinc metal bath during galvanizing, fatigue testing of the unstiffened socket connection was conducted to evaluate the fatigue resistance of galvanized and ungalvanized specimens (Ocel, 2014). With two set of test specimens from fabricator 1 and 2, it was realized that workmanship greatly affects in fatigue performance of socket connection and there was a one fatigue category reduction in galvanized specimen with a constant fatigue stress range as compared to ungalvanized specimen. Galvanized specimens showed a fatigue resistance less than category E' which represents the contradiction with the 6th edition of AASHTO specifications (2009).

Although there has been several previous research efforts to evaluate fatigue resistance of sign details, there is still a need to understand the fatigue performance of unstiffened connection details. A synthetic fatigue testing data analysis considering the key factors that significantly affect fatigue resistance was performed in Chapter III of this dissertation. Existing experimental results were grouped into eight different groups based on base plate thickness, galvanizing, peening and shape of tube. A statistical analysis was conducted assuming the log-normal distribution of slope A to set a fatigue design threshold for the commercial FEA software, ANSYS Workbench 17 used for fatigue analysis.

2.1.2 Stiffened socket connection detail: Tube-to-transvers plate connection with longitudinal stiffeners

Stiffened tube-to-transverse plate detail are typically designed to increase the stiffness of the fillet weld toe at the base plate and to decrease out-of-plane distortion

behavior of the tube wall (Roy et al. 2009; Roy et al. 2012). The fatigue design of this detail was firstly introduced in the AASHTO specification in 2001. The fatigue design category for weld terminations at the ends of longitudinal stiffeners varies from Category C to Category E depending on the length of stiffeners (short, medium and long). Figure 2.2 shows fillet-welded socket connection with longitudinal attachment.
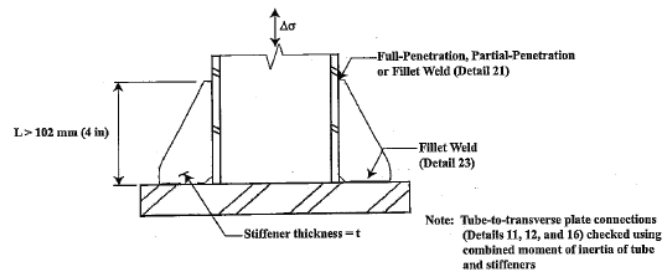
(a)
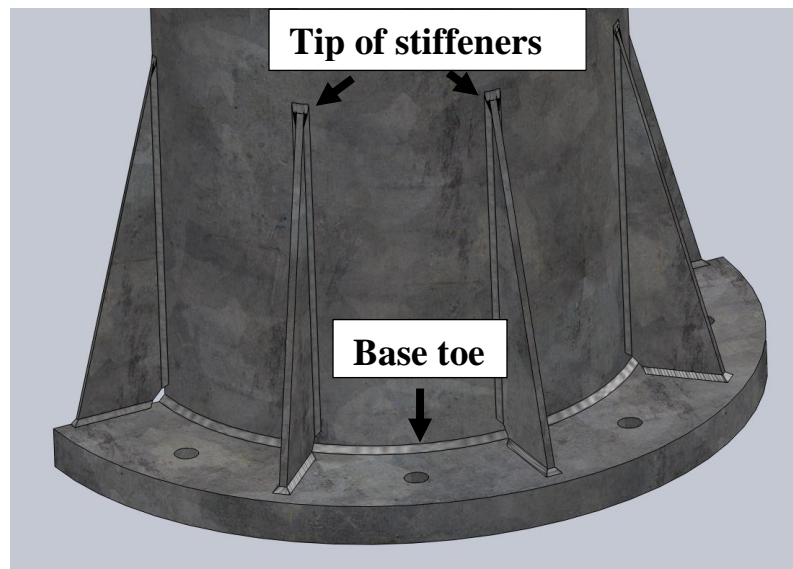
(b)

Figure 2.2 (a) Fillet-welded socket connection with longitudinal attachment (AASHTO, 2001) and (b) SolidWork model for Tube-to-transvers plate connection with longitudinal stiffeners

After the 2001 AASHTO specification, Valmont Industries performed fatigue

testing for both stiffened and unstiffened welded socket connections (Machietto, 2002). A total of six fillet-welded sockets utilizing gusset stiffeners were tested. In the synthetic data analysis in Chapter III only the first two fillet-welded gusseted specimens (Specimen #1 and #2) were considered in this study. Those two were designed in accordance with Detail #21 of the 2001 Specifications with 8 gussets fillet welded to the pole. This detail was categorized as category E because the height of stiffener was only 3.25 inch. The testing results showed that the fatigue resistance of the detail was above that of Category E. A fatigue crack was found at stiffeners for both specimens. The dead load stress was neglected in the Valmont study.

Another extensive fatigue study was carried out by Koenigs (Koenigs et.al, 2003) at The University of Texas at Austin. This study included 25 full scale fatigue tests for medium and long gusset stiffeners. The 2001 AASHTO specifications specify medium stiffeners as Category D detail and the long stiffeners as Category E detail. A significant finding was the examination of base flexibility on fatigue performance. Tests using 2 inch thick base plate showed substantial improvements as compared to 1.5 inch plate thickness. Testing results also revealed that at the same stress ranges, at least 3 long stiffener specimens are close to or above Category D detail and longer stiffeners improved the fatigue resistance compared to short stiffeners. The number of stiffeners provided does not seem to influence the fatigue Category. The pole thickness did not appear to have a significant impact on the fatigue resistance. It was also observed that the Ultrasonic Impact weld treatment enhanced the fatigue life of fillet-welded socket connection detail significantly.

The findings from their study appear to be inconsistent with the fatigue design

provisions (AASHTO, 2001) as the fillet or partial penetration weld termination for short stiffeners were identified as category C, while the long stiffeners are given a Category D or E (AASHTO, 2001)

Another experimental study (Ocel et al. 2006) was conducted for the multi-sided tube-to-transverse connections with gusset plate stiffeners. The test results have shown that the gusset plates could not prevent the fatigue crack at the corners of the tube and at the toe of the socket weld. It is believed that this is due to the nature of multi-sided tube shape which means that the higher stress range was at the corner of the tube. During the testing, cycling was paused once cracks were observed in the socket weld and then hammer peeing was applied at the cracked weld toes with the dead load. It was found that hammer peening introduced compressive residual stresses that resists fatigue crack growth and this procedure allowed cycling load to continue until the gusset plates cracked. In terms of fatigue resistance or fatigue category, the results have shown that the socket weld plots between category E_T and E' with the 97.5 percent of survivability line as compared to category K_2 for the unstiffened pole socket connections. The fatigue resistance of tips of the gusset show a lower bound resistance below category D.

In 2011, as the part of NCHRP study (Roy et al., 2011), galvanized stiffened tube-to-transverse plate connections which represent multi-sided high level luminaire support structure were tested at Lehigh University. It was discussed that increasing the stiffness of the transverse plate is the most cost-effective means of improving fatigue resistance of this connection (Roy et al., 2011). After the completion of an analytical study, the geometry of specimen was selected to be the most cost-effective fatigue design. This study introduced an optimized tube-to-transverse plate connection detail with longitudinal stiffener and three

factors were defined as follows: 1) a ratio of stiffener thickness to tube thickness of 1.25, 2) a ratio of stiffener height to stiffener spacing of 1.6 and 3) a stiffener termination angle of 15 degree. For multi-sided tubes, a minimum of eight sides and 1 inch bend radius were recommend to avoid the high stress concentration at the corner of the tube. An adequately designed and optimized stiffened tube-to-transverse plate fillet-welded connection provides a CAFT of 7.0 ksi which is AASHTO Category D while the prior specification (AASHTO, 2001; AASHTO, 2009) defines the CAFT of this connection as 2.6 ksi (Category E´). According to the research results presented in NCHRP Report 10-70 (2009), proposed recommendation were adopted for revision to AASHTO *Chapter 11:Fatigue Design* of the existing *AASHTO Specification for Highway Signs, Luminaire and Traffic Signal Support Structures, 5th Edition* (AASHTO, 2015).

2.2 Theoretical Background of Fatigue

The main purpose of fatigue analysis is to characterize the capacity (resistance) of the structural component under the cyclic loading. With repeated loading applied to structural members, fatigue failure occur although the stress level is lower than the yield strength. The stress level and the number of cycles are key parameters that determine fatigue performance of the structural members. Topics for the background of fatigue such as loading type, stress-life, strain-life analysis and fatigue reliability will be addressed in the following sections.

Fatigue (cyclic) loading phenomenon

Fatigue is damage accumulation phenomenon which is associated with repeated

loading that induce cyclic stresses. Loading amplitude and proportion are two components that distinguish fatigue loading. In general, constant amplitude cyclic loading is typically used for fatigue testing. The load-time waveform is typically sinusoidal function and it varies from a fixed minimum to maximum load or stress magnitude at defined frequency. In this dissertation, σ_a is determined as the stress amplitude and $\Delta\sigma$ is defined as the stress range, respectively. The constant amplitude with proportional loading is illustrated in Figure 2.3.
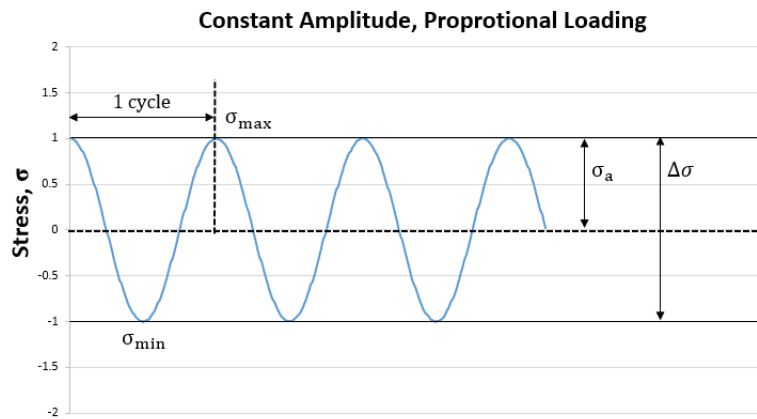
Figure 2.3 Constant amplitude, proportional loading

In the case of constant amplitude, fully-reversed loading occurs when an equal and opposite load is applied. This is the case when mean stress is equal to zero ($\sigma_m = 0$) and the stress ratio is set to -1 ($R = -1$). Zero-based loading occurs when cyclic fatigue loads are applied then removed. This is a case when the mean stress is equal to half of the maximum stress ($\sigma_m = \sigma_{max}/2$) and stress ration is equal to zero ($R = 0$).

Otherwise, if the amplitude of loading is not constant, this case is known as variable amplitude where mean stress is not equal to zero. In this case, the mean stress effect should be considered to evaluate fatigue performance and the detail of the mean stress correction theory will be addressed in a following section. Fatigue loading terms and corresponding

equations are summarized in Table 2.1.

Table 2.1 Fatigue loading terms and equations

Term	Equation
Stress Range	$\Delta\sigma = \sigma_{max} - \sigma_{min}$
Stress Amplitude (Alternating Stress)	$\sigma_a = \dfrac{1}{2}(\sigma_{max} - \sigma_{min})$
Mean Stress	$\sigma_m = \dfrac{1}{2}(\sigma_{max} - \sigma_{min})$
Stress Ratio	$R = \dfrac{\sigma_{min}}{\sigma_{max}}$
Amplitude Ratio	$A = \dfrac{\sigma_a}{\sigma_m}$

In addition, based on proportionality of fatigue loading, constant or non-constant amplitude loading can be divided into two loading types. Proportional loading means that the ratio of the principal stresses is constant, and the principal stress axes do not change over time. This essentially means that the response with an increase and reversal load are constant. Conversely, non-proportional loading means that there is no implied relationship in terms of changing loading components. Described fatigue loading components are the fundamental background in utilizing the fatigue tool in the ANSYS Workbench platform. In the light of loading amplitude and proportionality, four types of fatigue loadings are shown in Figure 2.4.
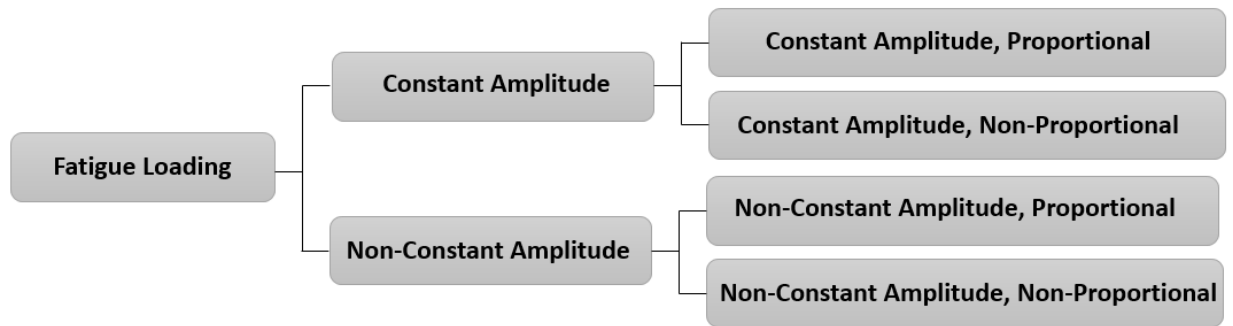
Figure 2.4. Fatigue loading types

2.2.1 Stress-Life Analysis

In this research, fatigue analysis will be performed by using the stress life analysis method. This approach is based on a traditional method that utilizes stress range versus the number of cycle curve, called S-N curve. Stress life is typically used for high cycle fatigue where the number of cycles exceeds 10 million with low stress range. Therefore, assumptions for the stress life analysis are elastic deformation (no yielding and plasticity). There are factors such as nominal stresses, strength of material and stress concentration that control fatigue performance.

2.2.1.1 Palmgren-Miner's rule

Miner's rule (Miner, 1945) is a simple and traditional fatigue analysis that does not include the sequence of loadings and it accounts the cumulative damage model for fatigue failure. In the light of fatigue design and analysis for overhead signs, luminaires, and traffic signal supports, Miner's rule is introduced by AASHTO specifications (AASHTO 2001, AASHTO 2009, and AASHTO 2015). Miner's rule can be expressed in the following equation 2.1,

$$N = A S_r{}^{-3} \quad (2.1)$$

Where N is number of cycle and S_r represents stress range and is considered as an independent variable. N and S_r are obtained from fatigue tests under the constant amplitude loading. To obtain the finite life constant A, Miner's rule also can also be written as,

$$A = n(S_{r,CAFL})^3 = N(S_r)^3 \quad (2.2)$$

Where n is the number of cycles using Miner's rule for the Constant Amplitude Fatigue Limit (CAFL) and N is the number of cycle to failure. $S_{r,CAFL}$ is stress range for CAFL. The fraction of fatigue life, C, consumed by exposure to N cycles at different stress level is given by,

$$C = \left(\frac{n}{N}\right) = \left(\frac{S_r}{S_{r,CAFL}}\right)^3 \quad (2.3)$$

When the fraction C reaches, failure occurs. The parameter n can be obtained from experimental test data as follows,

$$n = N \left(\frac{S_r}{S_{r,CAFL}}\right)^3 \quad (2.4)$$

The idea behind the Palmgren-Miner rule is that each cycle at a given mean stress and stress amplitude uses up a fraction of the available life. Based on this approach, fatigue failure is expected for cycles N at a given stress amplitude.

2.2.1.2 Mean stress correction theories

The original Goodman diagram (1899) defined the influence of mean and alternated stresses on the resulting cycles to failure with Wohler's data with linear projections as a function of material ultimate strength and applied mean and alternating stresses. A subsequent correction (inclusion of endurance limit) to improve agreement with data

results in the modified Goodman equation/diagram.

As illustrated in Figure 2.5, mean stress effect (i.e. dead load) should be considered if mean stress (σ_m) is not equal to zero. When the mean stress exists, it affects fatigue life by shifting of the S-N curve up or down. Therefore, the structural component can have longer or shorter fatigue life at a given stress range.
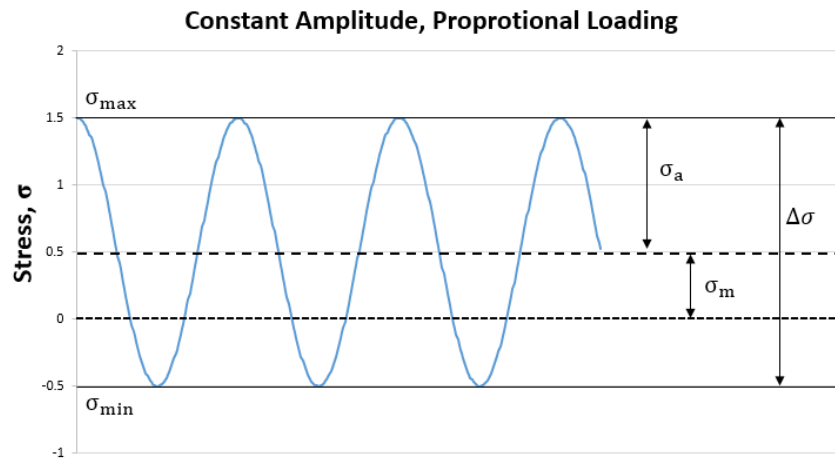
Figure 2.5 Mean stress effect for constant amplitude and proportional loading

To account for the mean stress effect, it is necessary to interpolate the material curves that defines the relationship between mean stress and strength of material. If there is no existing experimental data, several empirical curve options can be chosen including Gerber, Goodman, Soderberg and Morrow theories which utilize static material properties such as yield stress and tensile strength along with S-N data. Mean stress correction theories are summarized in Table 2.2.

Table 2.2 Mean stress correction theories

Mean stress correction theory	Equation
Soderberg (1930)	$\dfrac{\sigma_a}{\sigma_{ar}} + \dfrac{\sigma_m}{\sigma_y} = 1$

Goodman (1930)	$\dfrac{\sigma_a}{\sigma_{ar}} + \dfrac{\sigma_m}{\sigma_u} = 1$
Gerber (1874)	$\dfrac{\sigma_a}{\sigma_{ar}} + (\dfrac{\sigma_m}{\sigma_u})^2 = 1$
Morrow (1965)	$\dfrac{\sigma_a}{\sigma_{ar}} + (\dfrac{\sigma_m}{\sigma_f})^2 = 1$
Smith-Watson-Topper (SWT) (1970)	$\sigma_{ar} = \sqrt{\sigma_{max}\sigma_a}$

According to empirical fatigue testing data, experimental results can be determined between the Goodman and Gerber theories. Soderberg theory is usually overly conservative for mean stress effect. For brittle materials, the best fit can be obtained by the Goodman theory while the Gerber theory can be more representative for ductile materials. The difference among these is that the Gerber theory considers both negative and positive mean stresses as the same while the Goodman and Soderberg theories are not bounded when using negative mean stresses. In ANSYS Workbench platform, mean stress correction methods are provided.

2.2.2 Strain-Life Analysis

In this dissertation work, strain-life analysis was investigated to utilize proposed Strain-Life Smith-Watson-Topper (SWT) corrosion model for fillet-welded connection details. The fundamental concepts and theories in the light of strain-life analysis will be briefly described in this subchapter. The details of the SWT corrosion model and analysis results will be discussed in the Chapter 5.

With respect to strain-life fatigue analysis, the total strain is composed of two parts: elastic and plastic region. Ramberg-Osgood relationship for the stable hysteresis loop curve

is written in equation 2.5,

$$\varepsilon_{total} = \varepsilon_e + \varepsilon_p = \frac{\sigma}{E} + \left(\frac{\sigma}{K'}\right)^{1/n'} \qquad (2.5)$$

Where E is Young's modulus. n' is a measurement of the material's working hardening behavior and K' represents cyclic strength coefficient (Ramberg and Osgood, 1943). Due to the stress-strain behavior obtained from a monotonic test which is different with cyclic test, strain amplitude of plastic region is introduced in this equation. While cyclic properties are determined by stress-strain relationship, fatigue properties can be obtained from the steady-state hysteresis loop with symmetric deformation behavior in tension and compression (Stephens et al., 2000).

By following strain-controlled fatigue testing data (ASTM E606, 2012), the total strain amplitude can be resolved into elastic and plastic strain components and curves for both elastic and plastic are fitted separately as straight lines. At large strains, the plastic strain component is predominant while elastic strain is predominant at small strains. The intercepts of the two straight lines at $2N_f = 1$ are the elastic component and plastic component. The Morrow (1965) proposed the equation for the relation of the total strain amplitude and the fatigue life reversal to failure and it is expressed in equation 2.6,

$$\varepsilon_a = \frac{\Delta\varepsilon}{2} = \frac{\Delta\varepsilon_e}{2} + \frac{\Delta\varepsilon_p}{2} = \frac{\sigma'_f}{E}(2N_f)^b + \varepsilon'_f(2N_f)^c \qquad (2.6)$$

Where ε'_f is the fatigue ductility coefficient and σ'_f is the fatigue strength coefficient. The b and c represents the slopes of the elastic and plastic lines, respectively.
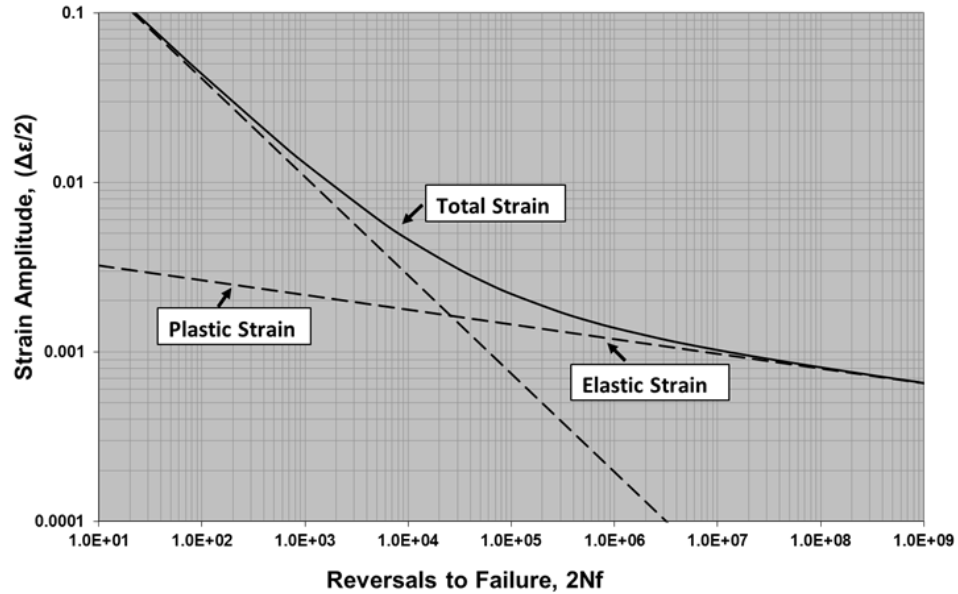
Figure 2.6 Strain amplitude versus reversals to failure for A595 Grade C

Using uniform material law (Baumel and Seeger, 1990), fatigue coefficients for strain life analysis can be obtained. According to ASTM Specification (ASTM A595, 2004), ASTM A595 Grade C weather-resistance steel of Young's Modulus, yield strength, ultimate tensile strength and elongation are 200,000 MPa, 410 MPa, 480 MPa and 21 percent, respectively. Fatigue coefficient values for strain-life fatigue analysis such as $K' = 1400$ MPa, $n' = 0.15$, $\sigma_f' = 720$ MPa, $b = -0.087$, $\varepsilon_f' = 0.59$ and $c = -0.58$ can be obtained for typical ASTM standard materials. Figure 2.6 shows Strain amplitude versus reversals to failure for A595 Grade C.

2.2.3 Reliability-Based Fatigue Assessment

Fatigue reliability is another part of the on-going research topic for various structural components such as ship, bridge and support structure. In the light of the cantilever sign

support structures, the long-term fatigue performance of under the non-constant amplitude wind load becomes critical due to high amplitude of vibrations with a low damping ratio which is less than one percent (Kaczinski et al. 1998). Therefore, the reliability of these type structures under the non-constant amplitude fatigue loading is an area that needs further study. It is important and worthwhile to address predicting the remaining fatigue life of existing structures using the principles of structural reliability at fatigue critical location where high stress concentration raised.

Limit state function or performance function for reliability-based fatigue assessment has been studied for the following fatigue life cycle formulation approaches (Ayyub et al. 2002). Using Miner's cumulative fatigue damage (Miner 1945), a limit state function of fatigue reliability has been investigated and used for many other structural applications such as offshore structures (Wirsching 1984), bridge structures (Kwon 2011), high-mast tower lights and others (Dawood et al 2014). Life cycle formulations for the fatigue reliability limit state function are defined by researchers (Foley and Diekfuss 2016; Ayyub et al) and by assuming parameters are statistically independent,

$$g(X) = N_c - N_T < 0 \text{ or } g(X) = \frac{T_c}{T_T} \leq 1 \qquad (2.7)$$

where N_c is the critical number of stress-range cycles resulting in crack initiation and N_T is the total number of applied stress-range cycles of any magnitude. The number of stress-range cycles can be also expressed in a form of service time intervals, T_c and T_T. A bias factor, B is introduced for wind demand uncertainties and prediction of stress-range magnitudes (Kwon 2011)

$$D = \frac{N_T(B^m \cdot S_{RE}{}^m)}{A} \geq \Delta \qquad (2.8)$$

where S_{RE} is stress range and m and A are constants corresponding to a specific

connection detail. Δ defines the damage parameter (Miner, 1945). The critical time, T_C needed for fatigue-induced crack initiation is defined as (Wirsching 1984),

$$T_c = \frac{\Delta \cdot A}{B^m \cdot \Omega} \quad (2.9)$$

where Ω is the semi-deterministic stress parameter (Foley and Diekfuss 2016). Further discussion of parameter Ω will be addressed in a later section. By applying developed time interval function above, the limit state function, $g(X)$, can be rewritten,

$$g(X) = \frac{T_c}{T_T} = \frac{\Delta \cdot A}{B^m \cdot \Omega \cdot T_T} \leq 1 \quad (2.10)$$

This function becomes a product of lognormal random variables and A, Δ and B, are assumed to be log-normally distributed random variables. The reliability index or safety index β is defined from the following equation from reference (Foley and Diekfuss, 2016),

$$\beta = \frac{ln\left(\frac{u_A u_\Delta}{u_B{}^m}\right) - \frac{1}{2} ln\left[\frac{\left(1 + CV_A{}^2\right)\left(1 + CV_\Delta{}^2\right)}{(1 + CV_B{}^2)^m}\right] - ln\Omega - lnT}{\sqrt{ln[\left(1 + CV_A{}^2\right)\left(1 + CV_\Delta{}^2\right)(1 + CV_B{}^2)^{m^2})]}} \quad (2.11)$$

It should be noted that if the limit state function is not a product of lognormal random variable, the limit state function becomes nonlinear function of random variables (Nowak and Collins 2000) and the equation for reliability index will not be applicable. Further, if the coefficient of variables are less than 0.2, the expression of the reliability index β in eq. (5) can be simplified as shown below (Nowak and Collins 2000).

$$\beta = \frac{ln\left(\frac{u_A u_\Delta}{u_B{}^m}\right) - ln\Omega - lnT}{\sqrt{[\left(CV_A{}^2\right) + \left(CV_\Delta{}^2\right) + (CV_B{}^2)^{m^2})]}} \quad (2.12)$$

The cumulative distribution function (CDF) describing the probability of fatigue crack-initiation is defined (Foley and Diekfuss 2016),

$$P_f = P[g(X) \leq 1.0] = \phi \left[\frac{ln(1) - u_{lng(X)}}{\sigma_{lng(X)}} \right] = \phi \left[\frac{u_{lng(X)}}{\sigma_{lng(X)}} \right] = \phi[-\beta] \quad (2.13)$$

To determine random variables that introduced in the fatigue limit state function, a comprehensive wind data analysis was performed for the long-term period of one hour averaged wind data collected from the National Climatic Data Center (NCDC) Automated Surface Observation System (ASOS). Then, collected wind speeds were simulated using the Kaimal spectrum to represent the non-constant and fluctuating natural wind speeds. A bias factor, *B* which represents uncertainties in modeling error was determined as the ratio of the simulated and measured one hour stress histories. In the light of the wind demand uncertainties, the stress parameter, Ω was defined as a semi-deterministic variable and parameters such as stress-ranges, number of cycles, wind direction, and combined probability, were accounted for in calculating the stress parameter. This procedure was performed for each year of wind data to obtain 44 years of stress parameters. To determine fatigue life uncertainties of the tube-to-transverse plate connection detail, fatigue coefficients m and *A* were determined by performing a least square regression analysis for stress range and number of cycle for fatigue crack-initiation. The details of fatigue reliability assessment will be addressed in Chapter 6.

2.2.4 Surface Treatment Effects

Material failures occur on the surface and most material failures, including fatigue fracture and corrosion (Zhang and Lindemann, 2005). Surface treatments of materials can effectively improve the structural performance globally.

In this subchapter, the background of surface treatment effects will be addressed with regard to fatigue resistance. Galvanization which produces the zinc barrier as the

corrosion protection and shot-peening treatment which has compressively stressed layer from multiple and progressively repeated impact are considered in the synthetic fatigue data analysis which will be presented in Chapter 3.

2.2.4.1 Galvanization

Hot-dip galvanizing is known as corrosion protection by forming the zinc patina as well as providing cathodic protection. According to American Galvanizers Association (AGA), hot-dip galvanized steel is produced by immersing steel in a bath of molten zinc. During dipping process, a protective coating is developed by a metallurgical reaction between iron and zinc and a tightly-bonded alloy coating provides cathodic protection (American Galvanizers Association, 2012). Hot-dip galvanizing process is shown in Figure 2.7.
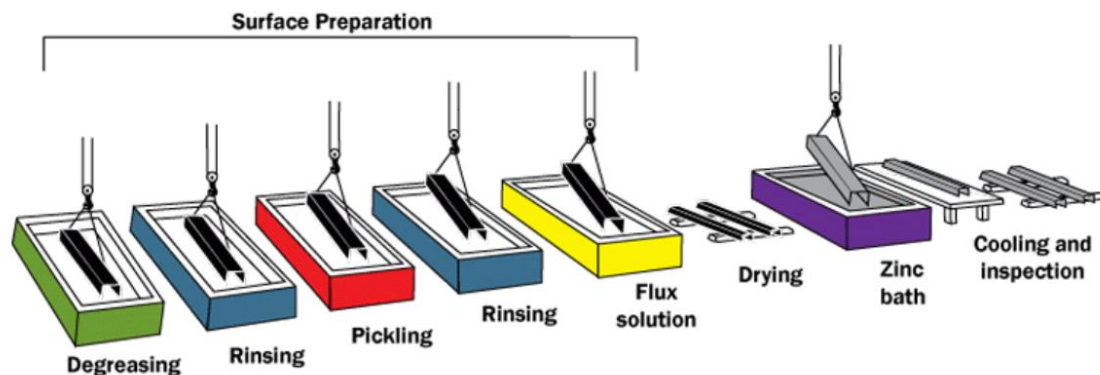
Figure 2.7 Hot-dip galvanizing process (American Galvanizers Association, 2012)

2.2.4.2 Shot-Peening

Shot-peering is the proven method to enhance the fatigue performance of structural materials such as steel, aluminum and titanium alloy (Zhang and Lindemann, 2005). Cold-

working the surface of structural components is a process by involving multiple and progressively repeated impact (Al-Obaid, 1995). Typically, spherical chilled shots made from iron or steel are projected against the surface being peened with sufficient velocities (ranges from 20 to 150 m/s) to indent the surface (Al-Obaid, 1995). With respect to the failure under cyclic loading, compressively stressed layer from the indentation at each point of impact is known as very effective in preventing premature failure (Al-Obaid, 1991, 1995). Compressive residual stress formation during the shot-peening is illustrated in Figure 2.8.
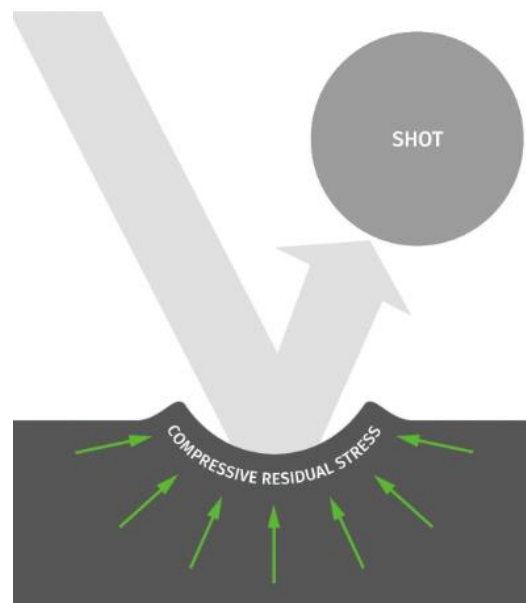
Figure 2.8 Compressive residual stress formation during the shot-peening (Stresstech, 2018)

2.3 AASHTO Luminaires and Traffic Signals (LTS) Specification

In the light of fatigue design and analysis of structural supports, most of state's DOT follows the AASHTO standard specifications for Structural Supports for Highway Signs, Luminaires and Traffic Signals (LTS). The fourth edition of specification (AASHTO, 2001) was the first specification that includes the fatigue design provision in Chapter 11 of the manual. The fifth edition of the AASHTO specification (AASHTO, 2009) was published in 2009 but there was no signification updates in a fatigue provision. After NCHRP Project 10-70, significant changes for fatigue design were adopted in AASHTO Load Resistance and Factored Design (LRFD) (AASHTO, 2015). This is the first edition that adopts the LRFD design concept for structural supports. In this chapter, an overview of the AASHTO specifications and fatigue provision for both unstiffened and stiffened fillet-welded tube-to-transverse connection detail will be addressed.

AASHTO Standard Specification (2001)

The AASHTO Specification 2001 is the result of National Cooperative Highway Research Program (NCHRP) Project 17-10 and NCHRP Report 412 (Kaczinski et al., 1998). The Specifications are intended to serve as a standard and guide for the design, fabrication, and erection of these types of supports. Structural supports are categorized as 1) sign support structures, 2) luminaire support structures, 3) traffic signal support structures, and 4) a combination of these structures. Due to changes in 2001 AASHTO, there were significant impacts in increasing of the size of sign support structures from previous version of AASHTO Specification published in 1994 (Valmont Structures, 2004).

In terms of load combinations and fatigue load, those are provided in Section 3.

Load combinations are based on the Allowable Stress Design (ASD) method. As shown in Figure 2.9, fatigue load combination is determined as the group load IV and the denote c indicates to see section 11 for fatigue loads and stress range limits. In addition, a 50-yr wind map from ASCE 7-95 was provided with "safety factors" with the ASD design method.

Group Load	Load Combination	Percentage of Allowable Stress[a]
I	DL	100
II	$DL + W$	133
III	$DL + Ice + 1/2(W)^b$	133
IV	Fatigue	c

Figure 2.9 Group load combinations (AASHTO, 2001)

Fatigue design criteria

In fatigue provisions of the 2001 AASHTO standard specification, fatigue design criteria is introduced to resist the equivalent static wind load effects. Due to the uncertainty of stress fluctuations and the corresponding number of cycles, category-based infinite fatigue life design methodology is recommended for each fatigue critical connection detail. Based on the connection type, fatigue design category is provided with corresponding the Constant Amplitude Fatigue Limit (CAFL) values. Fatigue details of cantilevered support structures is summarized and tabulated in Table 11-2.

With respect to fatigue critical details, the nominal stress approach with elastic section analysis is used. Stresses induced by the wind loading components such as galloping, natural-wind gust and truck-wind gusts should be lower than the CAFL value. In Table 2.3, constant-amplitude fatigue limit of each detail category is shown for both steel and aluminum support structure.

Table 2.3 Constant-Amplitude Fatigue Limits

Detail Category	Steel (ksi)	Aluminum (ksi)
A	24	10.2
B	16	6.0
B'	12	4.6
C	10	4.0
D	7	2.5
E	4.5	1.9
E'	2.6	1.0
ET	1.2	0.44
K_2	1.0	0.38

AASHTO-LTS LRFD Standard Specification (2015)

The LRFD AASHTO specification (AASHTO, 2015) provides the requirements for loads and fatigue design of cantilevered and noncantilevered steel and aluminum structural supports for highway signs, luminaires, and traffic signals. Since the design philosophy has been changes, significant updates were made with respect to design and analysis for structural supports.

By following the LRFD design philosophy which utilizes the corresponding limit state function, the load combinations and load factors are addressed. It has three load components such as 1) permanent, 2) transient, and 3) fatigue. Wind loads are considered in Extreme I, Service I and Service II with a load factor of 1.0. In terms of fatigue design and analysis, two fatigue limit states are provided for infinite life approach (fatigue I) and finite life approach (fatigue II), respectively. With the LRFD design philosophy, this specification uses only the infinite life approach which defines as fatigue limit state I. In Figure 2.10, the load combinations and load factors are shown and the load combinations herein were calibrated from NCHRP report 796 (Puckett, et al., 2014).

In the light of the design perspective under extreme or service limit sate, wind speed maps for Mean Recurrence Interval (MRI) are recalibrated with the reliability index, β, of

approximately 3.0 for 300-yr MRI, 3.0 to 3.5 for 700 MRI, and 3.5 to 4.0 for 1700-yr MRI, respectively. MRI wind speed is determined based on traffic volume, ADT (Average Daily Traffic) and risk category.

Load Combination Limit State	Description	Reference Articles	Permanent Dead Components (DC)		Transient Live Load (LL)	Wind (W)	Truck Gust (TrG)	Fatigue			
			Max/Min	Mean				Natural Wind Gust Vibration (NWG)	Vortex-Induced Vibration (VVW)	Combined Wind on High-level Towers	Galloping Induced Vibration (GVW)
								Apply separately			
Strength I	Gravity	3.5, 3.6, and 3.7	1.25		1.6						
Extreme I	Wind	3.5, 3.8, 3.9	1.1/0.9			1.0ᵃ					
Service I	Translation	10.4			1.0	1.0ᵇ					
Service III	Crack control for Prestressed Concrete				1.0	1.00					
Fatigue I	Infinite-life	11.7			1.0			1.0	1.0	1.0	1.0
Fatigue II	Evaluation	17.5			1.0			1.0	1.0	1.0	1.0
a. Use Figures 3.8-1, 3.8-2, or 3.8-3 (for appropriate return period)											
b. Use Figure 3.8-4 (service)											

Figure 2.10 Load combination and load factors (AASHTO, 2015)

Fatigue design criteria

In fatigue provision of the LRFD based AASHTO specification, fatigue design criteria is introduced for each fatigue-sensitive connection detail. This specification also provides the curve for stress range versus number cycles with the fatigue design category but Constant Amplitude Fatigue Threshold (CAFT) for infinite life design is determined by the Table 11.9.3.1-1. Fatigue Stress Concentration Factor (SCF) is the factor that determines the CAFT for the fatigue-sensitive connection detail. Stress induced by wind load components such as galloping, natural-wind gusts and truck-induced gusts is below the CAFT and it is written for nominal stress-based design,

$$\gamma(\Delta f)_n < \emptyset(\Delta F)_n = \emptyset(\Delta F)_{TH} \qquad (2.14)$$

Where $(\Delta f)_n$ is the wind-induced nominal stress range (ksi), $(\Delta F)_n$ is the fatigue

resistance for the various connection details and $\emptyset(\Delta F)_{TH}$ is the CAFT, respectively. γ is the load factor per the Fatigue I limit state defined in the load combination and load factors table and $\emptyset$ is the resistance factor equal to 1.0.

In the light of fatigue analysis, the assessment of the remaining fatigue life of existing structure can be made for a finite life. Nominal fatigue resistance can be determined,

$$\emptyset(\Delta F)_n = \emptyset(\frac{A}{N})^{\frac{1}{3}} \qquad (2.15)$$

Where A is the finite life constant and N is the number of wind load induced stress cycles expected during the life time of the structures. For finite life, fatigue constant of A for connection details is provided in Table 11.9.3.1-1 and this coefficient is determined by experimental and analytical study under NCHRP Project 10-70 (Roy et al., 2011). However, the remaining fatigue life approach is still relying on a traditional method which considers linear damage accumulation and no sequence of loading (Miner, 1945).

In addition, the fatigue details of support structures tested in the laboratory table (Table C11.9.3.1-1) provides fatigue constant of A and CAFT. With tested geometry of the specimen, both fatigue SCF for finite life, K_F and infinite life, K_I are addressed. Regarding the updates on the LRFD specification, there is a certain limitation in existing fatigue testing results which cannot represent geometries that varies in each state. CAFT is only applicable if the geometry is within a certain range and the resistance of fatigue-sensitive connection details determined by the local stress-based methodology should be verified experimentally.

2.4 Existing Studies on Fatigue Performance of Sign Details and Fatigue Failure

In past two decades, experimental and analytical studies in light of fatigue resistance were conducted for structural supports for overhead signs, traffic signals, and high-mast light poles. In this section, a comprehensive review of previous studies on fatigue resistance as well as failure investigations will be presented. Related research works will be presented in alphabetical order and it is also summarize in a tabular format in Appendix A.

Fatigue Behavior of Aluminum Light Pole Structures
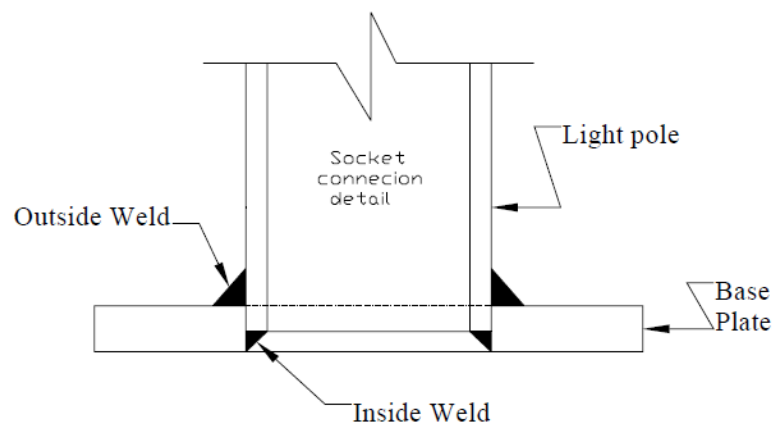
Figure 2.11 Fillet-welded through plate socket connection detail (Azzam, 2006)

This study by Azzam (2006) reported that there were a number of localized failures in the socket connections and the main cause of this type of failure is fatigue cracking near the welding area. Figure 2.11 shows fillet-welded through plate socket connection detail. Due to a lack of available fatigue testing data, full-scale fatigue testing was performed for aluminum light pole structures to observe fatigue performance of their connections. Tests were performed for plate socket connections (unstiffened) and for shoe base socket

connections to determine lower bound fatigue resistance for infinite fatigue life design which is designated as Constant Amplitude Fatigue Threshold (CAFT). Full-scale fatigue test set up at the University of Akron structural lab is illustrated in Figure 2.12. In addition, a parametric study was also conducted to evaluate the nature of the local stress fields due to changing geometries.

Figure 2.12 Fatigue test set up at the University of Akron testing laboratory

(Courtesy of University of Akron)

The plate socket connection was tested with the stress range of 0.9 ksi up to 4.5 ksi and the lower bound was much lower than the AASHTO category E' which has CAFL of 1.0 ksi for aluminum structure. Fatigue cracks developed along the weld toe for all tested specimens but cracks also formed along the toe opposite the bolts for 80 percent of the time.

For the shoe base socket specimens, the fatigue test was performed with stress range from 3.6 ksi to 8.6 ksi. The presence of compressive residual stresses at the surface of shoe base detail is the primary reason behind shifting the fatigue data above AASHTO category E'. Most of the data fell above the category D. At failure, the developed fatigue crack was observed at the weld toe area. Crack initiation occurred at the farthest distance from the

neutral axis and then propagated through the thickness and along the weld toe. Experimental results showed that relatively low strengths for the through plate socket connection as compared to the shoe base details. The difference in strength between two details was a factor of 3.5.

In the parametric study, it was found that a 30 percent of reduction in the longitudinal stress on the tube surface by changing the base plate thickness from 1 inch to 2 inch. In terms of attaching gusset stiffeners, those are mainly used to reduce the longitudinal stress level by stiffening and stabilizing the tube wall against distortion. According to the AASHTO Specifications 2001, stiffeners were sorted into short, medium and long. However, the stress category at tip of the stiffener with long stiffeners was described as the worst with a Category E. Also, attaching short triangular plate stiffeners raised a level of longitudinal stresses at the top of the stiffeners on the tube.

Therefore, the author concluded that results from analytical study were inconsistent with AASHTO 2001 Specification fatigue categories for light pole structures. (Azzam, 2006). In addition, it should be noted that the specimens were made of aluminum therefore the test results were not included in a synthetic analysis of fatigue life.

Numerical Study of Stiffened Socket Connections for Highway Signs, Traffic Signals, and Luminaire Structures

This study by Azzam and Menzemer (2008) mainly focused on a numerical investigation on the effect of geometric parameters of aluminum structural supports. An analytical study was conducted to evaluate the impact of local stresses near the tip of the stiffeners and along the weld toe between the tube and base plate. The analytical study also

investigated the effect of the base plate thickness and gusset stiffener. In addition, a statistical analysis was performed for existing fatigue data. Testing results from the University of Texas at Austin (Koenigs et al., 2003), Valmont industries (Macchietto, 2001) and the University of Minnesota (Ocel et al., 2006) was collected and analyzed to establish a lower bound of fatigue resistance.

The results of the analytical study and the statistical analysis demonstrated an improvement of fatigue resistance for unstiffened socket connection compared to stiffened connection. Nearly constant local stresses were observed for the stiffener that reached 4 inch of height. In addition, the highest stress was observed for short stiffeners defined as category C in the fourth edition of AASHTO (AASHTO, 2001). This finding revealed the contradiction of the specification (AASHTO, 2001) which addresses a better fatigue resistance for the short stiffener where the height is less than 2 inch. The study also emphasized the importance of the validation of analytical results and enough fatigue testing data for analysis.

Signal Mast Arm Failure Investigation

After failures in several cantilever mast arm in Missouri, Chen et al. (2003) performed a failure investigation and their failure investigation report concluded that the main cause of failures is due to fatigue. A signal mast arm in Missouri is shown in Figure 2.13 and for this connection fillet welds are provided in both outside and inside.

a) Arm-to-post connection   b) Cross section of a mast arm and base plate
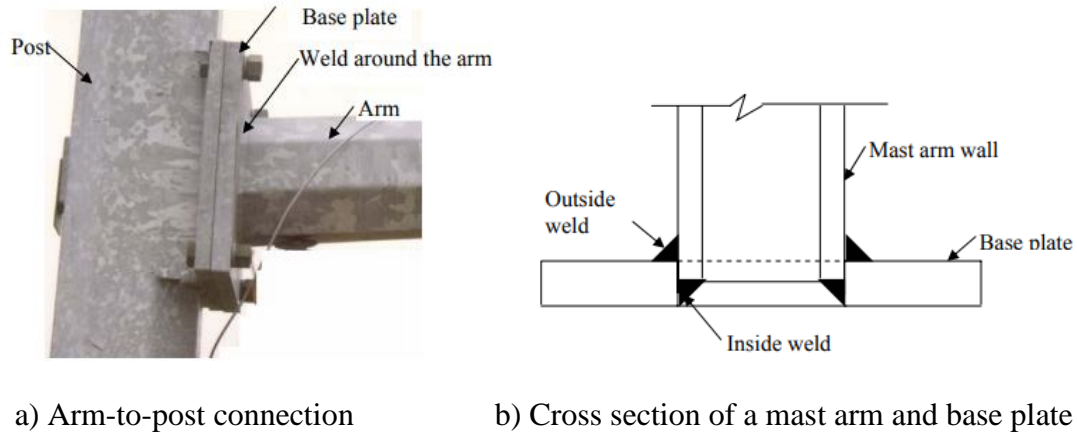
Figure 2.13 Signal Mast Arm in Missouri (Courtesy of Missouri DOT)

To evaluate the cause of as unexpected fatigue failure of the mast arm connection, a field level of study for the stress ranges, the number of cycles and the weld quality was carried out. A total of five specimens were tested in the lavatory and the failure mechanism and the weld quality were examined. According to the fatigue test results, fatigue crack initiation was observed on the outside weld at the weld toe. Differences in terms of fatigue resistance (number of cycle) were found among specimens which were manufactured by Valmont, JEM Inc. and Union Metals and this indicates that the fabrication error is significant factor in fatigue performance.

Failure investigation was performed through visual and metallographic examination and it was concluded that there was a poor quality of the welding such as lack of fusion and penetration. Therefore, the main cause of premature failure occurred due to the lack of fatigue resistance (i.e. poor weld quality). The calculated stress concentration factor was 2.63 at the weld toe of the arm-post connection and 2.88 at the corner of the octagonal section, respectively. These values of stress concentration indicate that there is a higher risk fatigue failure at the corner of the multisided tube.

Reliability-Based Fatigue Assessment of Mast-Arm Sign Support Structures

The motivation of this study by Diekfuss (2013) was the recent fatigue failure of mast-arm support in Wisconsin. The main objective of this work was to utilize the probability-based reliability fatigue assessment procedure to determine inspection protocols or intervals. Using a reliability-based approach to solve structural engineering problems requires a fundamental knowledge of the uncertainty associated with three variables: resistance, demand and modeling error.

The research work was focused on both fatigue wind load and resistance of the mast-arm connection and the study was divided into five main topics, 1) wind demand uncertainty, 2) fatigue life (resistance) uncertainty, 3) FE modeling, 4) modeling error uncertainty, 5) reliability-based inspection protocols.

Fatigue testing for both rounded and multisided (16 sided) socket connection with unequal leg fillet welded specimens on the outside and equal leg on the inside of the connection was conducted at two different testing locations: Marquette University (MU) and University of Wisconsin-Milwaukee (UWM). However, due to the unknown mean stress effect from UWM tests and the testing data from MU which has mean stress for a half time of stress range, testing results from the UWM tests were not considered for the synthetic test analysis of this study.

In addition, a synthesis of fatigue testing data analysis was performed to quantify fatigue life uncertainty. Existing fatigue testing results for the past three decades were collected. For a comprehensive data analysis, two approaches were proposed by utilizing 1) the new fatigue detail categories and 2) stress concentration factor. For the new fatigue detail category approach, all connection details were classified for the longitudinal

stiffness, tube type, welding type for a total of 12 categories. By utilizing equations for stress concentration factor (Roy et al, 2011), three proposed detail categories were introduced. For each proposed category, a least square regression analysis on log-log scale was performed to quantify the variance of fatigue coefficient, *A* which was determined from each test results with a given slope of *m*.

Fatigue Behavior of Steel Light Poles

This experimental study was performed by Fisher et al. (1981) to evaluate fatigue behavior of galvanized light poles fabricated to California Department of Transportation Standards. One half of twelve specimens has fillet welds with equal legs with A283 Grade D steel and the other half has fillet welds with unequal legs with A595 Grade A steel, respectively. It was observed that specimens with equal fillet weld legs showed a fatigue strength lower than category E' while unequal fillet weld legs specimen provides the same fatigue resistance as category E. The improvement of fatigue life for unequal leg specimens is due to a smoother stress transition from the mast wall through the weld to the connecting plate (Fisher et. al, 1981). For A283 Grade D steel, two additional specimens with unequal-leg fillet welds were fabricated and tested. The results showed an improvement in fatigue performance with unequal leg.

Fatigue cracks were observed at the toe of the welds at the base of the arm and at the base of the pole at approximately the same number of cycles. The authors emphasized that detecting cracks was a very difficult task due to galvanized coating and this might cause an inaccuracy in measuring the number of cycles at the stage of failure.

Fatigue Risks in the Connections of Sign Support Structure

Based on existing fatigue testing data and collected wind speed data, variability in fatigue life was mainly investigated by Foley et al. (2008). The term 'fatigue risks' represents a statistical fatigue analysis approach that estimates and predicts both wind load and resistance uncertainty. The variability in fatigue test data was tested by the Kolmogorov-Smirnov goodness fit and it was found that test results for stiffened connection of mast arms can be modeled using a normal cumulative distribution functions (CDFs) but a lognormal CDF was also suitable.

At low level of stress ranges, this study found that a fatigue sensitivity study for fatigue life is required because of a long-known trend that the variability in fatigue life increases as the stress level is decreased (Little and Jebe 1975). In addition, due to the long test duration at the low stress range, targeted mean interval was evaluated.

Another phase of their study included finite element analysis. In a single bi-directional bending moment condition, an increment of normal stresses (around 7 percent) in the mast-arm wall was observed due the loosening of bolts at base plate. Significant amplification of normal stress around the perimeter of the octagonal mast arm was induced by the flexibility of the base plate and the discrete load paths which is resulting from the arrangement of bolt connections.

Influence of base plate flexibility on the fatigue performance of welded socket connections

The main objective of this study by Hall and Conner (2008) was to evaluate the influence of base plate flexibility of welded socket connection which typically used in

cantilevered sign support structure. The effect of base plate flexibility on the stress distribution in the tube wall was extensively investigated experimentally and analytically. Figure 2.14 shows deflected shape of base plate and tube wall. A calibrated parametric study was conducted to evaluate the effect of base plate flexibility, anchor rod spacing and base plate side length. A method to quantitatively incorporate base plate flexibility into the infinite life nominal stress fatigue design approach in AASHTO was developed and proposed.
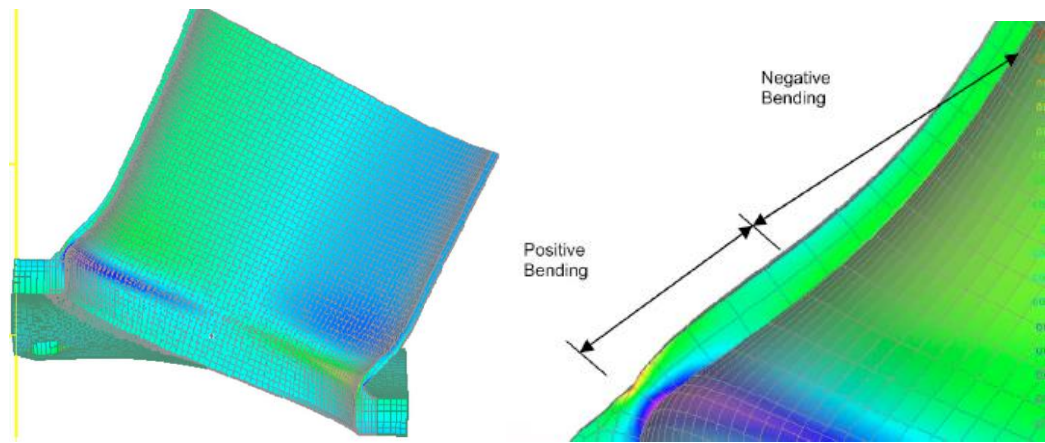
Figure 2.14 Deflected shape of base plate and tube wall (Hall and Connor, 2008)

The results has shown that base plate flexibility is a key parameter and has a significant impact on stress amplification in the tube wall. The authors addressed that increasing base plate thickness can be an effective way to improve the fatigue resistance of this detail. However, this conclusion raised the discussion in the light of cost-effective detail. In addition, the fourth edition of AAHSTO (AASHTO, 2001) does not provide specific guideline for the thickness of base plate for socket connection detail. The researchers pointed out that base plate thickness should be considered in fatigue design due to the effect on local weld toe stresses.

Parametric Study of Fatigue Light Pole Structures

Hosseini (2013) focused mainly on parametric study of fatigue light pole connection detail by utilizing a commercial FE software, ANSYS Workbench (ANSYS, 2012) – CFD (Computational Fluid Dynamics). The FE model was developed by following the dimensions from a manufacture, HAPCO and geometry of poles and mesh generated in ANSYS Mechanical is shown in Figure 2.15. To have a better understanding of the influence of geometric parameters on local stresses that determine the fatigue resistance. As the fatigue critical location, the hand-hole reinforcement width, hand-hole geometry and shoe base connection which can be sorted as stiffened socket connection for this work were investigated analytically.
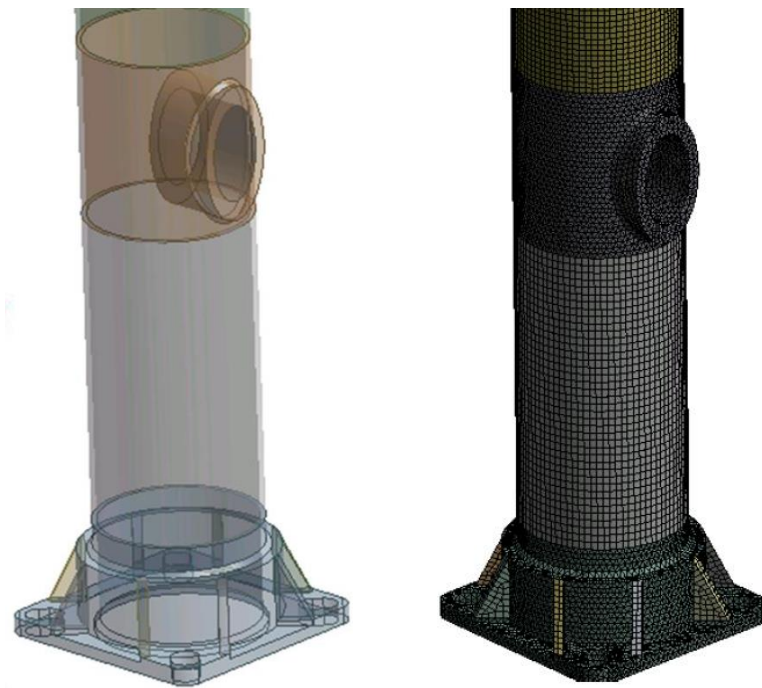
Figure 2.15 Geometry of poles and mesh generated in ANSYS Mechanical (Hosseini, 2013)

This study utilized the fatigue module in ANSYS Workbench. The fatigue output such as life, damage, safety factor was obtained by altering geometric parameters at fatigue

critical locations. In addition to this, fatigue sensitive study was performed for fatigue life with respect to load and tube thickness. The analytical investigation of this research work provided useful information regarding the effectiveness of the fatigue module for fatigue analysis in ANSYS Workbench.

The results indicates that light pole structures with tube thicknesses larger than 0.375 in are not susceptible to fatigue failure around shoe base connection. In addition, by increasing thicknesses of tube, the maximum stress around shoe base decreases. However, there is a need in the validation of FE model results by performing full scale fatigue testing.

Design of Highway Overhead Cantilever-Type Sign Support Structures for Fatigue Loads

As illustrated in Figure 2.16, fatigue failure occurred at the anchor bolts of a cantilevered support structure located at the I-565 and I-65 Interchange in Alabama in April 2006. Fatigue fracture was observed at anchor bolts due to combined and repeated axial and bending stresses. The bolt layout was designed according to an earlier version of the Specification (AASHTO, 2001) which did not consider fatigue design.

(a)   (b)

Figure 2.16 (a) Failure of cantilever sign support and (b) fractured anchor bolt (Ian, 2009)

A study of this fatigue failure by Ian (2009) emphasized that the fatigue design loads according to the fatigue provision of the 2009 edition do not adequately represent the wind-induced stresses since no updates were found from previous editions of the specifications (AASHTO, 2001). In addition, the provisions do not account for the variety of support structures in design, each with different configuration, sizes, shapes, and material properties that influence vibration behavior (Ian, 2009).

With measured stresses due to the wind-induced fatigue loading and CAFT from the specification, the failure index which is the ratio of the fatigue stress in the structure divided by the CAFT for the particular connection detail was proposed and then calculated. Fillet-welded tube-to-transverse plate connection and anchor bolt connection are shown in Figure 2.17. The largest strain was recorded at the anchor bolts followed by the post and chords and the stress range was defined as the peak-to-peak range from measured time history response. Except for the anchor bolts, the stress levels in the cantilever sign support structure were within the CAFT. The anchor bolts has the clearance length of 3 in showed much higher stress level.

(a)   (b)

Figure 2.17 (a) Fillet-welded tube-to-transverse plate connection and (b) anchor bolt

connection

Fatigue Testing and Failure Analysis of Aluminum Luminaire Support Structures

In 1996, the aluminum shoe base detail failures that occurred along route 147 in

New Jersey, where for 45 ft high poles. It was believed that during the night of the failure,

the poles experienced repeated stress ranges exceeding 12 ksi. Subsequent to the New

Jersey failures of aluminum light poles, an experimental and analytical study was

conducted to find out the main cause of failure (John and Dexter, 1998). It was concluded

that "fatigue strength of the shoe base socket connection detail was equal to Category E'

which has 2.6 ksi fatigue resistance limit. However, the data clearly indicated that all

failures occurred for the cases of the stress level above E' Category.

The purpose of the report was to determine the fatigue resistance of the socket

details for the NJDOT luminarie standards and also determine what caused the failure of

multiple luminarie supports on Route 147 in southern New Jersey. A total of twelve

luminaire support standards were tested to determine the fatigue resistance of the socket

joint at the pole to shoe base connection. Pull test were performed to observe the dynamic

characteristics such as stiffness, natural frequency and percent of critical damping of

NJDOT's luminaire standard. A finite element model was developed to validate the dynamic response measured from the pull tests. Figure 2.18 shows straight support standard positioned for pull test and actuator for fatigue test.

(a)   (b)
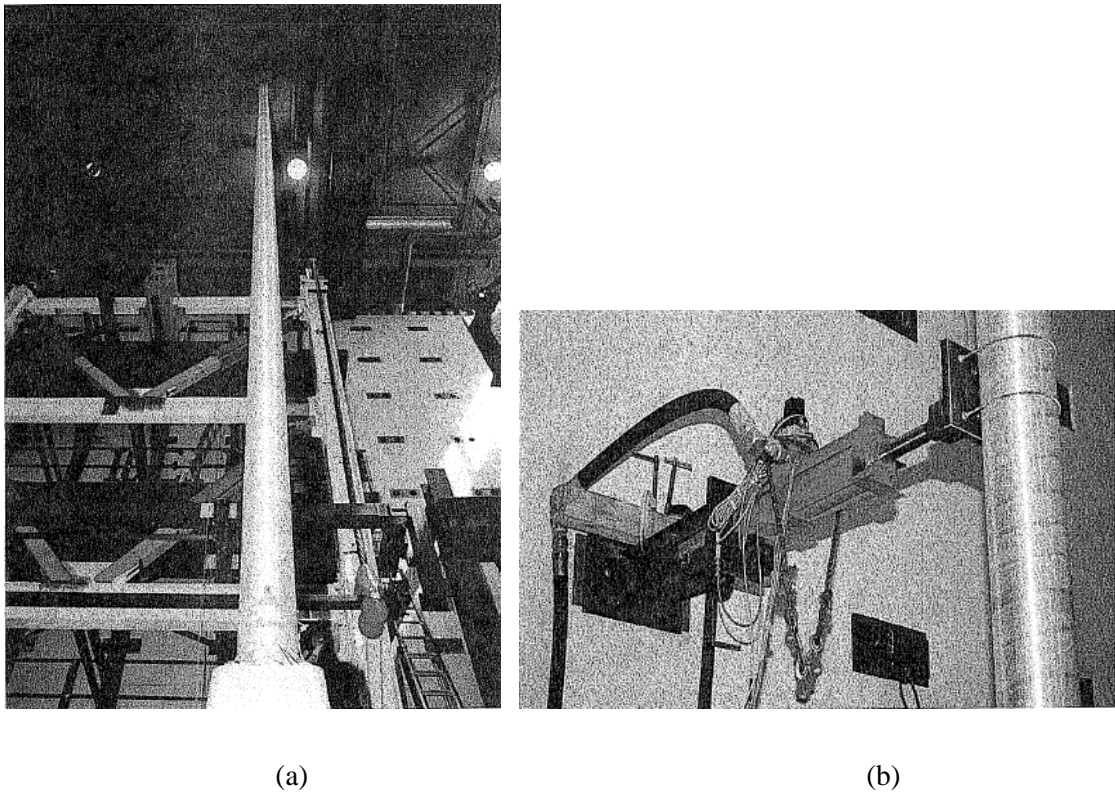
Figure 2.18 (a) Straight support standard positioned for pull test, and (b) Actuator for

fatigue test (Johns, K.W. and R. J. Dexter, 1998)

The following conclusions were drawn from the fatigue tests by Johns and Dexter (1998)*:*

- The fatigue strength of the shoe base detail was equal to AASHTO's fatigue category E.

- Fatigue cracks were observed in several transformer bases and most of fatigue cracks are caused by casting defects and notches in the base metal.

- The highest stress range was set to 12.2 ksi and fracture surface indicated that stress range for failure of Route 147 was higher than 12.2 ksi.

Recommendations for fatigue design were made for wind loads such as natural wind gusts, vortex shedding and shoe base-to-pole connections for fatigue resistance. The following improvements for the connection details were proposed,

- Bevel the inside top edge of the shoe base to reduce the shear stress on weld by having a larger welds leg along the pole.

- With the same reason above, use an unequal leg fillet on the top of the shoe base.

- Increase the geometric properties such as the pole diameters and/or thickness to reduce the bending stress by increasing stiffness.

- Use steel rather than aluminum.

Fatigue-Resistant Design of Cantilevered Signal, Sign, and Light Supports, NCHRP Report 412

NCHRP Report 412 was one of the most comprehensive studies with respect to fatigue loads and resistance prior to the fourth edition of AASHTO specifications. The results from the research performed Kaczinski (1998) were proposed for the modification of the fatigue provisions of the AASHTO specification. The wind induced loads such as galloping, vortex shedding, natural wind gust, and truck-induced wind gusts were determined as possible sources of large amplitude vibrations and those can be the main reason of fatigue failure.

The strengths of fatigue critical details (e.g. mast arm-to-column, column-to-base plate) were categorized according to the AASHTO fatigue design curve. It was noticed that

many fatigue sensitive connection details provided lower fatigue resistances compared to AASHTO category E'. In addition, fatigue performance of anchor bolt group was investigated by full-scale testing. A total of 47 specimens were tested and stresses at anchor bolt were accurately predicted from the flexure equation for bending stresses. According to testing results, the use of the CAFT for Category D was proposed for snug- and fully tightened axially loaded anchor bolts.

Based on an analysis of existing designs of cantilevered sign, signal, and luminaire support structures, the resulting applied stress range was on average 2.3 of times higher than the fatigue limits of the details. Therefore, the researcher recommendations were to: 1) increase the section modulus at the fatigue critical location by a factor of 2.3, 2) details within higher category must be chosen, and 3) adding stiffeners or gussets to improve fatigue resistance. The author also concluded that there remains a possibility that the proposed specifications may not be sufficiently conservative. With regards to existing support structures, the structure should remain resistant to excessive vibrations and fatigue cracking for a 25 year period or longer which represents the fatigue design for infinite fatigue life.

Fatigue Strength of Signal Mast Arm Connections

An experimental study of fatigue of full-size specimens to evaluate the fatigue strength of signal mast arm connections was conducted by Koenigs et al. (2003) at the University of Texas at Austin. A total fifty five full-size specimens was tested to evaluate fatigue performance of connection details. Fatigue resistance of fillet welded connection details were only considered for this work. As shown in Figure 2.19, unequal leg fillet weld

detail for socket connection with the long leg on the pole were based on the standard design that is used for the mast-arm. Unstiffened socket connections with unequal fillet welds showed fatigue resistance of Category E'.
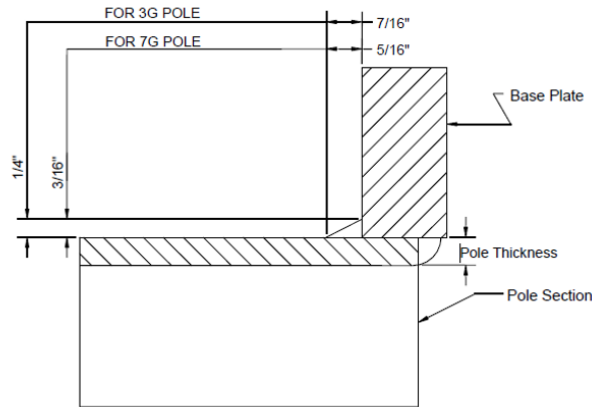
Figure 2.19 Fillet weld detail for socket connection

In the light of the fillet-welded socket connection with longitudinal stiffeners, it was observed that a longer stiffener provided a better fatigue behavior than a shorter stiffener at the same stress ranges. At least 3 long stiffener specimens are close to or above Category D detail and the longer stiffeners improved the fatigue resistance as compared to short stiffeners. This result appears to be inconsistent with the fatigue design provisions (AASHTO, 2001) as the fillet or partial penetration weld termination for short stiffeners are identified as category C, while long stiffeners are given a Category D or E (AASHTO, 2001). Also, the typical connections used in Texas for support structure did not meet the performance requirements from the specification.

Moreover, effect of base plate flexibility was determined as one of the most critical parameters that has a significant impact on fatigue performance. The use of 2 inch base plate thickness provides a substantial improvement of fatigue resistance as compared to 1.5 inch base plate thickness. By altering the number of stiffeners and pole thickness, no

significant impacts were observed.

The ultrasonic impact weld treatment enhanced the fatigue life of fillet-welded socket connection detail significantly. The fatigue testing data for fillet-welded socket connection details was collected for the synthetic data analysis and findings and conclusions take into account of the synthetic fatigue data analysis in chapter 3 for this dissertation.

Valmont Fatigue Testing Fatigue Testing Presentation

After the fourth edition of specification (AASHTO, 2001) was released, Valmont Industries performed fatigue testing to validate the fatigue resistance of unstiffened and stiffened socket connections using unequal leg fillet welds. Their research results were presented at AASHTO committee meetings (Machietto, 2002).

Socket connection specimens without stiffeners had similar details to that of Detail #16 in the 2001 AASHTO specifications having fatigue category of E'. However, inconsistencies with 2001 AASHTO specification were found from the test results where unstiffened fillet welded sockets showed a better fatigue resistance than category E. In addition, with respect to comparing unstiffened and stiffened specimen, results have shown that the fatigue resistance of the socket connection without stiffeners was significantly greater than the stiffened detail. This indicates that there was no significant contribution of the stiffeners which failed to reduce the level of stress at weld toe at base plate. The fatigue test results from this study were included for the fatigue data analysis proposed in this dissertation.

Fatigue-Resistant Design for Overhead Signs, Mast-Arm Signal Poles, and Lighting Standards

Ocel et al. (2006) tested full-scale 8-sided polygonal tube-to-transverse plate connection detail with varying tube diameters, tube thickness and base plate thickness at the University of Minnesota. The results have shown that multi-sided connection provided fatigue resistance of category K_2 and this is below the fatigue limit specified in 4th edition of AASHTO specification. An improvement of the fatigue performance to Category E' were made through treatment, hammer peening. As compared to 1.25 inch think specimen, 3 inch of base plate thickness specimen reached category E Category and this results indicate that the flexibility of the base plate has a significant effects on fatigue resistance of fillet weld connection detail.

With respect to the multi-sided tube-to-transverse connections with gusset plate stiffeners, the test results have shown that the gusset plates could not prevent the fatigue crack at the corners of the tube and at the toe of the socket weld. This result indicates that in terms of reducing stress concentration at critical locations, there was a no significant contribution by adding gusset stiffener. In addition, the failure at the corner of tube is due to the nature of multi-sided tube shape.

During the testing, cycling was paused once cracks were observed in the socket weld and then hammer peening was applied at the cracked weld toes with the dead load. By applying hammer peening, compressive residual stresses that resists fatigue crack growth and cycling loads were able to continue until the gusset plates cracked. The test results revealed that the socket weld plots between category E_T and E' with the 97.5 percent of survivability line as compared to category K_2 for the unstiffened pole socket connections.

The fatigue resistance of tips of the gusset showed a lower bound resistance below category D.

Fatigue Testing of Galvanized and Ungalvanized Socket Connections

To address the premature failure caused by cracking in the zinc metal bath during galvanizing, Ocel (2014) conducted fatigue testing of the unstiffened fillet welded socket connection to evaluate the influence of galvanization and fabrication error on the fatigue resistance. Specimens were fabricated from two different manufactures and test results has shown that workmanship greatly affects in fatigue performance of socket connection. One fatigue category reduction was found in galvanized specimen with a constant fatigue stress range as compared to ungalvanized specimen. Galvanized specimens showed a fatigue resistance less than category E' and this represents the contradiction with the 6th edition of AASHTO (AASHTO, 2009).

In terms of determining failure, the research team at the University of Texas at Austin proposed a ten percent of reduction in stiffness. However, a 12-inch-long crack around the perimeter of the tube was defined as the failure. The measured crack length and area from testing were recorded and illustrated in the report. With respect to fatigue testing data analysis, the authors believe that difference in failure definition should be taken into account. An error term was introduced in their statistical regression analysis. It was believed that the remaining life was small in comparison to the cycles to reach failure.

A plastic cracked section analysis was performed to assess the remaining moment capacity of tubes after cracking. Enough resistance for the fracture toughness of the plate material was observed under 12 inch long cracks at temperatures to -30 °F. It is believed

that there will be a future study to estimate and predict the remaining fatigue life of existing structure which already reached or above a yielding strength.

Effect of Galvanization on the Fatigue Strength of High Mast Illumination Pole

A thesis by Pool (2010) focused on determining the influence of galvanizing on the fatigue life of High Mast Illumination Pole (HMIP) in Texas. Their details are shown in Figure 2.20. Experimental work including destructive test was performed to compare fatigue performance of both multi-sided ungalvanized and galvanized connection details. The crack formed at the toe of the welding during the galvanization process was observed and the effects of initial cracks on fatigue performance were evaluated through experimental investigation.

Figure 2.20 High Mast Illumination Poles (HMIP) in Texas (Pool, 2010)

In the light of fatigue testing results, galvanized specimen provided a lower fatigue resistance as compared to ungalvanized pole. This is the same conclusion from the synthetic data analysis results for this dissertation which addressed in Chapter 3. It was also concluded that having external collar increase the fatigue life of the specimen.

However, the conclusion cannot be drawn for the specimens from two different fabricators and galvanizer due to the limitation in number of specimens. Also, this study did not include the effect of the fatigue resistance under the corrosive environments as well as analysis of material properties of the connection details.

NCHRP Project 10-70: Cost-effective Connection Details for Highway Sign, Luminarie, and Traffic Signal Structures

A comprehensive experimental and analytical study was performed to evaluate the fatigue performance of connection details for structural supports at Lehigh University under NCHRP project 10-70. Results from this study was recommended and then adopted to the new AASHTO specification (AASHTO, 2015).

To determine new cost-effective connection details in the light of fatigue resistance, fatigue testing program was developed for infinite life fatigue life. Approximately, eighty full size galvanized specimens for different welded connections such as groove-weld and fillet-weld were prepared for fatigue testing. In addition to experimental investigations, 3D Finite Element Model (FEM) was developed and also validated for both finite and infinite life regimes. For the range of applicable geometric dimensions, empirical equations for fatigue stress, and stress concentration factor were also proposed (Roy, 2012). Figure 2.21 shows Fatigue cracking of the pole-to-transverse plate at fillet welded toe on the tube wall and fatigue cracking from the stiffener to tube weld toe.
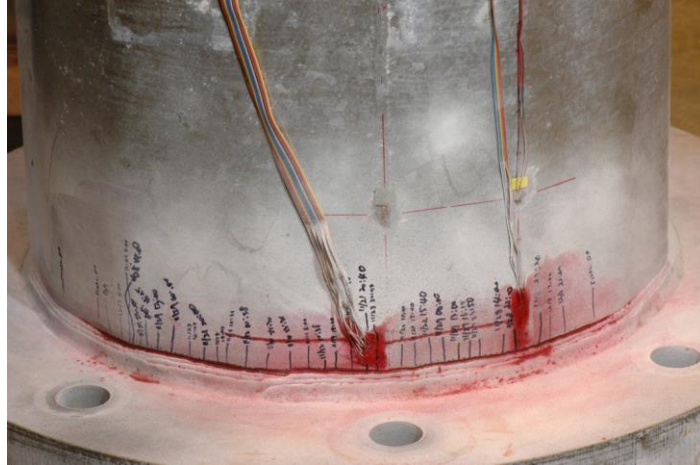
(a)
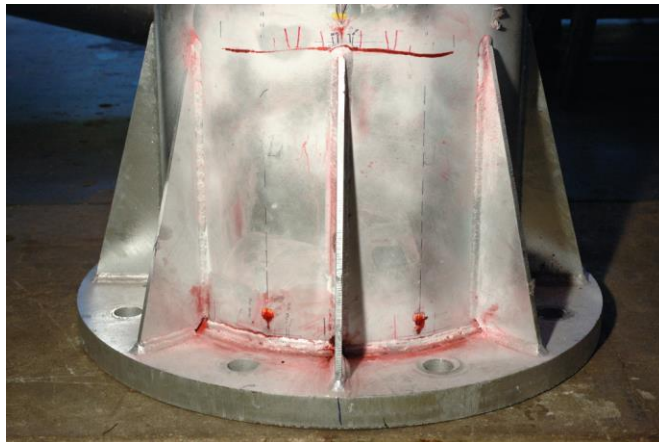
(b)

Figure 2.21 (a) Fatigue cracking of the pole-to-transverse plate at fillet welded toe on the tube wall and (b) Fatigue cracking from the stiffener to tube weld toe

This study demonstrated that fillet-welded tube-to-transverse plate connections are the most fatigue critical connection details. To enhance the fatigue resistance, increasing the stiffness of the transverse plate was recommended as the most cost-effective manner. Stiffeners in fillet-welded connection was initially developed to achieve a lower stress level at the fillet weld toe at the base by decreasing out-of-plane distortion at the pole wall (Roy

et al. 2009). However, a large stiffener thickness relative to the tube wall increases distortion of the tube and the potential for fatigue cracking at the stiffener terminus and the termination at the tip of stiffeners became more critical potential fatigue crack location (AASHTO 2015).

As a results of both experimental and numerical investigations, optimized stiffened tube-to-transverse plate fillet-welded connections was introduced as a cost-effective design which includes longitudinal stiffener and a ratio of stiffener thickness to tube thickness of 1.25, a ratio of stiffener height to stiffener spacing of 1.6 and a stiffener termination angle of 15 degree. An adequately designed and optimized stiffened tube-to-transverse plate fillet-welded connection provides a CAFT of 48.3 MPa (7.0 ksi) which is AASHTO Category D while the prior specification (AASHTO, 2001; AASHTO, 2009) defines the CAFT of this connection as 17.9 MPa (2.6 ksi) (Category E´).

With respect to multi-sided tube-to-transverse plate connections, the fatigue cracking initiates at the bend corners due to higher stress concentration. With fewer sides and sharper bend corners, the stress concentration increases resulting reducing fatigue resistance of the connections. It was suggested that a minimum of eight sides and 1 in (25 mm) bend radius should be used for multi-sided tubular structures.

Fatigue Life of Steel Base Plate to Pole Connections for Traffic Structures

This study was a pooled-funded project administered by the Texas Department of Transportation (Stam, 2011). This report is a final report that includes an extensive experimental and analytical examination of the fatigue behavior of the welded end connections for high-mast light structures and traffic signal masts. The main purpose of

this study was to develop the cost-effective connections that enhance fatigue resistance. The fatigue testing set-up was the also followed from the early study (Koenigs, 2003) and the socket connection and full penetration weld specimens are shown in Figure 2.22.
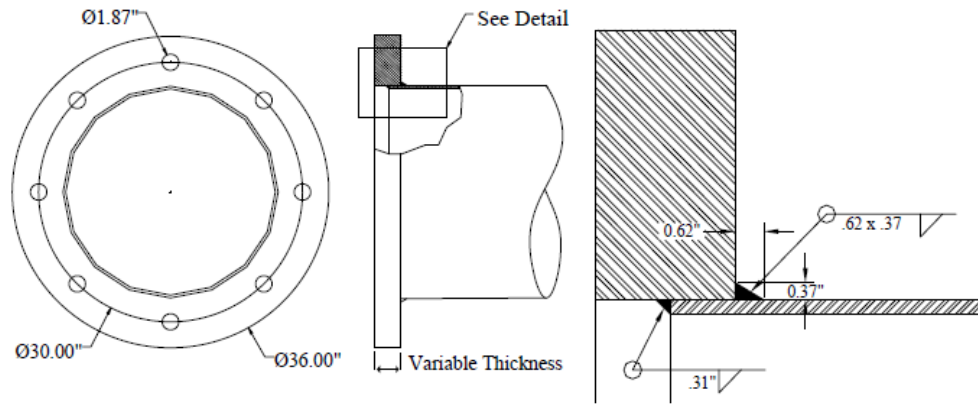
(a)
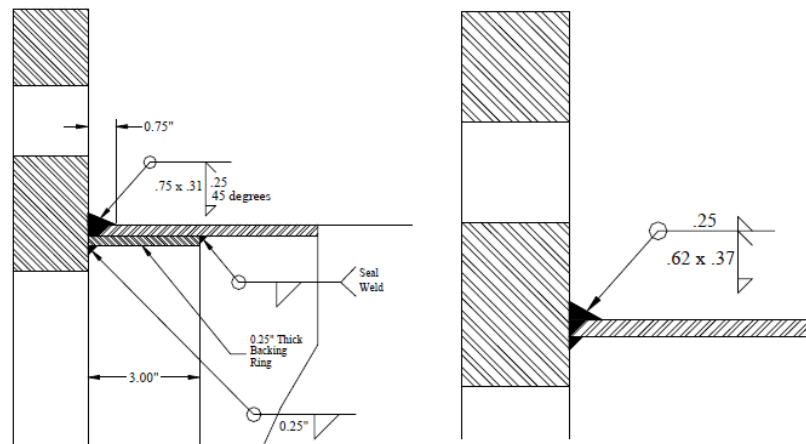
(b)

Figure 2.22 (a) Socket Connection and (b) Full Penetration weld for Wyoming (left) and Texas (right) (Stam, 2011)

According to the fatigue testing and analytic study results, it was stated that the influence of the geometry for the connection details with respect to fatigue performance cannot be accounted by the fatigue category approach in AASHTO specification

(AASHTO, 2001) because the same connection details with a different base plate thickness can produce a range of fatigue life (i.e. from Category B to E).

Reductions in fatigue strength due to the galvanizing was not observed in this study. The weld toe crack during galvanization process was investigated and it was found that initially formed the crack reduced fatigue strength. Also, using unequal welding leg, increasing base plate thickness, number of anchor bolts greatly affect fatigue resistance. Larger diameter or thicker poles requires thicker base plate to obtain the same level of fatigue strength. Recommendations for design, fabrication, and welding specification were addressed for fatigue resistance.

Evaluation of High-Level Lighting Poles Subjected to Fatigue Load

A thesis by Thompson (2012) at Lehigh University was completed as the part of the study under NCHRP project 10-70. More details regarding specimen description, fatigue testing and results were addressed.
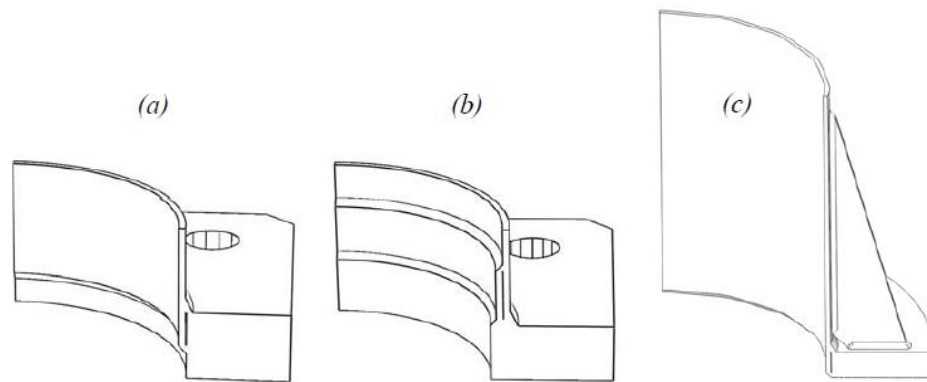
Figure 2.23 (a) Tube-to-base plate fillet-weld connection, (b) full penetration weld connection, and (c) stiffened fillet weld connection (Tompson, 2012)

Both fillet-welded and groove-welded connection details were experimentally

investigated and tube-to-base plate connections is shown in Figure 2.23. Additional study for retrofits using jacket was also performed and described. FE model validation in Chapter 4 of this dissertation was conducted by utilizing the strain gauge measurements from this study.

The fatigue testing were conducted at multiple stress range level to determine fatigue resistance for both finite and infinite region. During the test, fatigue crack location as well as propagation was observed and also recorded to evaluate fatigue crack prediction model and also to perform the post-mortem fracto-graphic study.

Fatigue testing results indicated that with a given geometry detail, the fatigue design limit of the stiffened fillet-welded connection for infinite fatigue life was determined as 7 ksi (48 MPa). The geometry used in the testing is defined as an optimized stiffened fillet-welded connection details (Roy et al., 2012). Fatigue cracking was observed at both the stiffener termination on the pole and at the fillet weld toe on the pole but the first fatigue crack was found at the tip of stiffeners due to the higher local stress. Figure 2.24 illustrates fatigue cracking for stiffened fillet-weld connection for first crack at weld toe and final crack at termination of fatigue testing. The finite life fatigue resistance was defined as Category E´. CAFT of unstiffened fillet-welded connection with a provided geometry was reached to 4.5 (31 MPa) as AASHTO Category E detail. Fatigue testing results for retrofit jacket was reached to 10 ksi (69 MPa) for infinite life fatigue resistance.

(a) (b)
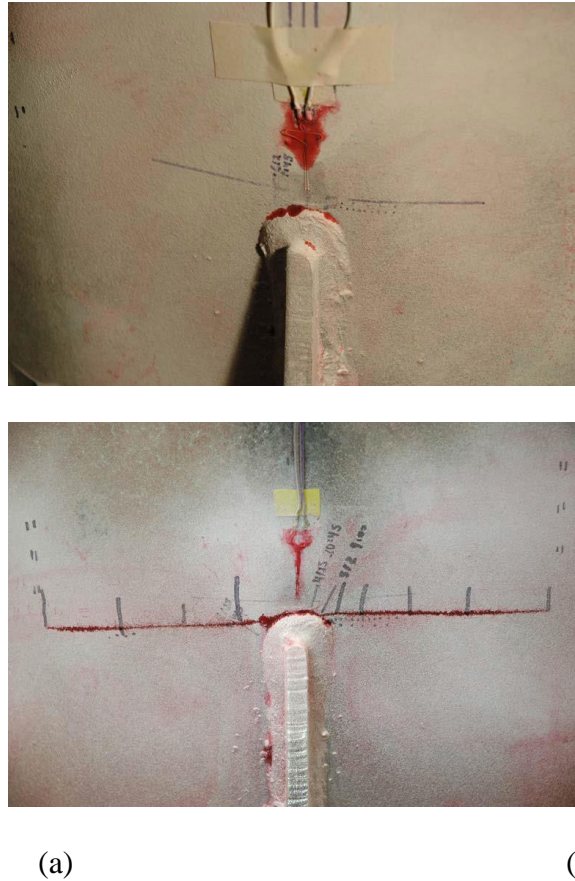
Figure 2.24 Fatigue cracking for stiffened fillet-weld connection (a) First crack at weld toe, (b) Final crack at termination of fatigue testing

This study was also noted that with respect to the scatter from the fatigue testing, this study addressed that it is mainly due to the inherent variability in macro- and micro-discontinuities at the weld toe. The variability in the weld toe angle from different manufactures or fabricators produced exceeding scatters in test results.

2.5 An overview of Fatigue Module in ANSYS Workbench

In this subchapter, an overview of fatigue module in ANSYS Workbench will be presented. In FE programs, a fatigue analysis is performed based on linear static analysis and fatigue calculations that supports only solid and surface bodies. To perform stress-life analysis, the fatigue module requires an S-N curve (Stress range – number of cycle) as an input material properties of the Engineering Data which can be obtained from fatigue testing results. In Workbench fatigue platform, the fatigue stress term is referred to as the 'alternating stresses or also called 'stress amplitude' (Raymond and Al, 2006).

The initial step of stress-life fatigue analysis in ANSYS requires the analysis type to be determined for stress-life and strain-life. Stress-life is based on the S-N curves and has traditionally dealt with high numbers of cycles, High Cycle Fatigue (HCF) which is typically greater than 10^5 cycles. In the fatigue provision of the current LRFD AASHTO-LTS specification (AASHTO, 2015), stress life analysis is used as a fatigue analysis method since more than 25 years of service life is anticipated for support structure.

For Low Cycle Fatigue (LCF) which refers to fewer than 10^5 cycles, the stain life approach can be used. This approach is typically utilized when strain can be directly measured from testing. While stress life takes into account the total number of cycles, strain life focuses on crack initiation and propagation. Lastly, the fracture mechanics approach is also used as an alternative fatigue analysis method. The fracture mechanics approach main focus is on fatigue crack growth referred to as crack life.

2.5.1 Fatigue Module

Determine fatigue analysis type – stress-life and strain-life

As discussed above, determining fatigue analysis type such as stress-life and strain-life is an initial step for fatigue analysis in ANSYS Workbench 17.1. In this process, the number of cycles is the key factor that determines fatigue analysis type. Stress-life is based on traditional S-N curves considering no plasticity while strain-life is based upon the strain life relationship by modeling material's yielding and plasticity. Stress-life is commonly used for high cycle fatigue and strain-life is appropriate for low cycle fatigue.

Fatigue loadings

Unlike static loading state, repeated cyclic loading over time is defined as fatigue loading. As discussed in Chapter 2.2, there are four types of fatigue loadings. ANSYS performs fatigue calculations for either constant amplitude loading or proportional non-constant amplitude loading. Common types of constant amplitude loading are fully reversed where a load ratio, R, is equal to -1 for an equal and opposite load and zero-based where the load ratio is set to zero. Fully reversed, zero-based, or a specified loading ratio can be defined in ANSYS's details view under the "Loading" section.

For the case of non-constant amplitude loading, the load ratio varies over time therefore use of a single load ratio to calculate the alternating and mean stress is not applicable. Cumulative damage calculations including cycle counting technique are required in the analysis process. In the Workbench platform, a Rainflow cycle counting method can be utilized to identify stress reversals. Recorded stress history data can be imported in the program as an input data. Figure 2.25 shows constant amplitude loading with an R ratio of -1 and a non-constant amplitude loading in ANSYS Workbench.

Constant Amplitude Load
Fully Reversed

Non-Constant Amplitude Load
History Data
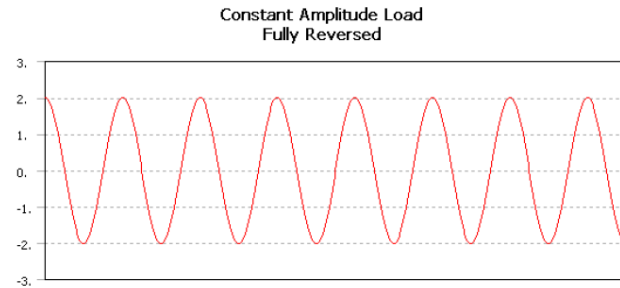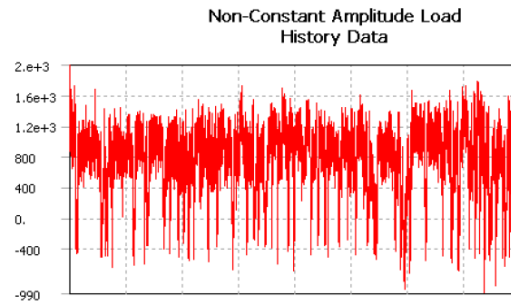
(a)   (b)

Figure 2.25 (a) Typical fully reversed constant amplitude loading, and (b) non-constant

amplitude loading for history data

In ANSYS Workbench fatigue module, the first three loading types of the following

loading types are available as input fatigue loading:

1) Constant amplitude, proportional loading

2) Constant amplitude, non-proportional loading

3) Non-constant amplitude, proportional loading

4) Non-constant amplitude, non-proportional loading

Mean Stress Correction

In light of stress-life analysis in the Workbench platform, the mean stress correction

is provided in the case where experimental data does not exist. Empirical options can be

chosen such as Gerber, Goodman and Soderberg theories and these methods utilizes static

material properties such as the yield stress and tensile strength. Figure 2.26 shows mean stress correction plots for Gerber, Goodman and Soderberg theories ANSYS Workbench and corresponding equations are in Table 2.2 in Chapter 2.2.3.

(a)   (b)

(c)
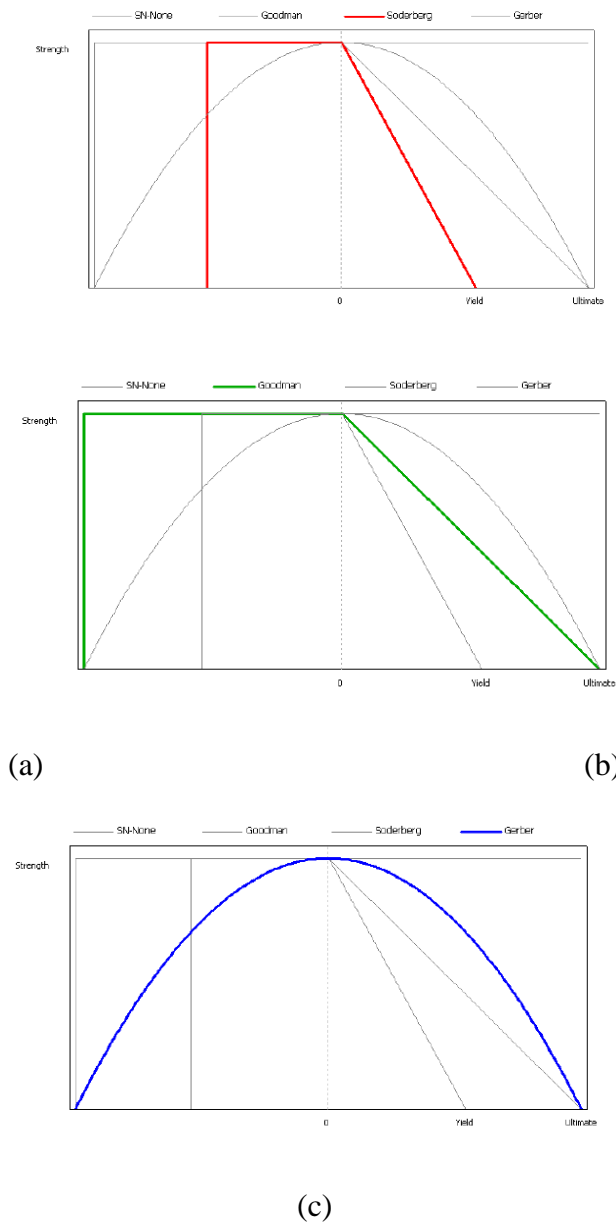
Figure 2.26 Mean stress correction plots for (a) Gerber, (b) Goodman and (c) Soderberg theories

Within the ANSYS Workbench fatigue module, the negative mean stress is

neglected for the alternating stress. Although the Goodman and Soderberg methods are conservative, empirically ignoring a negative mean stress is typically more conservative. This is because a compressive mean stress can retard fatigue crack growth. In the case of having negligible mean stress effect, the fatigue module platform also provides no mean stress option. Additional method for mean stress correction is the use of the mean stress curves from empirical data.

Fatigue Modification Factor

1) Infinite Fatigue Life

In ANSYS Workbench fatigue module, the user can define the infinite fatigue life value and it can be set a range from 10^6 cycles to 10^9 cycles. In the case of constant amplitude loading, the fatigue module will use the life at the last point on S-N curve if the alternating stress is lower than the lowest alternating stress.

2) Fatigue Strength Factor

The fatigue alternating stress is usually divided by fatigue strength factor that can be found in design handbooks. As defined, fatigue Strength Factor or K_f reduces the fatigue strength and this should be less than one. This factor can be used when the conditions are different from testing condition and does not affect the mean stress.

3) Loading Scale Factor

The loading scale factor will scale alternating and mean stresses by user specified value. This factor can be useful when the static model is analyzed to investigate the effects

of changing the magnitude of the FEM loads and converting a non-constant amplitude load history data into the appropriate values.

4) *Stress Life Interpolation*

The stress life analysis performed in Workbench requires the tabular S-N curve as one of the input parameters. The interpolation of S-N curve is performed to obtain an appropriate fatigue output value. Three different interpolation methods can be utilized such as log-log, semi-log and linear and analysis results will be varied by use of each method.

2.5.2 Results from Fatigue Module

Depending on the fatigue analysis types (stress-life or strain-life), fatigue analysis outputs can range from contour plots of a specific result over the whole model to information about the most critical or damaged location in the model. Results that are common to both types of fatigue analyses are listed below and details of fatigue analysis outputs are discussed.

- Fatigue life
- Fatigue damage at a specified design life
- Fatigue factor of safety at a specified design life
- Stress biaxiality
- Fatigue sensitivity chart
- Rainflow matrix output (Beta for Strain Life at 10.0)
- Damage matrix output (Beta for Strain Life at 10.0)

1) Fatigue Life

The fatigue life is defined as the available life for the given information based on fatigue analysis. The fatigue life contour plot of the FE model shows the available life. For constant amplitude loading, the fatigue life represents the number of cycles until the part will fail due to fatigue (Raymond and Al, 2006). The fatigue module determines cycles to failure from the S-N curve input data and a selected mean stress correction theory. If the loading is non-constant, this output represents the number of loading blocks cycles until failure. For example, if the given load history represents one hour of loading and the life was found to be 24,000, the expected model life would be 1,000 days.

2) Fatigue Damage

The fatigue damage is a contour plot of the fatigue damage at a given design life (Raymond and Al, 2006). As described in equation 2.16, the term 'fatigue damage' is determined as the design life divided by the available life. This result may be scoped and the default design life may be set through the control panel. If the fatigue damage values is greater than 1, it indicates the failure was reached before the design life is reached. Determining accurate fatigue design life from existing fatigue data analysis is the major tasks for this study.

$$Fatigue\ Damage = \frac{Design\ Life}{Available\ Life} \qquad (2.16)$$

3) Fatigue Safety Factor

The fatigue safety factor is another contour plot that is provided by fatigue module in Workbench. This output represents the factor of safety with respect to a fatigue failure

at a given design life (Raymond and Al, 2006). The maximum factor of safety displayed is 15. If output values are less than one, this indicates failure before the design life is reached. The fatigue design life value is the critical factor to enhance the accuracy of the Fatigue Safety Factor.

4) Biaxiality Indication

Fatigue material properties such as yield and ultimate strength are based on uniaxial stresses state. However, in field-level of structural response, multiaxial stress states typically occur. A value of zero for biaxiality indicates uniaxial stress states, a value of -1 corresponds to pure shear, and a value of 1 corresponds to a pure biaxial state, respectively (Raymond and Al, 2006).. In the case of non-proportional fatigue loading, multiple stress states can be found over the body and Workbench provides the average or standard deviation of stress biaxiality.

5) Fatigue Sensitivity

The fatigue sensitivity plot represents how the fatigue results change as a function of the loading at the critical location in the model. This plot can be constructed for fatigue outputs such as life, damage, or factor of safety. Linear, Log-X, Log-Y, or Log-Log scaling options can be chosen for chart display. Default values for the sensitivity study can be determined by the user through control Panel.

6) Rainflow and Damage Matrix Chart (Beta for Strain Life at 10.0)

The Rainflow matrix chart is a plot of the Rainflow matrix at the fatigue critical location. This result is only applicable for non-constant amplitude loading where Rainflow counting is required. In this 3-D histogram, the alternating stress and the mean stress are divided into bins and the size of bin should be determined for plotting. The z-axis represents the number of counts for a given alternating and mean stress bin. Under non-constant amplitude loading, this output provides a measure of the composition of a loading history (Raymond and Al, 2006).

Damage Matrix Chart is a plot of the damage matrix at the critical location in the model. For the three dimensional plot, the z-axis represents the percent damage that each of the Rainflow bin causes.

CHAPTER III

SYNTHETIC FATIGUE DATA ANALYSIS

In this chapter, synthetic fatigue data analysis using existing experimental data will be discussed to evaluate fatigue resistance of both unstiffened and stiffened fillet-welded connections. Analysis results will be utilized as an input parameters of fatigue module in ANSYS Workbench and also the results used to evaluate a modified SWT fatigue corrosion model. The fatigue test data were grouped based on those parameters that significantly affect fatigue resistance or has different material treatment types. A statistical analysis was then performed to establish the Constant Amplitude Fatigue Threshold (CAFT) that achieves infinite fatigue life. Details of the analysis are addressed in the following sections.

3.1 Fillet-welded Connection Details in AASHTO Specifications

Unstiffened fillet-welded tube-to-transverse connection detail

In Table 11-2 of the AASHTO specification, the unstiffened fillet-welded tube-to-transverse connection detail or called fillet-welded socket connection is introduced in Detail 16 with stress category of E' which has a Constant Amplitude Fatigue Limit (CAFL) of 2.6 ksi. The application of this detail can be column-to-base-plate or mast-arm-to-flange-plate socket connections. The fillet-welded socket connection is illustrated in Figure 3.1.
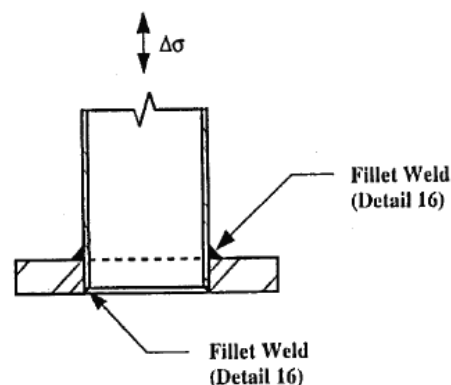
Fillet-Welded Socket Connection

Figure 3.1 Fillet-welded socket connection detail (AASHTO, 2001)

In Table 11.9.3-1 of AASHTO 2015, the fillet-welded tube-to-transverse plate connection or called socket connection is addressed in section 5.4 and it is shown in Figure 3.2. This connection is typically used for column-to-base-plate or mast-arm-to-flange socket connection and the potential fatigue crack location is defined in tube all along fillet-weld toe.

It is also observed that stress category no longer exists to determine CAFT. Fatigue stress concentration factors (SCF's) for both infinite and finite fatigue life are terms that are required for finite fatigue life constant and CAFT. Based on SCF for infinite life, three CAFTs are provided as 7.0 ksi, 4.5 ksi and 2.6 ksi, respectively. Although the stress category is not provided, the CAFT values are the same as Category D for 7 ksi, Category E for 4.5 ksi and Category E' for 2.6 ksi. As compared to the fourth edition of specification (AASHTO, 2001), stress category of E' which has CAFL of 2.6 ksi was the only fatigue limit that is provided for this socket connection detail.
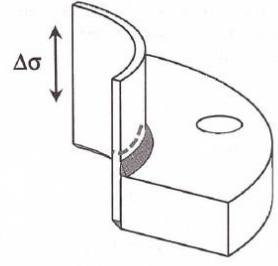
| 5.4 Fillet-welded tube-to-transverse plate connections | $K_F \leq 3.2$: 3.9 | $K_I \leq 4.0$: 7.0 $4.0 < K_I \leq 6.5$: 4.5 $6.5 < K_I \leq 7.7$: 2.6 | In tube wall along fillet-weld toe. | Column-to-base-plate or mast-arm-to-flange-plate socket connections. $\Delta\sigma$ |

Figure 3.2 Fillet-welded tube-to-transverse plate connections (AASHTO, 2015)

According to the laboratory test results for fillet-welded tube-to-transverse plate connection, finite fatigue life constant and CAFT values are provided for given geometric parameters and it is shown in Figure 3.3. Different CAFT's and fatigue SCF's are observed depending upon tube configuration and geometric parameters.
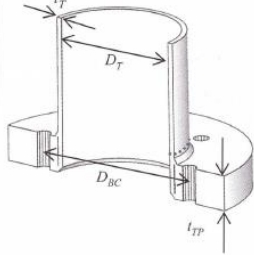
Description	Identification of Parameters	Tube Configuration	Detail Parameters	Finite Life Constant, $A \times 10^8$ ksi³	Threshold, ΔF_{TH} ksi
Fillet-welded tube-to-transverse plate connections		Round	$t_T = 0.179$ in. $D_T = 10$ in. $t_{TP} = 2$ in. $D_{BC} = 23.3$ in. $N_B = 4$	3.9 ($K_F = 2.8$)	4.5 ($K_I = 5.6$)
		Round	$t_T = 0.239$ in. $D_T = 13$ in. $t_{TP} = 2$ in. $D_{BC} = 20$ in. $N_B = 4$	3.9 $K_F = 2.9$	4.5 ($K_I = 6.2$)
		Multisided	$t_T = 3/16$ in. $D_T = 10$ in. $t_{TP} = 2$ in. $D_{BC} = 23.3$ in. $N_B = 4$ $N_S = 8$ $r_b = 0.5$ in.	3.9 ($K_F = 3.2$)	2.6 ($K_I = 6.6$)
		Multisided	$t_T = 1/4$ in. $D_T = 13$ in. $t_{TP} = 2$ in. $D_{BC} = 20$ in. $N_B = 4$ $N_S = 8$ $r_b = 0.5$ in	($K_F = 3.5$)	2.6 ($K_I = 7.6$)
		Multisided	$t_T = 5/16$ in. $D_T = 24$ in. $t_{TP} = 3$ in. $D_{BC} = 30$ in. $N_B = 16$ $N_S = 16$ $r_b = 4$ in.	3.9 ($K_F = 2.9$)	4.5 ($K_I = 6.5$)

Figure 3.3 Laboratory test results for fillet-welded tube-to-transverse plate connection (AASHTO, 2015)

Stiffened fillet-welded tube-to-transverse connection detail

Figure 3.4 shows the stiffened fillet-welded tube-to-transverse connection detail in the AASHTO specification. The fillet-welded tube-to-transverse connection detail with longitudinal attachments is introduced in detail 20 and stress categories varies from fatigue stress Category C to E based on the height and thickness of stiffener. Weld termination at the tip of longitudinal stiffener is determined as a fatigue critical location. However, inconsistency were found with fatigue testing results (Koenigs et.al, 2003) for the fatigue design provision of the 2001 specification and geometric factors such as base plate thickness and termination angle were not considered in determining CAFL for infinite fatigue life design.
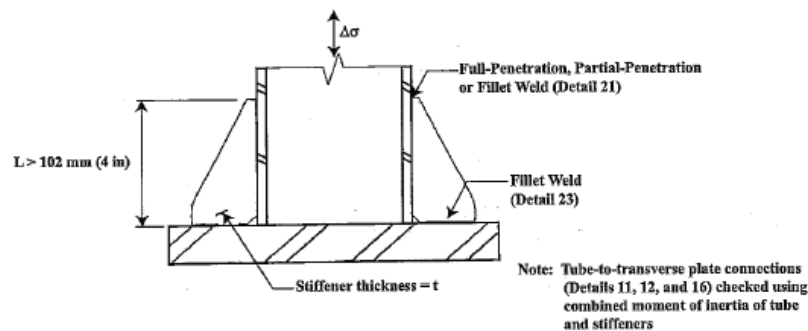
Figure 3.4 Stiffened fillet-welded tube-to-transverse connection detail (AASHTO, 2001)

Stiffened fillet-welded tube-to-transverse plate connection detail is addressed in both fatigue detail 6.2 and 6.3 of Table 11.9.3.1-1 as illustrated in Figure 3.5. In this fatigue provision, two sections were classified by considering potential crack locations. In a fatigue detail 6.2, fatigue-sensitive location is determined as in tube wall at toe of the stiffener and in the tube wall at the toe of tube-to-transverse plate weld. With respect to the design limit for infinite fatigue life, the CAFT for this detail is 7.0 ksi which is same as category D in

the prior specification. This threshold is only applicable when the stress concentration factor, K_I is less than 5.5 and this condition was proposed because the SCF affects the fatigue life and fatigue resistance of connections details depends on the relative stiffness of structural members at a connection (Thompson 2012). For fatigue detail 6.3, the CAFT is 10 ksi with a potential fatigue crack location in the base metal at the weld toe or through weld throat.
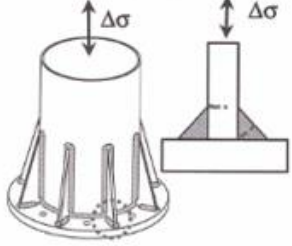
6.2 Tube-to-transverse plate connections stiffened by longitudinal attachments with partial- or full penetration groove-welds, or fillet-welds in which the tube is subjected to longitudinal loading and the welds are wrapped around the attachment termination.	$K_F \leq 2.5$: 11.0 (See detail 5.4)	$K_I \leq 5.5$: 7.0 (See detail 5.4)	In tube wall at the toe of the attachment to tube weld at the termination of attachment. In tube wall at the toe of tube-to-transverse plate weld.	
6.3 Transverse load-bearing partial joint penetration groove-welded or fillet-welded attachments where $t \leq 0.5$ in. and the main member is subjected to minimal axial and/or flexural loads (When $t > 0.5$ in., see note c).	44.0	10.0	In base metal at the weld toe or through weld throat.	Longitudinal stiffeners welded to base plates.

Figure 3.5 Stiffened fillet-welded tube-to-transverse connection detail (AASHTO, 2015)

Those fatigue limits for infinite fatigue life design can be used when geometric criterias are met. In section 5 of the LRFD specification, spefically in section 5.6.3 for transverse plate thickness and section 5.6.4 for stiffened base connection, respectively, geometric criterias are provided for an optimized and cost-effective stiffened connection. Fatigue design criterias in LRFD AASHTO and NJDOT design standard are compared and

summaried in Table 3.1.

Table 3.1 Fatigue design criteria for fillet-welded tube-to-transverse connection

Geometric parameter	Design criteria (AASHTO, 2015)	NJDOT standard (NJDOT, 2007)
Transverse plate thickness	2 inch, if section diameter > 8 inch 1.5 inch, if section diameter ≤ 8 inch	2 inch − 3 inch
Termination angle of stiffener	15 degree	24 degree − 32.8 degree
Thickness of stiffener	Minimum 0.25 inch	1 inch
Height of stiffener	Minimum 12 inch	18 inch
Number of stiffeners	8	8
Stiffener spacing	Not exceed 16 inch	8.42 inch − 15.31 inch
Ratio of the stiffness thickness to the tube-wall thickness	Not exceed 1.25	0.625 − 1.1

To utilize fatigue coefficients provided in the AASHTO specification, an optimimized detail provides a stiffener thinckness of 1.25 times the pole wall thickness, a stiffener height of 1.75 times the stiffener spacing, and stiffener termination angle of 15° (Roy et al., 2012) In addtion, it was addressed that increasing the transverse plate thickness can be the most cost-effective solution but this is not the best solution for the tube with a large diameter. In Figure 3.6, finite life constant and CAFT for stiffened fillet-welded tube-to-transverse plate connection is provided with given geometric parameters based on the laboratory test results.
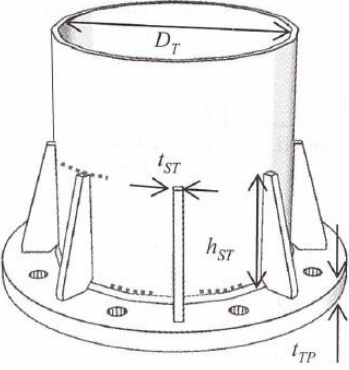
Tube-to-transverse plate connections stiffened by longitudinal attachments with partial- or full penetration groove-welds, or fillet-welds in which the tube is subjected to longitudinal loading and the welds are wrapped around the attachment termination.		Multisided	$t_T = \frac{5}{16}$ in. $D_T = 24$ in. $t_{TP} = 2$ in. $D_{BC} = 30$ in. $N_B = 8$ $N_S = 16$ $r_b = 4$ in $N_{ST} = 8$ $h_{ST} = 18$ in. $t_{ST} = \frac{3}{8}$ in.	Cracking at top of stiffener	
				11.0 ($K_F = 2.4$)	7.0 ($K_I = 5.3$)
				Cracking at end plate fillet-weld toe on tube wall	
				3.9 ($K_F = 1.9$)	7.0 ($K_I = 4.0$)

Figure 3.6 Laboratory test results for fillet-welded tube-to-transverse plate connection (AASHTO, 2015)

Stress Concentration Factor (SCF)

For infinite fatigue life design of tubular connections, the fatigue stress concentration factor should be calculated and the equations are only valid for given geometric ranges. The equations for fatigue SCF for finite life K_F, are provided in Table 11.9.3.1-2 and it is shown in Figure 3.7. The infinite fatigue life stress concentration factor K_I can be obtained using the proposed equation in section 11.9.3.1. The adopted fatigue SCF is determined by empirical equations based on both analytical and experimental study performed under NCHRP Project 10-70 and verified with experimental results (Roy et al. 2011).

Section Type	Detail	Location	Fatigue Stress Concentration Factor for Finite Life, K_F	Section Type
Round	Fillet-welded tube-to-transverse plate connections	Fillet-weld toe on tube wall	$K_F = 2.2 + 4.6 \times (15 \times t_T + 2) \times (D_T^{1.2} - 10)$ $\times (C_{BC}^{0.03} - 1) \times t_{TP}^{-2.5}$ Valid for: 0.179 in. $\leq t_T \leq$ 0.5 in.; 8 in. $\leq D_T \leq$ 50 in.; 1.5 in. $\leq t_{TP} \leq$ 4 in.; 1.25 $\leq C_{BC} \leq$ 2.5	(11.9.3.1–2)
	Groove-welded tube-to-transverse plate connections	Groove-weld toe on tube wall	$K_F = 1.35 + 16 \times (15 \times t_T + 1) \times (D_T - 5)$ $\times \left(\dfrac{C_{BC}^{0.02} - 1}{4 \times C_{OP}^{-0.7} - 3} \right) \times t_{TP}^{-2}$ Valid for: 0.179 in. $\leq t_T \leq$ 0.625 in.; 8 in. $\leq D_T \leq$ 50 in.; 1.5 in. $\leq t_{TP} \leq$ 4 in.; 1.25 $\leq C_{BC} \leq$ 2.5; 0.3 $\leq C_{OP} \leq$ 0.9	(11.9.3.1–3)
	Fillet-welded tube-to-transverse plate connections stiffened by longitudinal attachments	Weld toe on tube wall at the end of attachment	$K_F = \left(\dfrac{t_{ST}^{0.4}}{t_T^{0.7}} + 0.3 \right) \times \left(0.4 \times \dfrac{D_T^{0.8}}{N_{ST}^{1.2}} + 0.9 \right)$ Valid for: 0.25 in. $\leq t_{ST} \leq$ 0.75 in.; 8 $\leq N_{ST}$; 0.25 in. $\leq t_T \leq$ 0.625 in.; 24 in. $\leq D_T \leq$ 50 in.	(11.9.3.1–4)
	Fillet-welded tube-to-transverse plate connections stiffened by longitudinal attachments	Fillet-weld toe on tube wall	$K_F = \left[\left(130 \times \dfrac{D_T^{0.15}}{N_{ST}^{1.5}} + 1 \right) \times \left(\dfrac{0.13}{h_{ST} + 7} \right) \times \left(\dfrac{6.5}{t_{ST}^{0.5}} - 1 \right) \right.$ $\left. \times K_F \text{ as per Eq. 11.9.3.1-1} \right]$ Valid for: 12 in. $\leq h_{ST} \leq$ 42 in.; 0.25 in. $\leq t_{ST} \leq$ 0.75 in.; 8 $\leq N_{ST}$; 24 in. $\leq D_T \leq$ 50 in.	(11.9.3.1–5)
Multisided	As above	As above	Multiply respective K_F above by: $\left[1 + (D_T - r_b) \times N_S^{-2} \right]$ Valid for: 8 in. $\leq D_T \leq$ 50 in.; 1 in. $\leq r_b \leq$ 4 in.; 8 $\leq N_S \leq$ 16	(11.9.3.1–6)

Figure 3.7 Fatigue stress concentration factor, K_F (AASHTO, 2015)

3.2 Fatigue Data Analysis

Statistical analysis of fatigue data

The S-N curve for stress-life fatigue analysis were constructed on log-log scale with key parameters such as the stress range under constant-amplitude and the number of cycles to failure. The linear regression on the S-N curve represents the relationship between stress-range and the number of cycles. According to Miner's rule (Miner, 1935), the fatigue life curve is generally expressed by Equation (3.1):

$$N \cdot S_R{}^m = A \qquad (3.1)$$

Where *m* represents the slope of the linear line in log-log scale and *A* is the value of the intercept on the x-axis. The fatigue coefficient, *A,* is assumed to be a log-normal random variable according to the recommendation from a previous study (Wirsching 1984). The variance of *A* is calculated as follows:

$$\sigma_A{}^2 = \frac{\sum_{i=1}^{k}(A_i - \bar{A}_i)^2}{k-2} \qquad (3.2)$$

Where *k* is the number of test specimens and the term *(k-2)* in the denominator is used instead of *k* to make the variance of *A* an unbiased estimator of the normal population variance.

Least square regression analysis of fatigue data

In this dissertation, a least square regression analysis was performed following the procedures in ASTM Standard (ASTM E739-91, 2007). In linear form, the regression equation, it can be written as,

$$Y = a + b \cdot X \qquad (3.3)$$

In the light of stress life fatigue analysis for lognormal random variables, equation (3.3) can be rewritten as shown in equation (3.4) (Wirsching, 1983),

$$logN = logA - m \cdot logS_R \qquad (3.4)$$

The value *a* and b in the linear form represent the value at the x-intercept and slope of the regression fit, respectively. These values can be evaluated (Wirsching, 1983) in equations (3.5) and (3.6),

$$\hat{b} = \frac{\sum_{i=1}^{n}(X_i - \bar{X}) \cdot (Y_i - \bar{Y})}{\sum_{i=1}^{n}(X_i - \bar{X})^2} \qquad (3.5)$$

$$\hat{a} = \bar{Y} - \hat{b} \cdot \bar{X} \qquad (3.6)$$

$\hat{a}$ and $\hat{b}$ are the predicted value of a and b respectively and $\bar{X}$ and $\bar{Y}$ represents the sample mean values. Hence, the least squares line for stress life fatigue data analysis is given as,

$$\hat{Y} = \hat{a} + \hat{b} \cdot X \quad (3.7)$$

In this study, the value of 3 was used for m parameter for the fatigue data analysis by following AASHTO Specification.

Fatigue coefficient A and fatigue design life

To take into consideration the residuals from regression fit, the fatigue coefficient, A, can be determined as lognormal random variable. It can expressed by,

$$Y = \ln(A) \quad (3.8)$$

If A is lognormally distributed, Y is a normal distribution where A is greater than zero. (Nowak and Collins, 2000). Since Y is normally distributed, standard normal function can be written,

$$F_A(a) = F_Y(y) = \Phi\left(\frac{y - u_Y}{\sigma_Y}\right) \quad (3.9)$$

Where $u_Y = u_{\ln(A)}$ is a mean value of $\ln(A)$ and $\sigma_Y = \sigma_{\ln(A)}$ is a standard deviation of $\ln(A)$, respectively. The variance and mean of $\ln(A)$ can be expressed as follows (Nowak and Collins, 2000),

$$\sigma^2{}_{\ln(A)} = \ln\left[1 + \left(\frac{\sigma_A}{u_A}\right)^2\right] \quad (3.10)$$

$$u_{\ln(A)} = \ln(u_A) - \frac{1}{2} \cdot \sigma^2{}_{\ln(A)} \quad (3.11)$$

To establish the fit lines for the fatigue experimental data, a regression analysis was performed for the existing testing data for both unstiffened and stiffened fillet-welded

socket connections. By utilizing equations 3.1 through 3.11 above, the mean minus two standard deviation regression lines were established from the regression fit. The linear regression line for the mean minus two standard deviation was shifted down slightly to establish a lower bound and this approach is commonly used for design purposes and is associated with a 2.3 percent probability of failure assuming the life logarithms to be normally distributed (Fisher et al. 1998 and Schneider and Maddox, 2003). In addition, the fatigue design life used for the calculation of fatigue damage and safety factor is considered as the fatigue design life corresponding to the number of cycle that ranges from 10 million to 20 million cycles for infinite fatigue life (Puckett et al. 2014).

3.2.1 Fillet-welded socket connection detail: Tube-to-transvers plate connection

Several researchers performed fatigue tests on unstiffened fillet-welded socket connections (Macchietto, 2002; Koenigs, 2003; Ocel et al., 2006; Roy et. al, 2011; Stam et al., 2011; Ocel 2014). This unstiffened fillet-welded socket connection is similar to the fillet-welded tube-to transverse plate connection given in Table 11.9.3.1-1 in the LRFD specifications (AASHTO, 2015). These fatigue tests were performed after the fourth edition of AASHTO fatigue provisions were published (AASHTO, 2001). Figure 3.8 shows a plot of the existing test data from the above mentioned researchers along with Category E'. As can be observed in Figure 3.8, there is a large scatter in the test data.
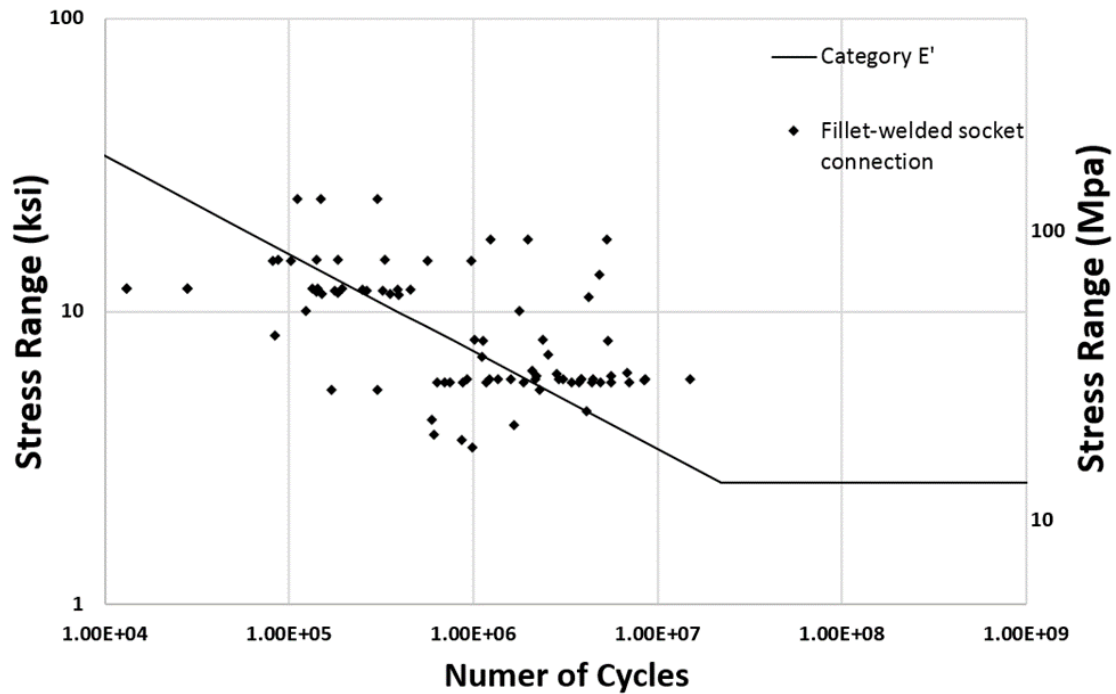
Figure 3.8 Fatigue data for unstiffened fillet-welded socket connection

Due to the many parameters that influence fatigue resistance, the test data were divided into eight (8) groups based on: base plate thickness, peening, galvanizing and the shape of tube as shown in Table 3.2. Table 3.2 also shows the fatigue coefficient, A from the regression line representing the mean minus two standard deviation. For instance, the fatigue data listed under Group 1, the base plate thickness was greater than 50.8 mm (2 inch) and the tube had a round shape. For the tested specimens in Group 1, there was no peening and no galvanization. The tests in Group 2 were tested under the same conditions as in Group 1 but the test specimens were galvanized. Figure 3.9 shows the fatigue test data for both Group 1 and Group 2 with category E' and with the fatigue limit which represents the mean minus two standard deviation regression line. Test results from Group 2, in which the test specimens were galvanized, show a reduction of fatigue limit. A detailed description of geometric parameters for the post, base plate and fillet welding of

unstiffened fillet-welded socket connection are summarized in Table 3.3.
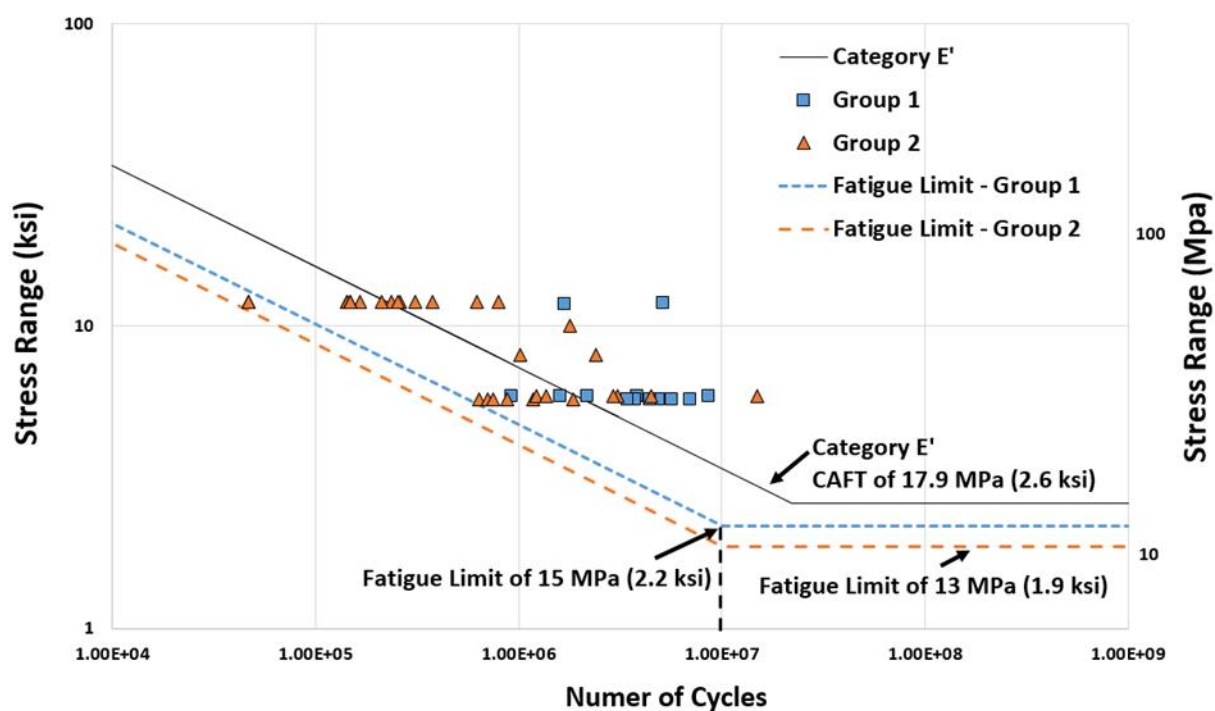
Figure 3.9 Unstiffened fillet-welded socket connection sorted by base plate thickness of 2

inch

Table 3.2 Summary of test groups and coefficients for unstiffened fillet-welded socket

connection

	Plate thickness		Peened	Galvanized	Tube shape		$A_{MEAN-2\sigma}$	Number of testing data
	t ≥ 50.8 mm	t < 50.8 mm			Round	Multi		
Group 1	Yes	No	No	No	Yes	No	1.04E+08	14
Group 2	Yes	No	No	Yes	Yes	No	6.58E+07	30
Group 3	Yes	No	No	No	No	Yes	9.76E+07	8
Group 4	No	Yes	No	No	Yes	No	2.03E+08	17
Group 5	No	Yes	No	No	No	Yes	7.33E+06	9
Group 6	No	Yes	No	Yes	Yes	No	2.65E+07	8
Group 7	No	Yes	Yes	No	No	Yes	1.71E+08	8
Group 8	No	Yes	Yes	No	Yes	No	2.25E+08	4

To evaluate the fatigue damage and safety factor using the fatigue module in ANSYS Workbench, fatigue design limit in terms of stress range was calculated for both 10 million cycles and 20 million cycles which were established for infinite fatigue life (Puckett et al. 2014).

Table 3.3 Geometric parameters for unstiffened fillet-welded socket connection test data

	Post dimension (mm)	Post thickness (mm)	Base plate dimension (mm)	Base plate thickness (mm)	Fillet welding thickness (mm)
Group 1	254 – 457	6.4 – 55.3	483	50.8	4.8 x 7.9
Group 2	254 – 609	4.5 – 7.9	305 x 457 – 914 x 914	50.8 – 76.2	9.4 x 15.9
Group 3	-*	4.8 – 7.9	-	63.5	-
Group 4	254	4.5 – 6.1	483	38.1	4.8 x 7.9 – 6.4 x 11.2
Group 5	-	7.9	-	31.8	-
Group 6	254 – 609	4.5 – 7.9	483	38.1 – 44.5	4.8 x 7.9 – 9.4 x 15.9
Group 7	-	7.9	-	31.8	-
Group 8	254	4.5 – 6.1	483	38.1	4.8 x 7.9

* - indicates that information is unknown or missing.
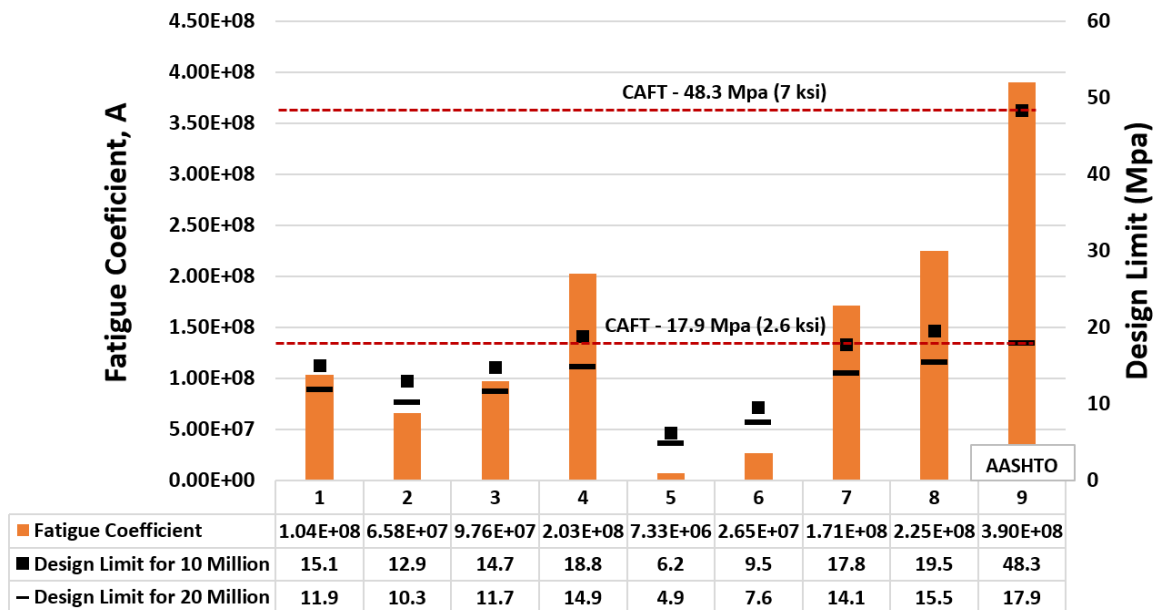
Figure 3.10 Fatigue coefficients and fatigue design life

In Figure 3.10, a bar chart represents the fatigue coefficient *A*, for the mean minus two standard deviation regression line for the eight groups of test data compared to the AASTHO fatigue limits (designated as Group 9 in Figure. 3.10). The right axis in Figure. 3.10 represents the fatigue design limit. Group 9 which represents the values from the AASHTO specification (AASHTO 2015) was added in Figure. 3.10. It shows comparisons between AASHTO and the eight test data groups.

With respect to galvanization, the reduction in fatigue design life is observed for Groups 1 and 2. Also, for Groups 4 and 6 where the plate thickens is less than 2 inch with a round tube and no peening, the fatigue coefficient and fatigue design limit have decreased significantly compared to other test data in Figure. 3.10. The tube geometry was another important parameter investigated in the data analysis in this study. For Groups 1, 3, 4 and 5 as well as Groups 7 and 8, there is a reduction in fatigue design life with multisided tube due to the stress concentration at the corner of the tube. Group 5 shows the worst fatigue performance with base plate thickness of 54.6 mm (1.25 inch).

With regard to the effect of surface treatment, the peening treatment seems to improve the fatigue resistance. The effect of peening can also be observed by comparing Groups 5 and 7 as well as comparing Groups 4 and 8. As illustrated in the bar chart in Figure. 3.10, the highest fatigue coefficient is found in the data in Groups 8. Although this group has a base plate thickness less than 2 inch, the peening treatment seems to have improved the fatigue resistance substantially. It is worth noting that there were only four tests in Group 8 compared to the other groups which had more tests per group.

According to previous studies (Hall et al. 2008; Stam et al. 2011), it is believed that the base plate thickness is one of the most critical factors that affect fatigue performance

of socket connections. In this study, comparing Groups 1 and 4, and Groups 2 and 6, and Groups 3 and 5, it was observed that there are reductions in fatigue design limit for thinner base plates except Group 4 where has 38.1 mm (1.5 inch) of plate thickness.

The synthetic fatigue data analysis performed in this chapter shows that there are considerable discrepancies in the fatigue design life for 10 million and 20 million cycles. According to the Section 5.4 in Table 11.9.1-1 in the AASHTO specifications, the CAFT's are determined by K_I and those vary from 17.9 MPa (2.6 ksi) to 48.3 MPa (7.0 ksi) as illustrated in Figure 3.10. The fatigue coefficient is defined as 3.9 x 10^8 when K_F is less than 3.2. It is observed that in terms of fatigue coefficient and CAFT fatigue performance of unstiffened socket connection details is overly predicted with a mean minus two standard deviation regression lines. Each group represents significant disparity in fatigue performance. The results of the fatigue test data analysis evaluated for the eight groups earlier will be further discussed in light of the finite element analysis results in the next sections.

3.2.2 Stiffened fillet-welded socket connection

The fatigue test results for stiffened fillet-welded socket connection detail from several researchers (Machietto, 2002; Koenigs et al., 2003; Ocel et al., 2006; Roy et al., 2011) were analyzed in this section. The detail is also named tube-to-transverse plate connections stiffened by longitudinal attachments with fillet-weld. In this detail the tube is subjected to longitudinal loading and the welds are wrapped around the stiffener termination (AASHTO, 2015). This detail was defined as category E' for a CAFL of 17.9 MPa (2.6 ksi) in the fourth edition of specification (AASHTO, 2001). As can be seen in a

previous chapter, Figure. 3.2 shows a typical stiffened socket connection detail tube-to-transverse plate connection with longitudinal stiffeners. Modifications were made to this detail in the LRFD specification (AASHTO, 2015). By considering two potential fatigue crack locations: at the weld location at the base and at the weld location at the tip of stiffeners, a CAFT of 48.3 MPa (7 ksi) is introduced when the stress intensity factor, K_I, is less than 5.5. Based on the fatigue crack location, collected data is sorted out into two groups and the testing data is plotted on S-N curve with fatigue categories as shown in Figure. 3.11.
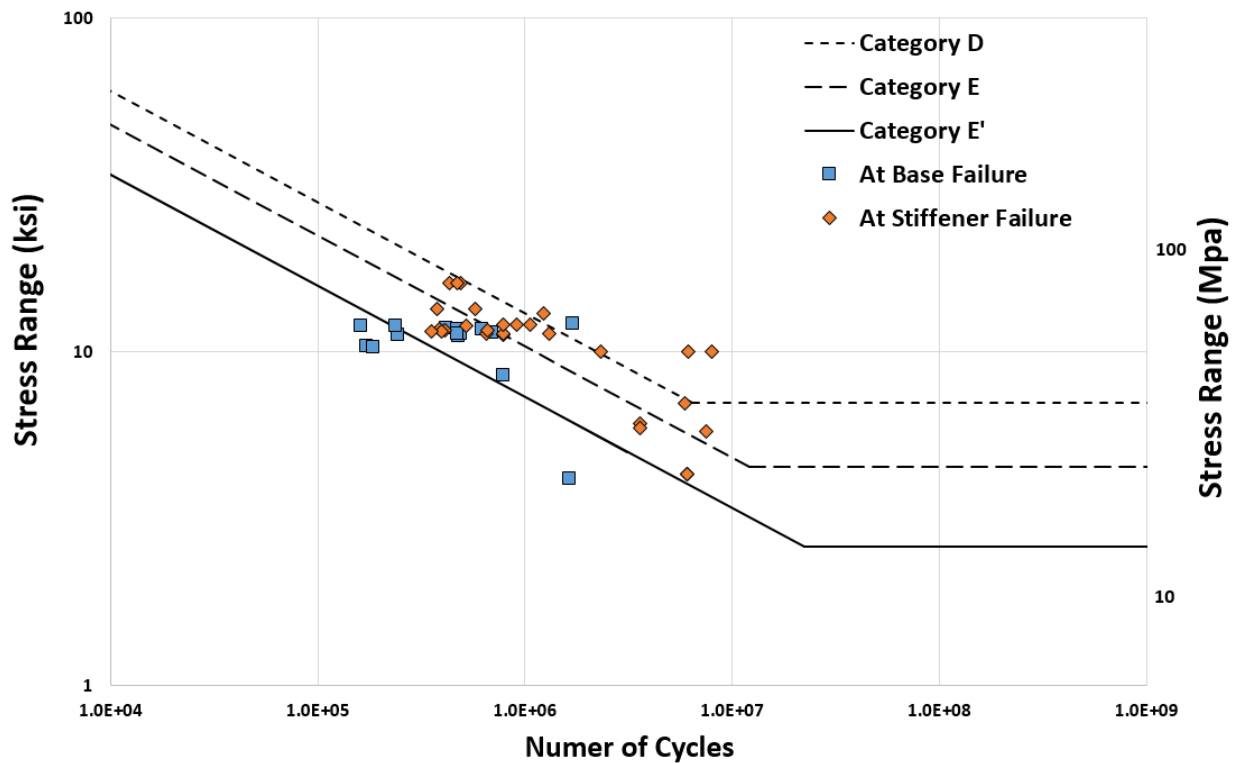
Figure 3.11 Fatigue data of stiffened fillet-welded socket connection with respect to crack location at base and at stiffeners

From the test data analysis procedure, significant differences were observed in the fatigue resistance at crack location at the tip of stiffener due to the geometric effects of stiffeners. Because of that, the fatigue data is further sorted into another two groups: the

socket connection with eight stiffeners (Machietto, 2002; Roy et. al, 2011) and the socket connection with four stiffeners (Koenigs, 2003; Ocel, 2006). Except for two test results (Machietto, 2002), the first group presents a CAFT of 48.3 MPa (7.0 ksi) and it was defined as an optimized stiffened tube-to-transverse connection detail (Roy et al., 2012) with eight stiffeners.
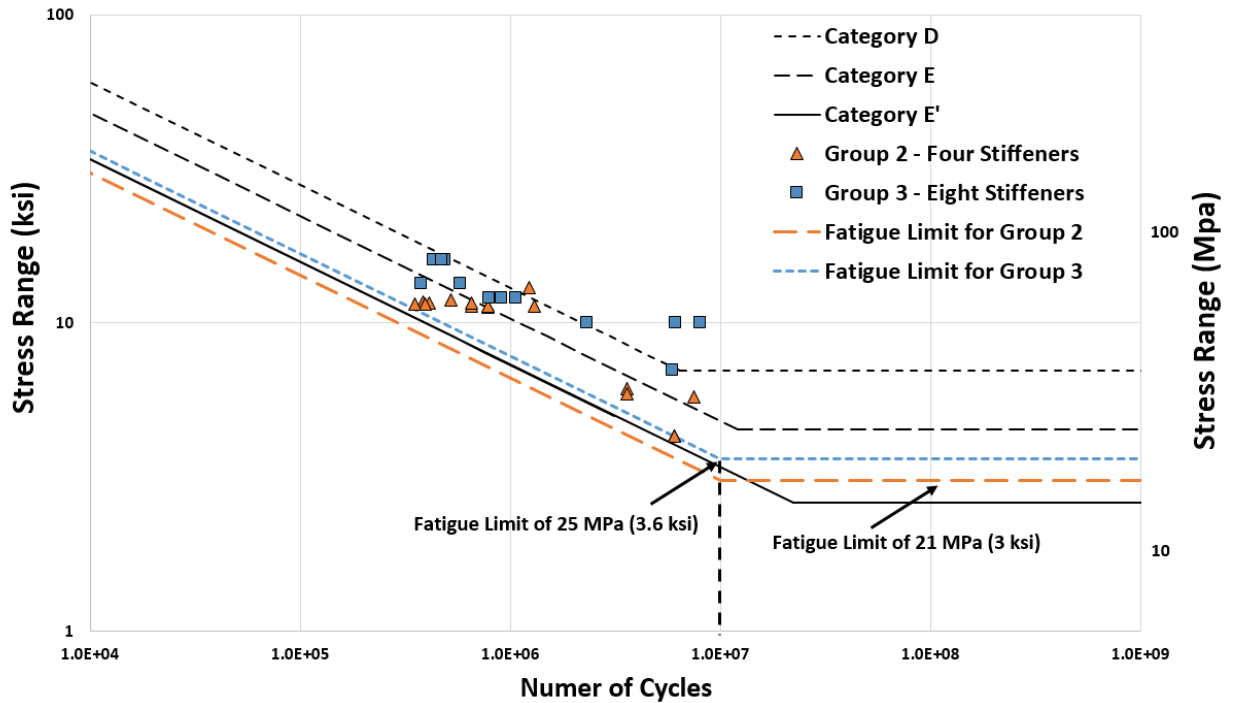
Figure. 3.12 Established fatigue limit for stiffened fillet-welded socket connection

A statistical regression analysis was performed on the test data to establish fatigue limits and design life. Figure 3.12 shows mean minus two standard deviation lines from the least square regression analysis for the two test data groups. The connection with eight stiffeners shows higher fatigue resistance. The test groups are summarized in Table 3.4 with failure location, number of stiffeners, fatigue coefficient and number of testing data. The geometric parameters for the post, the base plate and the thickness of fillet welds are shown in Table 3.5. The stiffener parameters are summarized in Table 3.6.

Table 3.4 Summary of testing cases and coefficients for stiffened fillet-welded socket connection

	Failure location	Number of stiffeners	$A_{MEAN-2\sigma}$	Number of testing data
Group 1	Base	4 - 8	9.46E+07	15
Group 2	Stiffener	4	2.90E+08	16
Group 3	Stiffener	8	4.74E+08	12

Table 3.5 Geometric parameters for stiffened fillet-welded socket connection

	Post dimension (mm)	Post thickness (mm)	Base plate dimension (mm)	Base plate thickness (mm)	Fillet welding thickness (mm)
Group 1	254 – 610	4.5 – 7.9	483 – 914	31.8 – 50.8	4.8 x 7.9 – 9.5 x 15.9
Group 2	254	4.5 – 7.9	483	31.8 – 38.1	4.8 x 7.9
Group 3	610	7.9	914	50.8	9.5 x 15.9

Table 3.6 Geometric parameters for stiffener

	Height (mm)	Width (mm)	Thickness (mm)	Angle (mm)
Group 1	76 – 457	51 – 122	6.4 – 9.5	15 – 45
Group 2	76 – 152	51	6.4 – 9.5	45
Group 3	83 – 457	122	9.5	15

As was done in the test data analysis for the socket connection-tube-to-transvers plate connection in the previous section, the fatigue design life is calculated with a lower range of 10 million cycles and an upper range of 20 million cycles. In Figure 3.13, a bar chart represents the fatigue coefficient, A, from obtained from the mean minus two standard deviation regression analysis line of the test data. Figure. 3.13 also shows fatigue design limit on the right hand vertical axis. As presented in Table 3, Group 1 represents a fatigue failure at base, Groups 2 and 3 are for tests with four stiffeners and eight stiffeners

respectively. In addition, Group 4 was added to Table 3 to show comparisons of the test data from Groups 1, 2, and 3 to the limits given in the AASHTO (2015) Specifications represented in Group 4. The fatigue resistance at the base which is represented by Group 1 tests in Table 3.3, is the lowest fatigue performance compared to Groups 2 and 3. This indicates that local stress was higher at base toe than at tip of stiffeners and failure was observed at base toe only. Because of the geometric parameters, the stiffeners fail to reduce or minimize the level of stress at the toe. On the other hand, Group 3 tests which has eight stiffeners represents the best fatigue resistance in terms of fatigue coefficient, A, and design life.

According to the Section 6.2 in Table 11.9.1-1 of the AASHTO specifications, the CAFT of 48.3 MPa (7 ksi) is can be used when K_I is less than 5.5. The fatigue coefficient, A, for this case is given as 11×10^8 when K_F is less than 2.5. For a fatigue design life range between 10 million and 20 million cycles and using a mean minus two standard deviation regression line, the analysis of the test data from Group 3 and comparing them to AAHSTO (Group 9) shows that the CAFT values from AASHTO is conservative for connections with eight stiffeners (Group 3) . However, for Group 2 (four stiffeners) and Group 1 (at base failure with various number of stiffeners), the data analysis shows that the AASHTO fatigue limit (Group 9) is overestimated.
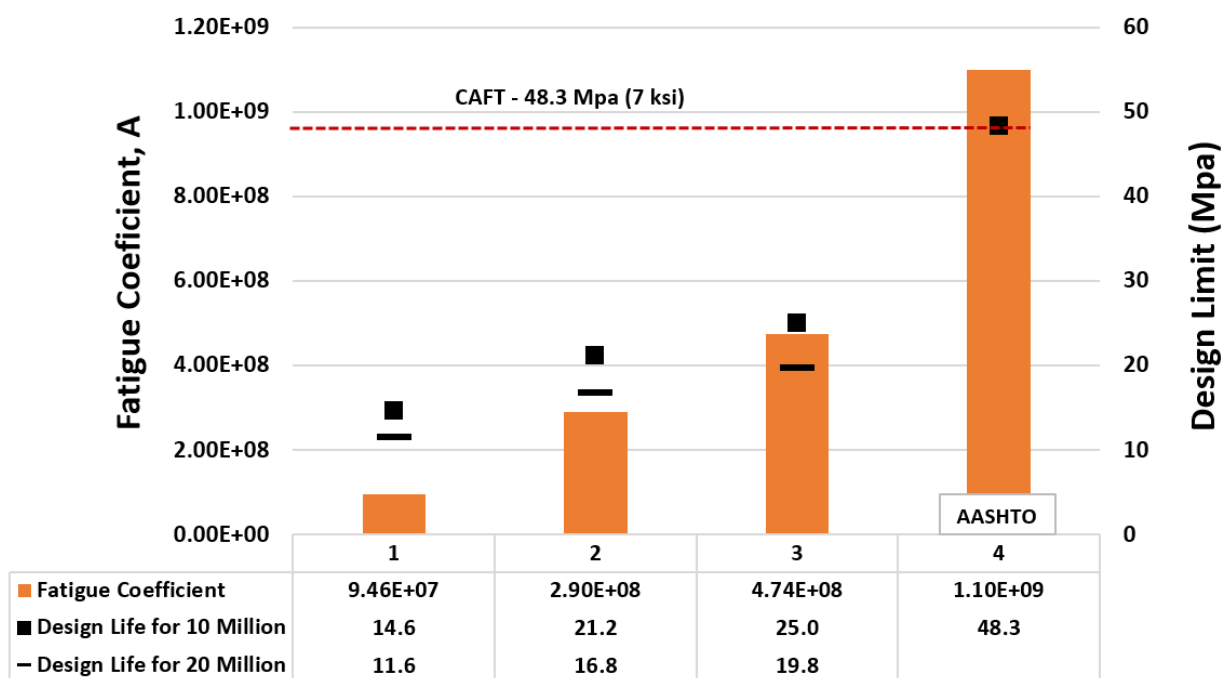
Figure. 3.13 Fatigue coefficients from statistical analysis for each group

CHAPTER IV

FE MODEL DEVELOPMENT

This chapter describes the development of three-dimensional Finite Element Method (FEM) model including material properties, meh generation, contact regions, boundary regions, and fatigue input and output tools. The FE model will be utilized to evaluate the fatigue resistance of fillet-welded unstiffened and stiffened connection details for sign support structures. The geometry of FE model was originally constructed using SOLIDWORK 2010 then it was exported to the commercial Finite Element Analysis (FEA) software ANSYS Workbench 17.1. In this study, a static structural option was chosen for an imported solid model and then the model was regenerated into a design module. Contact regions, boundary conditions and meshes were also determined under the model tap in the Workbench platform. A detailed procedure for FE model development and model validation will be further discussed in following subsections.

4.1 FE Model Development

A tube-to-transverse plate connection detail stiffened with eight longitudinal welded stiffeners was constructed. The model was validated using experimental data and

also compared to the nominal stresses from basic mechanics. For mesh generation, ANSYS

Solid 187 elements were selected because they are relatively tolerant of irregular shapes of

FE model. The Workbench platform does not support shell elements for fatigue analysis.

The round tube (post) is 146-inch-long and 5/16-inch-thick and it was attached to the base

plate using fillet welds on top and bottom as shown in Figure 4.1. It should be noted that

the fillet welds with equal legs were constructed with 3/8 inch x 3/8 inch due to the

limitation with regard to welding geometry in SOLIDWORK 2010. The acceptable

maximum gap between the tube and the base plate was deliberately set as 0.063 inch. The

round shape base plate was 2-inch thick with eight ϕ30 mm diameter holes positioned such

that one hole is located between two stiffeners as shown in Fig. 4.1.
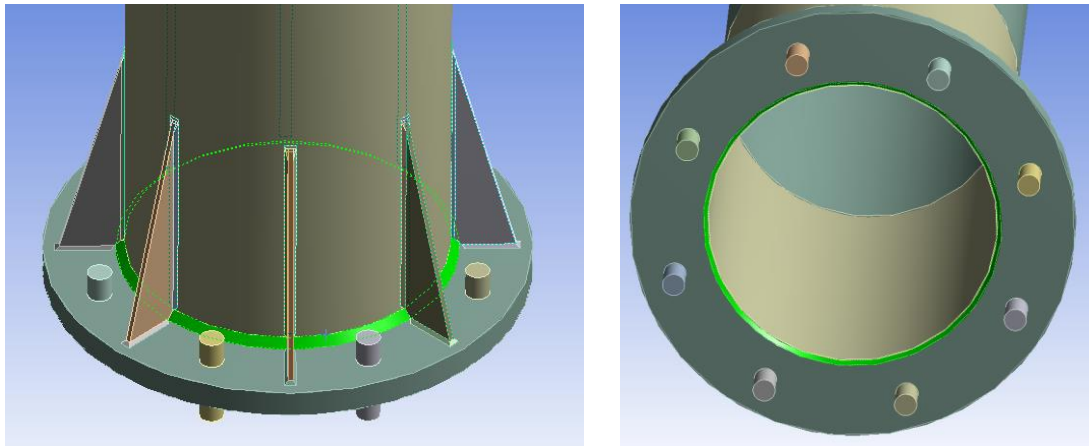
Figure 4.1 Fillet welding between post and base plate

Each stiffener (attachment) is 18-inch-long and 3/8-inch-thick with a 15 degree

stiffener termination angle on the tube. As illustrated in Figure 4.1, stiffeners are attached

to both the post and the base plate with 1/2 inch thick fillet weld. The stiffeners are welded

at the tip and each side and the base plate were also connected by enclosed inside of fillet

weld. A square loading plate 20 inch x 20 inch x 2 inch was provided the top of the tube to

simulate both static and cyclic load application. A three-dimensional FE model of the tube-

to-transverse plate connection is shown in Fig. 4.2.
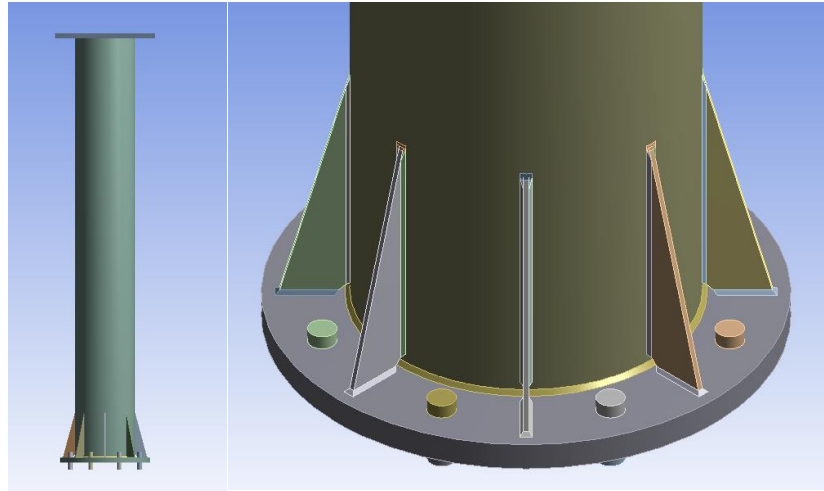
Figure 4.2 3D FE model for tube-to-transverse plate connection detail

Material Properties

Two material properties were defined in the FE model: one material property for the structural steel and the other for the welds. According to a prior experimental work (Thompson, 2012), Grade 50 steel which has 50 ksi of yield strength was used for the tube, the base plate, and the stiffeners. The weld yield strength and ultimate strength was 70 ksi. The modulus of elasticity and Poisson's ratio were also determined as an input parameter. Table 4.1 summarizes the material properties.

Table 4.1 Material properties for structural steel and welding profile

	Structural Steel	Welding Profile
Modulus of Elasticity, E	29000 ksi	29000 ksi
Poisson's Ratio, v	0.3	0.37
Yield Strength	50 ksi	70 ksi
Ultimate Tensile Strength	70 ksi	70 ksi

Fatigue properties such as alternating stress and the number of cycle for stress-life analysis were obtained from the synthetic data analysis results (Chapter 3) and then stored

in a tabulated format in Workbench platform. In addition to stress-life properties, a fatigue design life that achieves infinite fatigue life was used as an input parameter following the proposed CAFT from synthetic data analysis. For instance, existing experimental fatigue testing data (Roy et al., 2011) has shown that their testing results were close to Category D, which has a fatigue coefficient, A, equal to 11×10^8 and a slope, m equal to 3, respectively. As illustrated in Fig. 4.3, the Constant Amplitude Fatigue Threshold (CAFT) of 7 ksi was determined with a design life of 3.21×10^6.
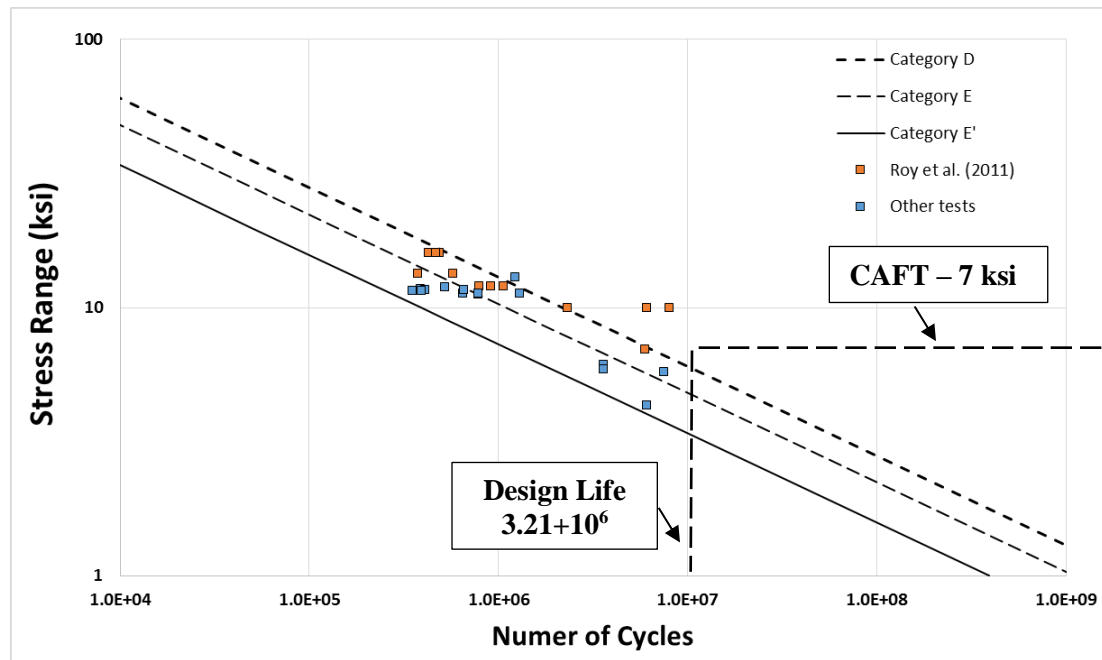
Figure 4.3. Experimental results (Machietto 2002; Koenigs 2003; Ocel 2006; Roy et al., 2011) with AASHTO-LTS Categories D, E and E'

Contact Regions

In this study, defining contact regions was another important process with respect to FE model development. Manual contact regions were inserted under the connections tap in Workbench platform and contact bodies and target bodies were manually designated.

The following contact regions were defined: 1) fillet welding between post and base plate, 2) fillet welding between stiffener and post, 3) fillet welding between stiffener and base-plate, and 4) bolts-base plate contact areas. These contact regions are illustrated in Fig. 4.4.
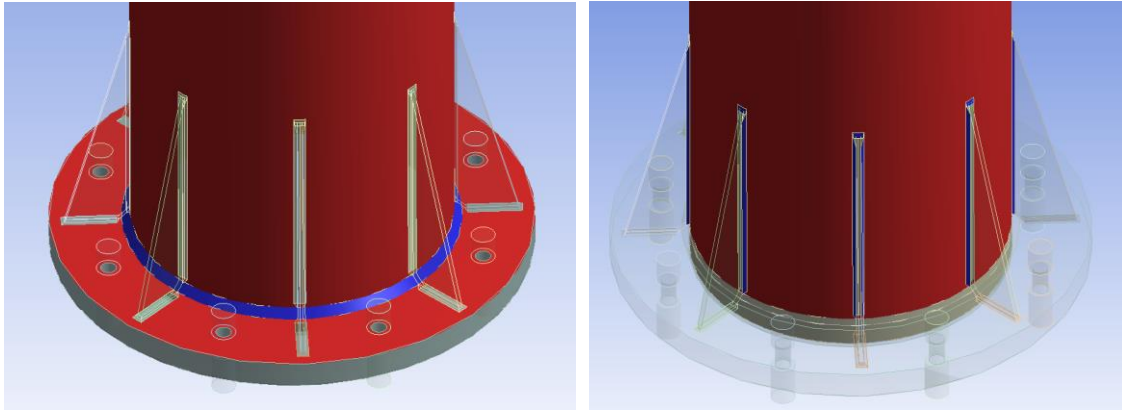
(a)   (b)
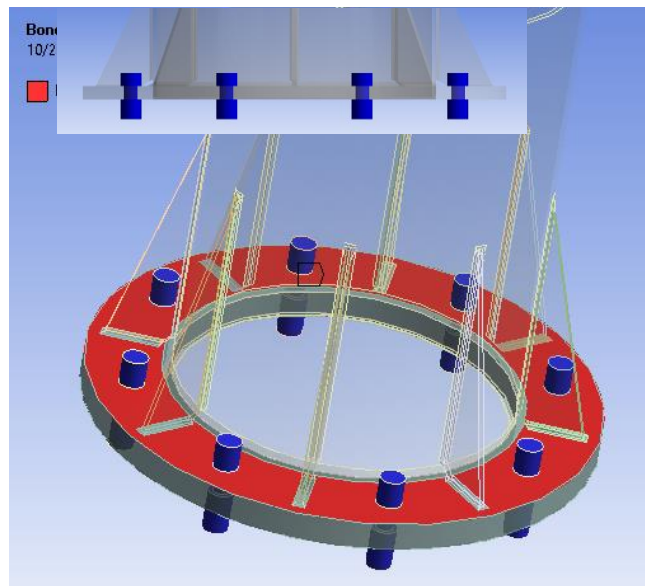
(c)

Figure 4.4. Contact regions for (a) fillet welding between post and base plate, (b) stiffeners connections for post and base plate, and (c) bolts and base plates

Mesh Generation

Generating the mesh was one of the most challenging task in the FE model development. Due to the multiple surface intersections and an initially defined gap between post and base plates, failure messages were received and it was carefully reviewed. Furthermore, the flat surface of the stiffness and a rounded shape of tube caused an error in mesh generation. Mesh iterative solver was used to enhance the topological surface intersections with other surfaces. Adaptive size function for the stiffness matrix and active assembly for initial size seed was set for the mesh generation. A total of 99,579 nodes and 59,433 elements were generated and as shown in Figure. 4.5.

A recent research (Hall III, 2004) has indicated that elements with 0.25 inch lengths along the weld toe area, representing 0.3% of the model height can adequately capture the behavior of the connection details. This recommendation was used in selecting the element size of the weld elements.
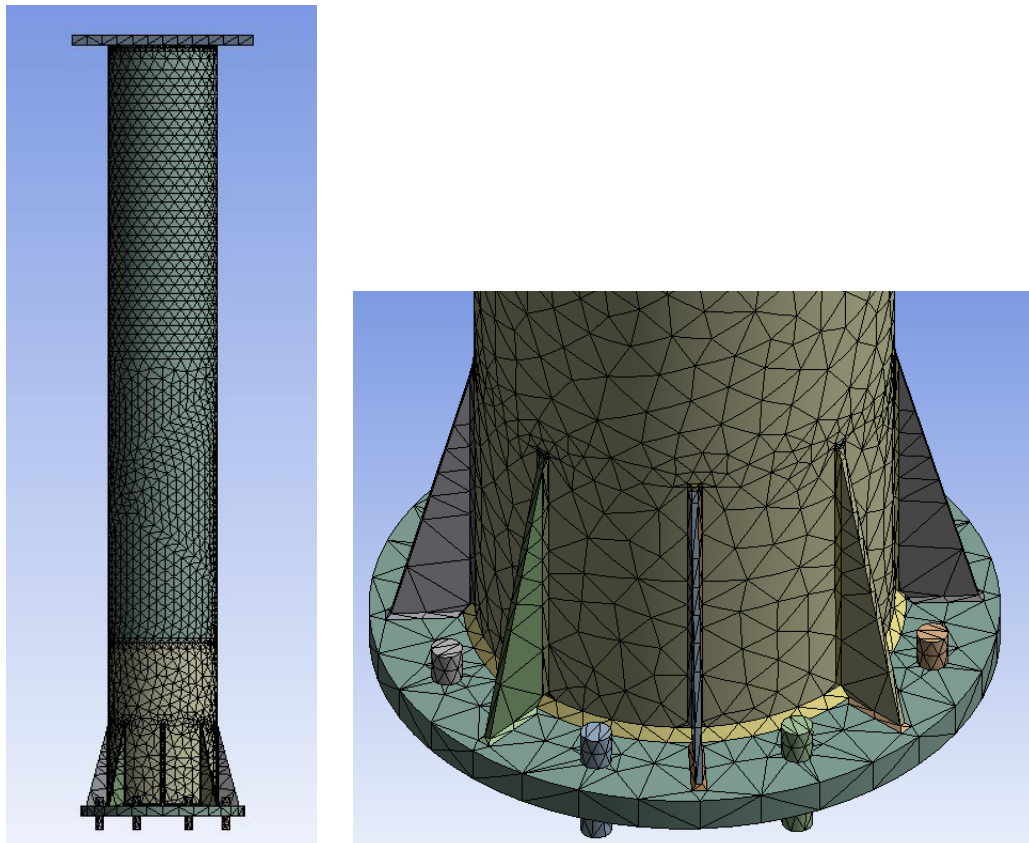
Figure 4.5. Mesh generation

Boundary Conditions

Boundary conditions were set through the static structural window. Many cases of boundary conditions were tested to validate the FEM model. Based on the level of the maximum principle stresses obtained from the FE model, two fixed boundary conditions were investigated: 1) fixed conditions at the bottom of the eight bolts, and 2) fixed conditions at the surface areas of the eight bolts. Fig. 4.6 shows the two fixed boundary conditions applied in the FE model. It should be pointed out that the applied boundary condition in this study was not exactly the same as a previous numerical study (Roy et al., 2011) and the details of contact surfaces and fixed support is shown in Fig. 4.6 (c).

(a)   (b)

(c)
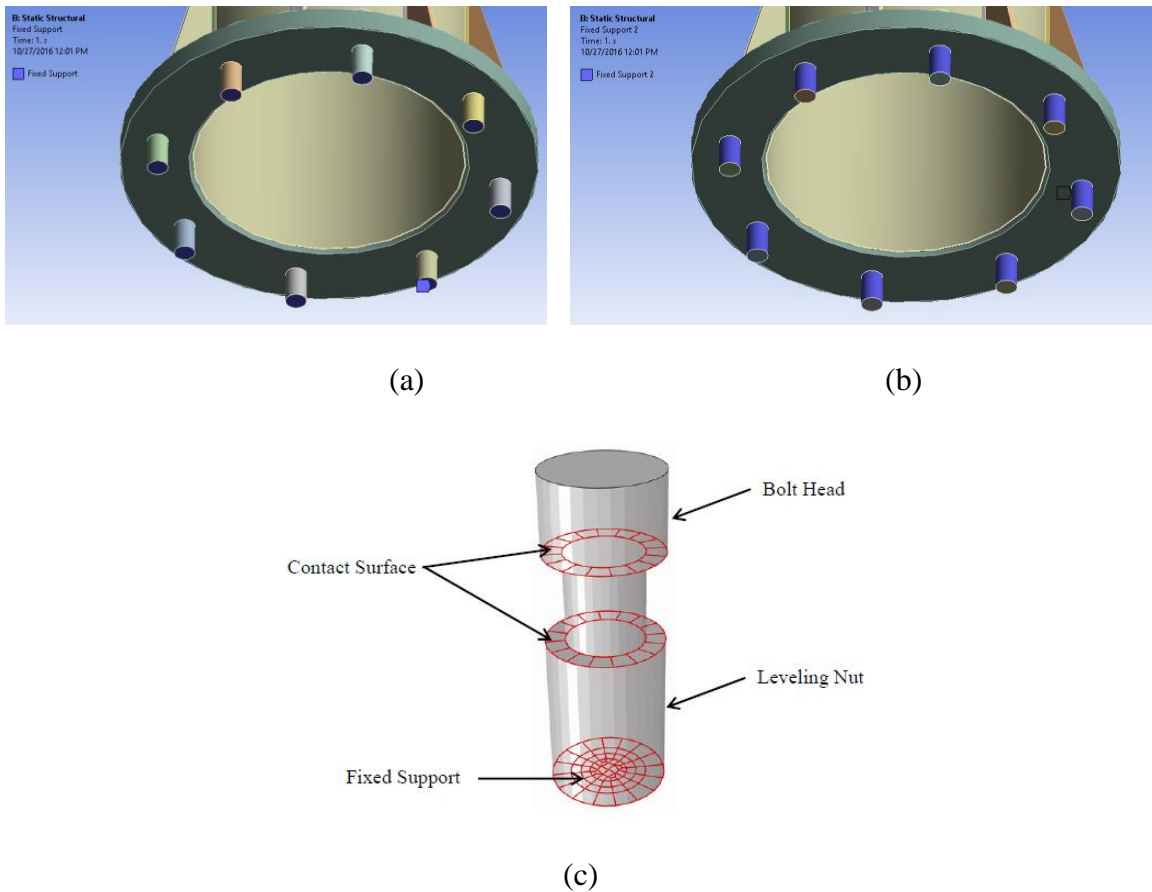
Figure 4.6 Applied boundary conditions: (a) fixed conditions at the bottom of bolts, (b)

fixed conditions at the surface areas of the eight bolts, and (c) contact surfaces and fixed

support from NCHRP 10-70 (Roy et al., 2011)

Fatigue tools

Under the solution tap, an inserted fatigue tool option was required to perform the stress-life fatigue analysis. As described in Chapter 2.5, the detailed view of the fatigue tool was used to define the various aspects of a fatigue analysis such as loading type, analysis type, mean stress theory and stress component. All fatigue results were based on input fatigue material properties and stress components. In this study, the maximum principle stress was used as stress component type indicator

For an applied constant amplitude fatigue loading case, the fatigue outputs such as life, damage and safety factor were obtained by altering loading ratios such as fully reversed, zero-based, or a specified loading ratio. Stress-life analysis using traditional S-N curves was used to achieve no plasticity in the structural components.

Conducting fatigue testing under a uniaxial loading by applying a fixed or zero mean stress state is cost-prohibitive and also has time limitations. It is anticipated that results from FE model utilizing ANSYS Workbench fatigue tool platform would be beneficial to have a better understanding of fatigue performance in both stiffened and unstiffened fillet-welded connection details.

4.2 FE Model Validation

For FE model validation, a finite element model of the tube-to-transverse plate connection detail was constructed with identical dimensions and geometry of tested specimen. (Thompson, 2012) Based on static test results, the load versus stress plot was

constructed for fatigue critical locations such as at the top of stiffeners and base toe. To obtain the stress values at these specific locations, selected nodes were defined. Fig. 4.7 shows the load versus maximum principle stress from the FE model and from experimental results (Thompson, 2012). The figure shows good agreement between the FE results and the experimental values.
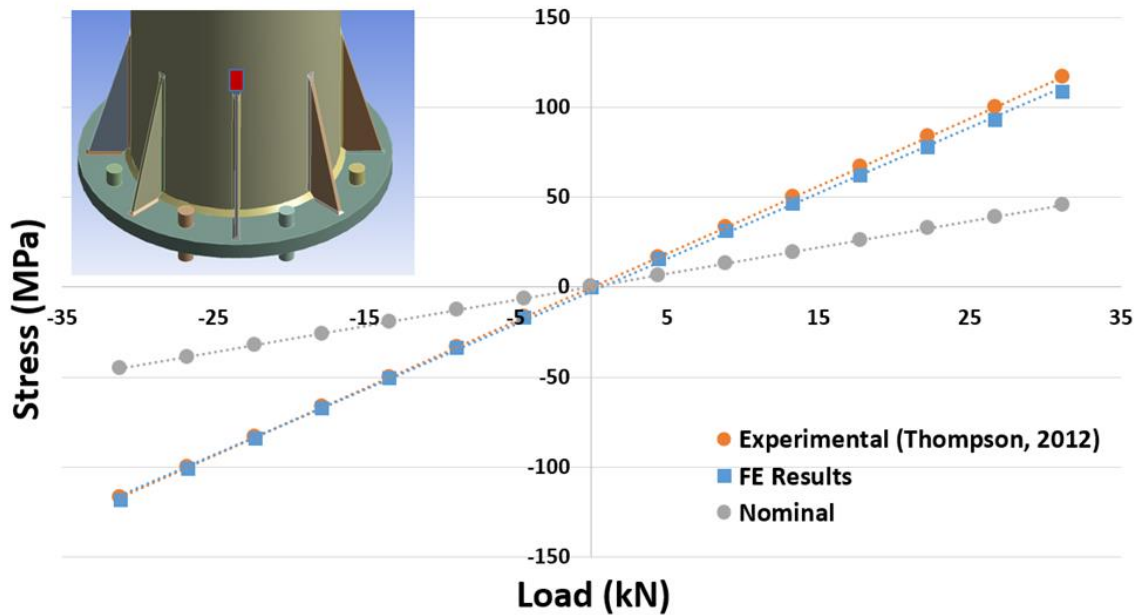
Figure 4.7 Load versus maximum principle stress at the top of stiffeners

Results from the FE model were also used to obtain the Stress Concentration Factor (SCF) at the fatigue critical locations. In Fig. 4.8, a SCF (approximately 2.5) was observed at the top of stiffeners then gradually decrease along the tube as anticipated. Overall, the SCF pattern from the FE model results shows higher stress level but relatively reasonable agreement with experimental results (Thompson, 2012).
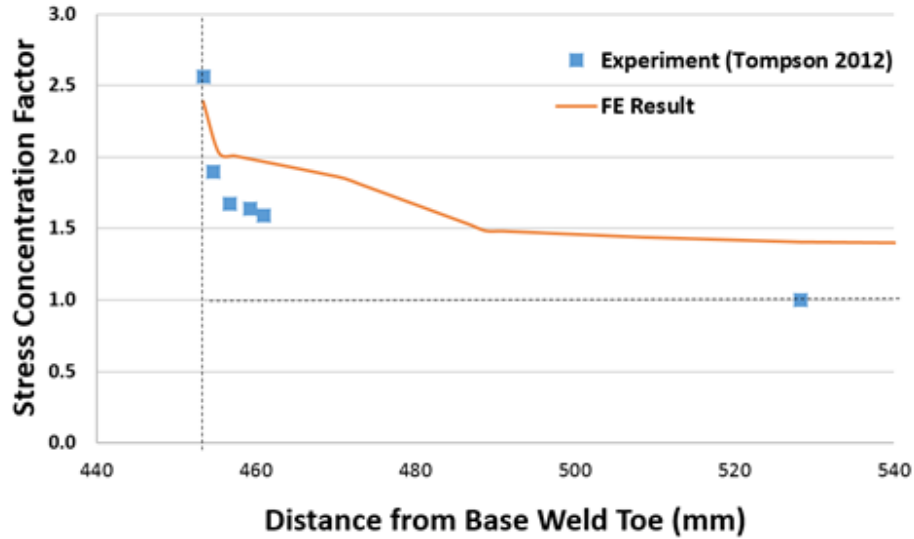
Figure 4.8 Stress Concentration Factor (SCF) at the top of stiffeners to the post

The SCF at the base weld connecting the base plate to the post is shown in Fig. 4.9. Results from the FE analysis showed that the SCF at the base weld was about 3.0 compared to SCF of about 3.7 from experimental results. The higher SCF from experimental results may be attributed to residual stresses which the FE model does not take account. As shown in Fig. 4.9, both stress patterns along the tube gradually decreased as distance from the base weld toe increased as expected.
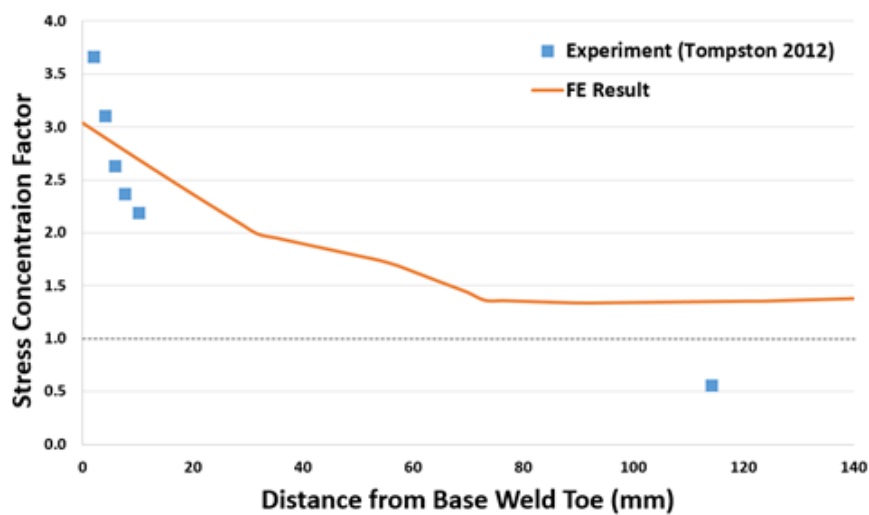
Figure 4.9. Stress Concentration Factor (SCF) at the base weld to the post

4.3 Results and Discussion

4.3.1 FE Analysis Results

In the static FE model, the local principle stresses at the fatigue critical locations were evaluated by altering the base plate thickness, the number of stiffeners and the boundary conditions. The plate thickness varied from 1.5 inch (38.1 mm) to 3 inch (76.2 mm). The number of stiffeners evaluated were: eight, four, two, and no stiffneres. Two boundray conditions were invesitgated: a fixed boundary at the base plate and partially fixed boundary at the base plate. The fixed condition was modeled as mast-arm fixed connection while the partially the fixed boundary was simulated by using fixed support conditions on the bottom and side of the bolts connecting the base plates to the foundation.

The input data into the ANSYS FE model include the following: the stress range and number of cycles of the detail under the constant amplitude stress life analysis, and the fatigue design life. For this study, the proposed S-N curve for fatigue design was obtained from the synthethic fatigue testing data analysis by considering the characerics of the connection such as the base plate thickness, galvanazation, peening, and tube shape. Due to the fact that FE model was developed with a round tube, the test results for multi-sided tube (Group 3, 5, 7) were not cosidered as S-N data input into FE model. The base plate thickness for FE model was adjusted to 1.5 inch (38.1 mm) for Group 4, 6 and 8, respectively. An average plate thinckness of 30 specimen was 2.33 inch (56.6 mm) for Group 2 and 1.58 inch (40.1 mm) for Group 6. Table 4.2 shows base plate thickness from the experiments and the plate thickness used in the FE model.

Table 4.2 Base Plate Thickness for experiments and FE model

Base Plate Thinness	Base Plate Thinness

	(Experiments)	(FE model)
Group 1	50.8 mm	50.8 mm
Group 2	50.8 mm – 76.2 mm	50.8 mm
Group 4	38.1 mm	38.1 mm
Group 6	38.1 mm – 44.5 mm	38.1 mm
Group 8	38.1 mm	38.1 mm

For each run of the FE model, the following output was obtained: the fatigue damage, the factor of fatety, and the fatigue life. It is noted that the fatigue damage and safety factor have a range as the fatigue design life has a range of 10 to 20 million cycles. The advantage of usieng two fatigue resistance terms is the simplicity by representing fatigue performance while the stress range and number of cycles needs log-log space. The results will be presented in the form of contour plot as well as table format.

4.3.2 Static FE Analysis Results

Effect of base plate thickness

The first developed FE model has partially fixed boundary conditions, 50.8 mm (2 in) thick base plates and no stiffeners. The effect of the base plate thickness was evalauted for unstiffened fillet-welded connections by varying the thickness from 38.1 mm (1.5 in) to 76.2 mm (3 in). Under the constant applied focrce, the FE model results showed that there is an decrease in the local principal stress as the thickness of the base plate increased. The effect of the base plate thickness, the number of stiffeners, and boundary condition are summarized in Table 4.3.

Table 4.3 Effect of base plate thickness, number of stiffeners and boundary condition

Base Plate Thickness (mm)	Principal Stress (MPa)	Number of Stiffeners	Principal Stress (MPa)	Boundary Condition	Principal Stress (MPa)
38.1 mm (1.5 inch)	198.9	8	108.6	Partially fixed	185.8

50.8 mm (2 inch)	185.8	4	142.9	Fully fixed	119.9
63.5 mm (2.5 inch)	145.2	2 (side)	185.6		
76.2 mm (3 inch)	127.6	0	185.8		

Effect of the number of stiffeners

For a connection with eight stifferenrs, the maximum local principal stress dropped by 42 percent compared to the case with no stiffeners. The maximum principal stress in the unstiffened socket connection was at base toe while the stiffened connections showed the maximum principal stress at the tip of stiffeners. It is important to note that this FE model was developed with an optimized stiffener configuration that was introduced in the AASHTO-LRFD Specifcation (AASHTO, 2015) and also can minmize the local stress level at the base. For the case of the connection with four stiffeners, Table 4.3 shows that the the local principal stress at the base and the the tip of stiffener were similar. Fig. 4.10 shows the local principal stress at the base toe and at the tip of the stiffener for stiffened connections with different number of stiffener.
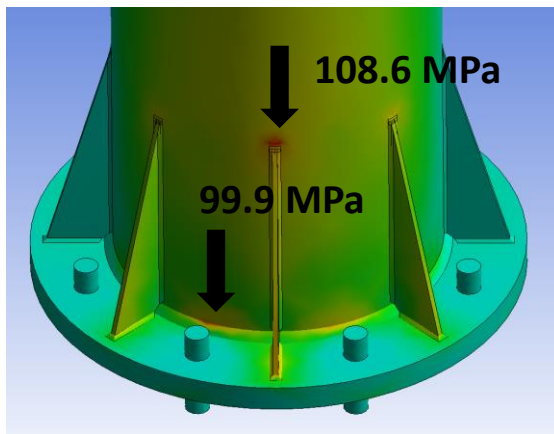
(a) Eight stiffeners   (b) Four stiffeners

(c) Two stiffeners (side)   (d) No stiffener
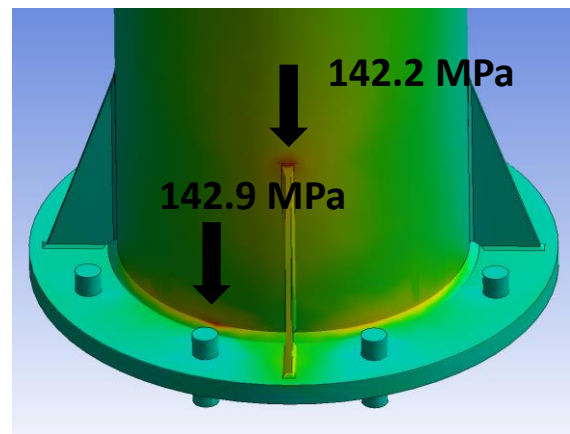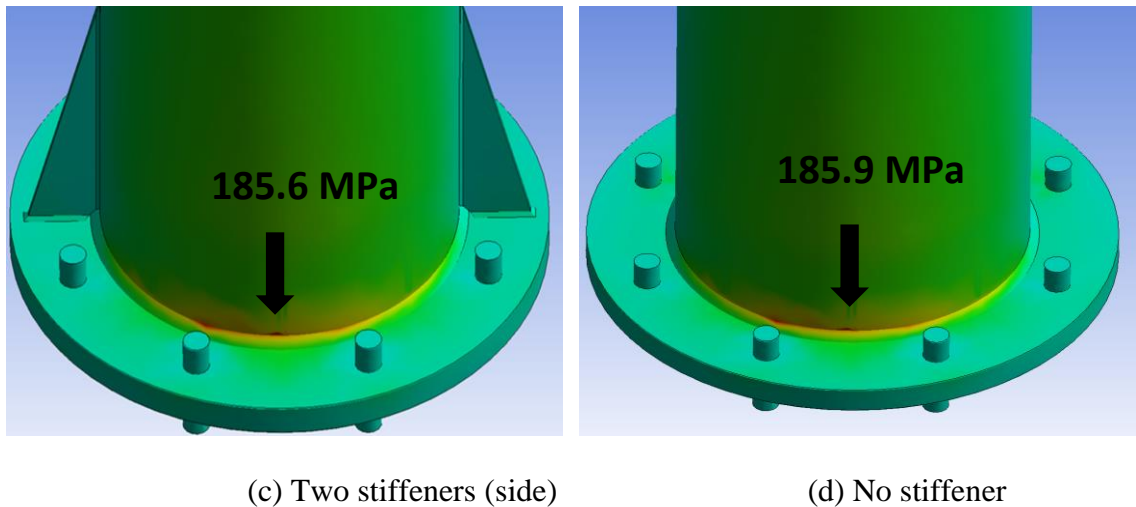
Figure 4.10 Local principal stress at the base and at the tip of the stiffener for stiffened

connections with different number of stiffeners

Effect of boundary conditions

As discussed earlier, two boundary conditions were investigated: fixed and partially

fixed conditions. It was observed that fully fixed condition mitigated significant level of

local principal stress at the base by enhancing the rigidity of the base plate as shown in

Tables 4.3 and 4.4. The FE model of the stiffened connection with eight stiffeners showed

a similar level of principal stress at the tip of stiffners for both partially fixed and fully

fixed conditions. At the base toe, the model showed the principal stress at the base tow was

significantly less that that at the tip of the stiffener.

The analysis resutls of the FE model of the stiffenned connection with four

stiffeners with partially fixed boundary condition showed similar local principal stresses at

both, the tip of stiffeners and at the base. When the boundary conditions are changed to

fully fixed boundary conditions, the principal stresses at base toe decreased. This is due to

completely restrained bottom side of base plate which enables to make the base plate more

rigid. Table 4.4 also shows a comparison of the principal stresses of stiffened connection with two stiffeners and unstiffened connection (zero stiffeners). The results show that the local principal stress at the base toe for the fixed condition is about 37 percent less than that of the partially fixed boundary condition for both connections.

Table 4.4 Effect of number of stiffeners and boundary condition on local principal stress

Number of Stiffeners	Boundary Condition	Locations	Principal Stress (MPa)
8	Partially fixed	Tip of stiffener	108.6
	Partially fixed	Base	99.9
	Fully fixed	Tip of stiffener	110.2
	Fully fixed	Base	53.8
4	Partially fixed	Tip of stiffener	142.2
	Partially fixed	Base	142.9
	Fully fixed	Tip of stiffener	133.9
	Fully fixed	Base	69.9
2	Partially fixed	Base	185.6
	Fully fixed	Base	119.8
0	Partially fixed	Base	185.9
	Fully fixed	Base	119.9

4.3.3 Fatigue FE Analysis Results

As discussed earlier, the S-N curve from synthetic data regression analysis and fatigue design life were used as input variables for fatigue module in the ANSYS Workbench platform. In this study, only the test groups that have a round shape tube were considered. The base plate thickness was 38.1 mm (1.5 in) for test Group 4, 6 and 8, respectively. For a constant applied force of 4.45 kN (1 kip) at the top of the round tube,

the resutling local principal stresses and fatigue resistances were determined. Figure 4.11 (a), 11 (b), and 11 (c) show the contour plots of fatigue resistance outputs for fatigue life, fatigue damage and fatigue safety factor for the unstiffened connection, respectively. The fatigue life represents the number of cycles corresponding to the local principal stress while fatigue damage represents the ratio of the design life to the available life. When the fatigue damage is greater than 1.0, this indicates that fatigue failure has occurred before its intended design life. The fatigue safety factor represents the factor of safety for fatigue failure at a given design life. When the safety factor is less then 1.0, that means failure has occurred before reaching its intended design life.

(a) Fatigue Life   (b) Fatigue Damage
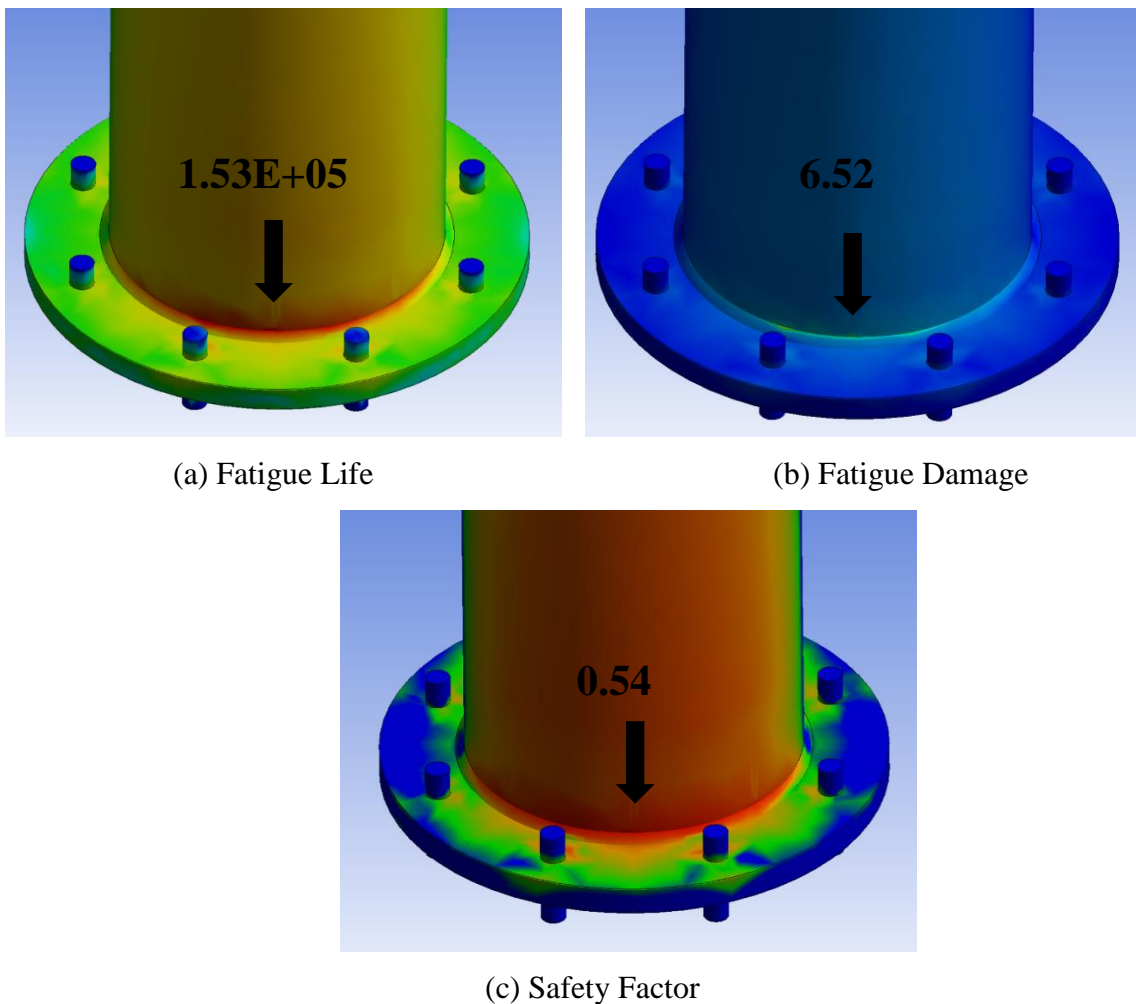
(c) Safety Factor

Figure 4.11 Fatigue life, fatigue damage and safety Factor for the unstiffened connection

Effect of Galvanization

To evaluate an effect of galvanizations on fatigue resistance, the S-N curve from the synthetic analysis of the test data of Groups 1 and 2 were used for model input. Groups 1 and 2 have plate thicknesses greater than 2 inch with a round tube and no peening treatment. Results from the FE analysis showed that without galvanization (Group 1), a fatigue life of 1.53E+05 cycles was achieved with stress range of 53.1 MPa compared 9.70E+04 cycles was obtained with galvanization (Group 2). This shows that the fatigue resistance (fatigue life, damage and safety factor) were reduced due to the galvanization and fatigue design life of 10 million cycles for Group 1 and 2 was increased from 6.52 to 10.31. On the other hand, the safety factor decreased from 0.54 to 0.46. Similar trend was observed for Group 4 and 6 which has the plate thinness of 38.1 mm (1.5 in). The FE results using input data from Groups 4 and 6 showed a fatigue life of 2.53E+05 and 3.31E+04, respectively. Table 4.5 shows the stress range and fatigue resistance of each group.

Effect of Peening Treatment

The peening surface treatment showed an improvement of fatigue resistance of the socket connection details. The analysis results were compared with Group 4 and 8 which have plate thickness is less than 2 inch with a round tube and not galvanized. With a stress range of 56.9 MPa, fatigue life of 2.53E+05 and 2.81E+05 cycles were obtained for input data from Groups 4 and 8?respectively. As such, the resulting fatigue damage and safety factor values showed that peening treatment has enhanced the fatigue resistance.

Effect of base plate thickness and boundary conditions

The base plate thickness was an important parameter that affects the fatigue performance of socket connections. The thickness of base plate was adjusted for FE model for the sake of comparing Groups 1 and 4, and Groups 2 and 6. It was anticipated that there are reductions in fatigue resistance for the specimen that has a thin base plate. However, Group 4 showed a higher fatigue resistance in terms of fatigue life, damage and safety factor compared to Group 1 which has a larger thickness. This result was unexpected and may be attributed to workmanship, weld quality, inherent defects and others. Future tests and analyses may be needed to verify this result. For Group 6 , which has galvanized connections, a lower fatigue resistance was observed with base plate thickness of 38.1 mm as compared to Group 2.

For the fully fixed boundary condition, the fatigue resistance of all groups improved by achieving a lower stress range. In the case of Group 6, a fatigue life of (3.31E+04) was obtained with partially fixed condition while a higher fatigue life (3.99E+05) was observed with fully fixed condition. In addition to the effect of base plate thickness, this result also can be compared to fatigue life of 9.70E+04 where base plate thickness was increased to 50.8 mm. Fig. 9 summarizes the effects of the base plate, number of stiffeners, and boundary conditions on fatiue life, fatigue damage, and safety factor for the various test groups.

Table 4.5 Effect of base plate, number of stiffeners, and boundary conditions on fatigue life, fatigue damage, and safety factor

Group	Base Plate Thickness (FE model)	Boundary Condition	Stress Range	Life	Damage	Safety Factor

1	50.8 mm	Partially Fixed	53.1 MPa	1.53E+05	6.52 – 13.05	0.54 – 0.42
		Fully Fixed	34.3 MPa	7.51E+05	1.33 – 2.66	0.91 – 0.72
2	50.8 mm	Partially Fixed	53.1 MPa	9.70E+04	10.31 – 20.62	0.46 – 0.36
		Fully Fixed	34.3 MPa	4.75E+05	2.11 – 4.21	0.78 – 0.62
4	38.1 mm	Partially Fixed	56.9 MPa	2.53E+05	3.95 – 7.89	0.63 – 0.50
		Fully Fixed	27.9 MPa	3.05E+05	0.33 – 0.66	1.45 – 1.15
6	38.1 mm	Partially Fixed	56.9 MPa	3.31E+04	30.2 – 60.5	0.32 – 0.25
		Fully Fixed	27.9 MPa	3.99E+05	2.51 – 5.02	0.74 – 0.58
8	38.1 mm	Partially Fixed	56.9 MPa	2.81E+05	3.56 – 7.12	0.65 – 0.52
		Fully Fixed	27.9 MPa	3.39E+06	0.29 – 0.59	1.50 – 1.19

CHAPTER V

MODIFIED STRAIN-LIFE SMITH-WATSON-TOPPER (SWT) CORROSION MODEL

In this chapter, a modified Strain-Life Smith-Watson-Topper (SWT) corrosion model is developed for fillet-welded connection details of highway sign support structures. Chemical components and material properties of corrosion-resistant weathering steel and low-carbon steel were investigated using ASTM specifications. To estimate the corrosion

resistance, corrosion Index, *I*, was obtained by following the equations from ASTM G101 Standard (ASTM G101, 2004). Hot-dip galvanized steel which protects from corrosion by forming the zinc patina was also studied to determine the corrosion resistance. Strain-life fatigue coefficients and a modified strain-life corrosion model was developed and will be described in the following sections. Results from the developed model include a range for the Constant Amplitude Fatigue Thresholds (CAFT) for various corrosion categories.

5.1 Chemical Composition and Material Properties of ASTM Steels

ASTM A595 and A572 are specified as steel materials for structural supports for highway signs, luminaires, and traffic signals according to AASHTO (AASHTO 2015). To use the strain-life corrosion fatigue life prediction model for ASTM A588 Grade B weathering steel (Aghoury and Galal, 2014) for structural supports, the chemical requirements and material properties are investigated herein.

ASTM A595 Grades A and B low-carbon steel or high-strength low-alloy steel composition are used. A595 Grade C steel has weather-resistance steel composition and it has the same chemical compositions as A588 steels. Another type of structural steel used for support structures is high-strength low-alloy columbium-vanadium A572 steel structural steel (ASTM A572, 2015). Nickel (Ni), copper (Cu) and chromium (Cr) are the key components for the weathering steel that provides higher corrosion resistance (ASTM A588, 2004). Chemical requirements of ASTM A588, A595 and A572 are summarized in Table 5.1. Certain chemical elements such as silicon (Si) and phosphorus (P) affect hot-dip galvanizing and zinc coating by prolonging the reaction between iron and molten zinc in the surface (ISO 14713-2, 2009).

Table 5.1 Chemical Requirements of ASTM A588, A595 and A572

Designation	Grade	C	Mn	Si	P	S	Cr	Ni	Cu
ASTM A588	Grade A	0.19	0.18-1.25	0.30-0.65	0.03	0.03	0.40-0.65	0.4	0.25-0.40
	Grade B	0.20	0.75-1.35	0.15-0.50	0.03	0.03	0.40-0.70	0.5	0.20-0.40
ASTM A595	Grade A	0.15-0.25	0.30-0.90	0.060	0.035	0.035	-	-	-
	Grade B	0.15-0.25	0.40-1.35	0.060	0.035	0.035	-	-	-
	Grade C	0.19-0.22	0.50-1.35	0.15-0.65	0.04	0.05	0.40-0.70	0.5	0.20-0.50
ASTM A572	Grade 42 - 65	0.21-0.26	1.35	0.15-0.40	0.03	0.03	-	-	-

With respect to the material properties of ASTM steels, the yield strength, ultimate tensile strength, and elongation are obtained from ASTM Standard Specifications (ASTM A595, 2014; ASTM A588, 2015; ASTM A572, 2015) and it is summarized in Table 5.2. These properties will be used to determine fatigue coefficients for strain-life analysis using the uniform material law (Baumel and Seeger, 1990).

Table 5.2 Material properties and corrosion-resistance index of weathering and low-carbon steel

Designation	Grade	Yield strength (MPa)	Ultimate tensile strength (MPa)	Elongation (%)	Corrosion-Resistance Index 6.3.1	Corrosion-Resistance Index 6.3.2
ASTM A588	Grade A	345	485	21	5.07-6.86	5.53-7.74
	Grade B	345	485	21	5.07-6.86	5.53-7.74
ASTM A595	Grade A	380	450	23	0.13-0.69	0.68-1.57
	Grade B	410	480	21	0.13-0.69	0.89-2.35
	Grade C	410	480	21	5.07-6.86	5.53-7.74
ASTM A572	Grade 42	290	415	24	0.74-1.11	2.80-3.78
	Grade 50	345	450	21	0.74-1.11	2.83-3.81
	Grade 55	380	485	20	0.74-1.11	2.85-3.83
	Grade 60	415	520	18	0.74-1.11	3.84
	Grade 65	450	550	17	0.74-1.11	4.15

5.2 Corrosion Resistance Index – ASTM G101

ASTM G101 Standard (ASTM G101, 2004) provides the guide to estimate the atmospheric corrosion resistance of low-alloy weathering steels. The corrosion-resistance index, I, can be obtained by utilizing the chemical composition of the steel. In section 6.3.1

of ASTM G101, the modified Legault-Leckie equation is introduced from the industrial atmospheric exposure test data (Legault and Legault, 1974). Based on statistical analysis of the effects of chemical composition, the averaged corrosion-resistance index can also be calculated using the corrosion loss data from three different locations (Townsend, 1999).

Using both methods, the corrosion-resistance indices are obtained in the form of range of values to evaluate the corrosion resistance of various ASTM steels used for highway signs, luminaires, and traffic signals. Weathering steels such as A558 and A595 Grade C have higher corrosion indices as compared to low-carbon steels. Since higher index values represent greater corrosion resistance, it is expected to observe lower reductions in fatigue resistance of weathering steels compared to low carbon steels. Obtaining corrosion indices for hot-dip galvanized steel was not possible because ASTM G101 does not provide guidelines for calculating corrosion index for hot-dip galvanizing steel similar to those given for weathering steel and low carbon steel.

5.3 Hot-Dip Galvanization and Weathering Steel

Hot-dip galvanization protects corrosion by forming the zinc patina as well as providing cathodic protection. According to the American Galvanizers Association (AGA), hot-dip galvanized steel is produced by immersing steel in a bath of molten zinc. During the dipping process, a protective coating is developed by a metallurgical reaction between iron and zinc and a tightly-bonded alloy coating provides cathodic protection (American Galvanizers Association, 2012).

Weathering steel is known as corrosion-resistance steel and the presence of the rust layers produces a protective barrier that prevents further oxidation of the metal. Weathering

steel contains chemical components such as nickel (Ni), copper (Cu) and chromium (Cr) that provides higher corrosion resistance as compared to low-carbon steel (ASTM G101, 2004). However, weathering steel exhibits accelerated corrosion when frequent high humidity or fog conditions exist (American Galvanizers Association, 2012). Although hot-dip galvanization protects corrosion, it was observed that the fatigue resistance was reduced for galvanized steel (Ocel, 2014). The same result was also found in Chapter 3, the synthetic data analysis results. Unstiffetic socket connection details groups are used in the strain-life fatigue analysis in this chapter. The strain-life fatigue analysis will be applied to connections made of hot-dip galvanized steel, weathering steel or low-carbon steel in the light of different corrosion categories.

5.4 Strain-Life Model Development

5.4.1 Strain-Life Fatigue Coefficients

In strain-life fatigue analysis, the total strain is composed of two parts: the elastic strain region and plastic strain region. The cyclic stress-strain behavior is represented by the Ramberg-Osgood relationship expressed in equation 5.1:

$$\varepsilon_{total} = \varepsilon_e + \varepsilon_p = \frac{\sigma}{E} + (\frac{\sigma}{K'})^{1/n'} \qquad (5.1)$$

Where E is Young's modulus. n' is a measurement of the material's working hardening behavior and K' represents cyclic strength coefficient (Ramberg and Osgood, 1943). While the cyclic properties are determined from the stress-strain response, the fatigue properties can be obtained from the steady-state hysteresis loops. The total strain amplitude can be resolved into an elastic and plastic strain components and curves for both elastic and plastic strains are fitted separately as straight lines as shown in Figure 5.1. At large strains, the plastic strain component is predominant but the elastic strain is

predominant at small strains. The intercepts of the two straight lines at $2N_f = 1$ are the elastic component and plastic component of the strain. This is represented by equation 5.2 (Morrow, 1968):

$$\varepsilon_a = \frac{\Delta\varepsilon}{2} = \frac{\Delta\varepsilon_e}{2} + \frac{\Delta\varepsilon_p}{2} = \frac{\sigma'_f}{E}(2N_f)^b + \varepsilon'_f(2N_f)^c \qquad (5.2)$$

Where ε'_f is the fatigue ductility coefficient and σ'_f is the fatigue strength coefficient. The factors b and c represents the slopes of the elastic and plastic lines respectively.
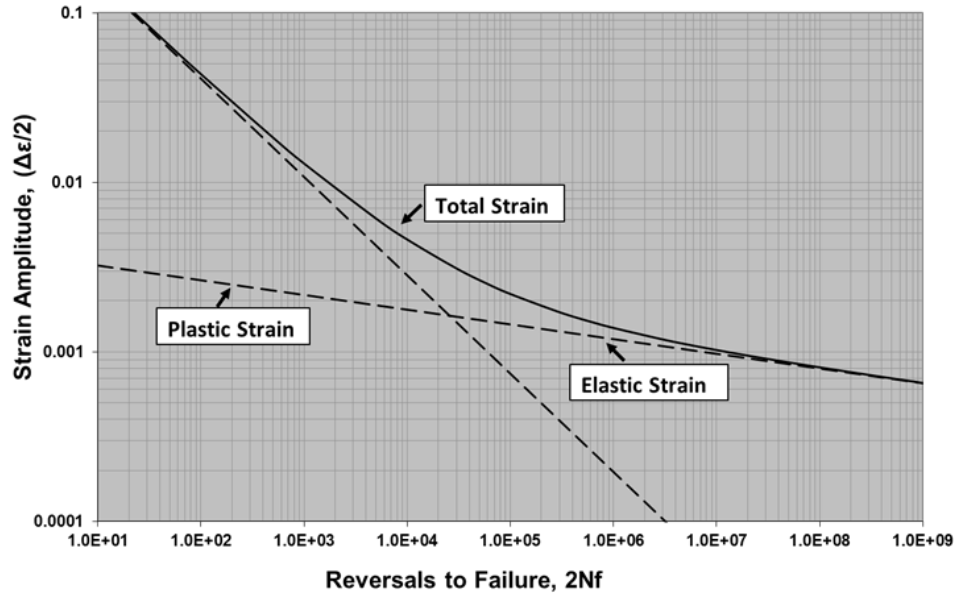
Fig. 5.1 Strain amplitude versus reversals to failure for A595 Grade C

Using the uniform material law (Baumel and Seeger, 1990), coefficients for strain life analysis were obtained. For example, when using ASTM A595 Grade C weathering steel for tube-to-transverse connection details, the Young's Modulus, the yield strength, the ultimate tensile strength and the elongation were 200,000 MPa, 410 MPa, 480 MPa and 21 percent, respectively. The coefficients needed for strain-life analysis: K', n', σ_f', b, ε_f',

and c were obtained using the uniform material law from uniaxial tensile test results for smooth specimens. In this study, the strain-life coefficients were obtained by fitting the curve for the notches at tip toe of fillet-welding that raise localized stress concentration. These values were the following: $K' = 1400$ MPa, $n' = 0.15$, $\sigma_f' = 720$ MPa, $b = -0.087$, $\varepsilon_f' = 0.59$ and $c = -0.58$. Figure 5.1 shows the strain amplitude versus reversals to failure for A595 Grade C steel.

5.4.2 Smith-Watson-Topper (SWT) Corrosion Model

To take into account the long-term corrosion effect, a recent study (Aghoury and Galal, 2014) proposed the strain-life corrosion model using the Smith-Watson-Topper (SWT) equation (Smith et al. 1970). This model was validated through the experimental work (Albrecht and Shabshab, 1994) with A588 Grade B steel. In their experimental work, twenty four (24) rolled beams were weathered for five to six years and were boldly exposed to air, moist freshwater, and sprayed with a salt solution to simulate the use of deicing salts. The results obtained for the expected life for each specimen are presented as a range of values and a good agreement was observed using their strain-life corrosion model (Aghoury and Galal, 2014). The modified SWT strain-life corrosion model (Aghoury and Galal, 2014) can be written as shown in equation (5.3):

$$\varepsilon_a \sigma_{max} = \varepsilon_a(\sigma_a + \sigma_m) = \frac{(\sigma'_f)^2}{E}(2N_f)^{2b'} + \sigma'_f \varepsilon'_f (2N_f)^{b'+c'} \quad (5.3)$$

Where σ_{max} is maximum applied tensile stress which is obtained by adding stress amplitude, σ_a and mean stress, σ_m. In the SWT model, it is assumed that the SWT parameter defined as the strain energy density remains constant with different combinations of the strain amplitude and the maximum stresses for a given life (Stephens et al., 2000). To take into account the corrosion effects, new factors b' and c' are

introduced and are defined in equation (5.4) and (5.5):

$$b' = b(1 + \gamma_{corr}\gamma_\alpha\alpha_b) \quad (5.4)$$

$$c' = c(1 + \gamma_{corr}\gamma_\alpha\alpha_c) \quad (5.5)$$

According to ISO-9224 (International Organization for Standardization) (ISO, 1992; ISO, 2012), the corrosion factors, γ_α represent the average corrosion rate and the high corrosion penetration rates yield higher value of γ_{corr} as compared to unity environmental condition corresponding to an upper limit exposure to 3,5% NaCL solution for typical fatigue tests (Aghoury and Galal, 2014). To evaluate the modified SWT strain-life corrosion model, the highest values corresponding to the worst environmental case are used for each corrosion category. Based on examining several values for the γ_α factor (Aghoury and Galal, 2014), the range of the values of ± 0.05 proved to result in more accurate fatigue life predictions. Table 5.3 summarizes the γ_α values for hot-dipped zinc galvanized steel, weathering steel, and low-carbon steel from ISO 1992. In this study, the maximum values of γ_α and γ_{corr} were selected for each corrosion category.

Table 5.3 γ_α values for hot-dip galvanized, weathering and carbon steel (ISO 9224, 1992)

Corrosion Category	γ_α, Average corrosion rate (um/year)		
	Hot-dip galvanized Steel	Weathering Steel	Low Carbon Steel
C1	$\gamma_\alpha \leq 0.1$	$\gamma_\alpha \leq 0.1$	$\gamma_\alpha \leq 0.5$
C2	$0.1 < \gamma_\alpha \leq 0.5$	$0.1 < \gamma_\alpha \leq 2$	$0.5 < \gamma_\alpha \leq 5$
C3	$0.5 < \gamma_\alpha \leq 2$	$2 < \gamma_\alpha \leq 8$	$5 < \gamma_\alpha \leq 12$
C4	$2 < \gamma_\alpha \leq 4$	$8 < \gamma_\alpha \leq 15$	$12 < \gamma_\alpha \leq 30$
C5	$4 < \gamma_\alpha \leq 10$	$15 < \gamma_\alpha \leq 80$	$30 < \gamma_\alpha \leq 100$

The two corrosion material constants $\alpha_b = 0.182$ and $\alpha_c = 0.034$ proposed by Aghoury and Galal (2014) were also used in this study (Aghoury and Galal, 2014). It should be noted that these factors were derived from a two-year JIS-JMS weathering steel fatigue test data (Kunihiro et al., 1972). Therefore, future experimental fatigue data needed

is required to update and adjust the corrosion material constants for the low-carbon steel. The descriptions of the proposed γ_{corr} for each corrosion category are summarized in Table 5.4 (ISO 14713-1, 2009; Aghoury and Galal, 2014). The SO_2 compound represents the concentration of sulfur dioxide in a particular steel.

Table 5.4 Corrosion categories and Proposed γ_{corr} (ISO 14713-1, 2009; Aghoury and Galal, 2014)

Corrosion Category	Corrosivity	Descriptions	Proposed γ_{corr}
C1	Very Low	Dry or cold zone, atmospheric environment with very low pollution and time of wetness	$0 < \gamma_{corr} \leq 0.09$
C2	Low	Temperature zone, atmospheric environment with low pollution ($SO_2 < 5$ ug/m^3)	$0.09 < \gamma_{corr} \leq 0.29$
C3	Medium	Temperate zone, atmospheric environment with medium pollution (SO_2: 5 ug/m^3 to 30 ug/m^3)	$0.29 < \gamma_{corr} \leq 0.47$
C4	High	Temperate zone, atmospheric environment with high pollution (SO_2: 30 ug/m^3 to 90 ug/m^3)	$0.47 < \gamma_{corr} \leq 0.57$
C5	Very High	Temperate and subtropical zones, atmospheric environment with very high pollution (SO_2: 90 ug/m^3 to 250 ug/m^3)	$0.57 < \gamma_{corr} \leq 1.00$

5.5 Results and Discussions

In this section, the analysis procedure for the SWT corrosion model for the AASHTO Fatigue Categories and the results from the synthetic data analysis as well as results and discussions will be presented. The strain-life SWT corrosion model flowchart is illustrated in Figure 5.2.
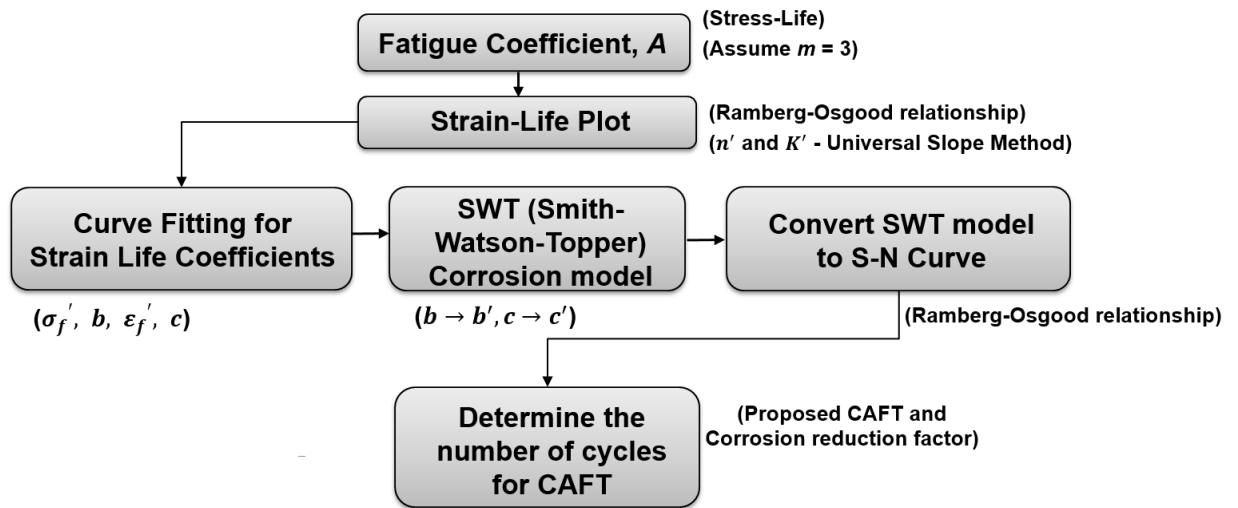
Figure 5.2 A Strain-life SWT corrosion model flowchart

5.5.1 Evaluation of Fatigue Resistance for AASHTO Categories

To evaluate the modified SWT strain corrosion model, AASHTO Fatigue Categories which indicate fatigue design limits or thresholds were plotted on strain-life plot. The y axis represents the strain amplitude and the x axis represents the reversals to failure. The Ramberg-Osgood relationship which was described in equation (5.1) was used in developing the strain-life plots. The fatigue coefficients *K'* and *n'* were obtained using the universal material method (Baumel and Seeger, 1990). The obtained cyclic strength coefficient *K'* was 1400 MPa (203 ksi) and the cyclic strain hardening component *n'* was 0.15. These coefficients are used to obtain the plots in Figure 5.3.
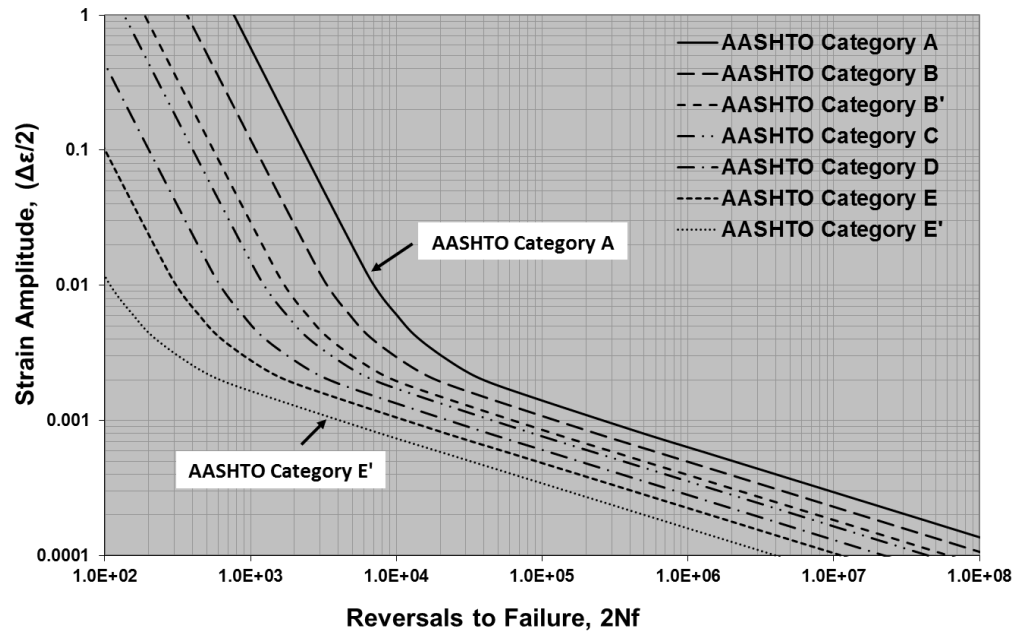
Figure 5.3 Strain amplitude versus reversals to failure for AASHTO categories

Strain-life coefficients b and c which determine the slope of the strain-life curve for the elastic and plastic curves were obtained by fitting the two curves curve. The values for b and c were -0,33 and -2.25 respectively. It is worth noting here that the obtained values of b and c are applicable to all other AASHTO Categories. The proposed modification corrosion factors γ_{corr} for hot-dip galvanized steel, weathering steel, and low-carbon steel were calculated using equations (5.4) and (5.5) and are and it is summarized in Table 5.5.

Table 5.5 Corrosion factors for hot-dip galvanized, weathering and low-carbon steel

Hot-dip galvanized Steel / Category	b	b'(min)	b'(max)	c	c'(min)	c'(max)	$\gamma_{corr}\gamma_\alpha$(min)	$\gamma_{corr}\gamma_\alpha$(max)
C1	-0.330	-0.33	-0.33	-2.25	-2.25	-2.25	0.00	0.01
C2	-0.330	-0.34	-0.34	-2.25	-2.26	-2.26	0.12	0.17
C3	-0.330	-0.38	-0.39	-2.25	-2.31	-2.33	0.84	1.04
C4	-0.330	-0.45	-0.48	-2.25	-2.41	-2.44	2.08	2.48
C5	-0.330	-0.90	-0.96	-2.25	-2.98	-3.05	9.50	10.50
Weathering Steel/ Category	b	b'(min)	b'(max)	c	c'(min)	c'(max)	$\gamma_{corr}\gamma_\alpha$(min)	$\gamma_{corr}\gamma_\alpha$(max)

	b	b'(min)	b'(max)	c	c'(min)	c'(max)	$\gamma_{corr}\gamma_{\alpha}$(min)	$\gamma_{corr}\gamma_{\alpha}$(max)
C1	-0.330	-0.33	-0.33	-2.25	-2.25	-2.25	0.00	0.01
C2	-0.330	-0.36	-0.37	-2.25	-2.29	-2.30	0.48	0.68
C3	-0.330	-0.53	-0.58	-2.25	-2.51	-2.57	3.36	4.16
C4	-0.330	-0.79	-0.89	-2.25	-2.85	-2.96	7.80	9.30
C5	-0.330	-4.89	-5.38	-2.25	-8.06	-8.68	76.00	84.00
Low-Carbon Steel/ Category	b	b'(min)	b'(max)	c	c'(min)	c'(max)	$\gamma_{corr}\gamma_{\alpha}$(min)	$\gamma_{corr}\gamma_{\alpha}$(max)
C1	-0.330	-0.33	-0.33	-2.25	-2.25	-2.26	0.02	0.07
C2	-0.330	-0.40	-0.43	-2.25	-2.34	-2.38	1.20	1.70
C3	-0.330	-0.63	-0.70	-2.25	-2.64	-2.73	5.04	6.24
C4	-0.330	-1.27	-1.45	-2.25	-3.44	-3.67	15.60	18.60
C5	-0.330	-6.04	-6.64	-2.25	-9.52	-10.28	95.00	105.00

For AASHTO Category E, a modified SWT strain-life equation presented by Aghoury and Galal (2014) was utilized to account for the corrosion effects for category C2 for hot-dip galvanized steel, weathering steel and low carbon steel as shown in Figure 5.4. In the SWT plot in Figure 4, the y axis represents the strain energy density defined as the strain amplitude multiplied by the maximum applied stress. As expected, significant reductions in fatigue life were observed for low-carbon steel while for hot-dip galvanized steel the reduction in fatigue life was not significant.
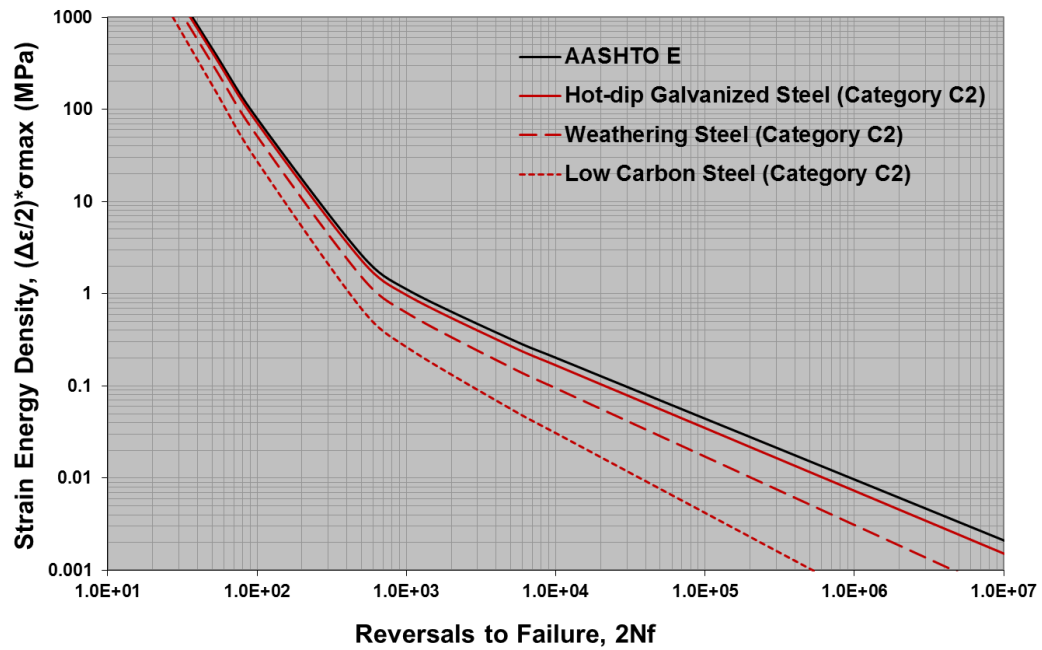
Figure 5.4 Corrosion effects on AASHTO fatigue category E for steel designation C2

To convert a modified SWT stain-life plot to a stress-life plot, the total strain which is obtained by using the Ramberg-Osgood relation (Ramberg and Osgood, 1943) is transferred to a stress range with a cyclic strength coefficient K' of 1400 MPa (203 ksi) and a cyclic strain hardening exponent n' of 0.15, respectively. Using fatigue coefficient A and slope m of 3 from the AASHTO Specification, the number of cycles that can achieve infinite fatigue life were determined. The proposed CAFT range for each corrosion category is summarized in Table 5.6. The abbreviations HGS, WS, and LS represent Hot-dip Galvanized Steel, Weathering Steel, and Low-carbon Steel, respectively.

Table 5.6 Proposed CAFT range for AASHTO categories

Fatigue Category		E'	E	D	C	B	A
CAFT (AASHTO)	HGS, WS, and LS	2.6 ksi	4.5 ksi	7 ksi	10 ksi	16 ksi	24 ksi
Proposed CAFT (C1)	HGS	2.58 – 2.58	4.45 – 4.47	6.95 – 6.98	9.89 – 9.95	15.8 – 15.9	23.6 – 23.8
	WS	2.58 – 2.58	4.45 – 4.47	6.95 – 6.98	9.89 – 9.95	15.8 – 15.9	23.6 – 23.8
	LS	2.54 – 2.58	4.33 – 4.44	6.73 – 6.92	9.56 – 9.86	15.2 – 15.7	22.7 – 23.5
Proposed CAFT (C2)	HGS	2.48 – 2.51	4.17 – 4.24	6.38 – 6.55	8.98 – 9.26	14.2 – 14.7	21.1 – 21.9
	WS	2.19 – 2.30	3.37 – 3.64	4.95 – 5.44	6.72 – 7.50	10.2 – 11.6	14.9 – 17.0
	LS	1.76 – 1.96	2.41 – 2.81	3.31 – 3.97	4.21 – 5.20	5.84 – 7.53	8.12 – 10.7
Proposed CAFT (C3)	HGS	2.03 – 2.12	2.95 – 3.17	4.24 – 4.61	5.61 – 6.19	8.23 – 9.24	11.8 – 13.4
	WS	1.05 – 1.24	1.35 – 1.60	1.75 – 2.09	2.07 – 2.50	2.52 – 3.13	3.18 – 4.04
	LS	0.69 – 0.88	0.89 – 1.13	1.16 – 1.46	1.35 – 1.72	1.62 – 2.06	1.99 – 2.56
Proposed CAFT (C4)	HGS	1.49 – 1.69	1.97 – 2.17	2.62 – 2.94	3.21 – 3.66	4.20 – 4.92	5.61 – 6.72
	WS	0.37 – 0.50	0.49 – 0.65	0.65 – 0.86	0.77 – 1.01	0.92 – 1.21	1.14 – 1.49
	LS	0.05 – 0.10	0.08 – 0.14	0.11 – 0.20	0.14 – 0.24	0.17 – 0.30	0.23 – 0.38
Proposed CAFT (C5)	HGS	0.29 – 0.36	0.39 – 0.47	0.52 – 0.61	0.61 – 0.73	0.73 – 0.89	0.92 – 1.10
	WS	0.00 – 0.00	0.00 – 0.00	0.00 – 0.00	0.00 – 0.00	0.00 – 0.00	0.00 – 0.00
	LS	0.00 – 0.00	0.00 – 0.00	0.00 – 0.00	0.00 – 0.00	0.00 – 0.00	0.00 – 0.00

As expected, HGS that has a zinc coating layer showed the best corrosion protection by achieving the highest proposed CAFT values for all AASHTO categories. Under the corrosion category 1, no significant reductions were observed in both HGS and WS. However, under the severe corrosion environments such as category 3 and 4, significant reductions in fatigue life were observed in both WS and LS. For corrosion Category C5 which has a 3.5 percent of NaCL solution environment in subtropical area with atmospheric environment of very high pollution, the CAFT values from the proposed analysis were very small number as if indicating not alternative designs should be considered or additional protective measures form the severe corrosion should be implemented.

5.5.2 Evaluation of Fatigue Resistance for the Synthetic Data Analysis

To estimate the effects of surface treatments such as hot-dip galvanized or zinc coating, the synthetic data analysis results were used. Based on the regression analysis results of existing test data for unstiffened fillet-welded socket connection (Koenigs, 2003; Stam et al., 2011; Ocel 2014), the mean minus two standard deviation regression lines were shifted down slightly to establish a lower bound. With a 2.3 percent probability of failure and assuming the fatigue life logarithms to be normally distributed (Fisher et al. 1998 and Schneider and Maddox, 2003), this approach is commonly used for design purposes.

According to the synthetic data analysis results in Chapter 3, the unstiffened fillet-welded socket connection details were grouped to take into account the parameters that significantly influence the fatigue resistance. Group 1 represents non-galvanized round tube shape specimens that has plate thicknesses greater than 50.8 mm (2 inch). Group 2 has the same condition as Group I except that the surface treatment has zinc bath coating. The fatigue coefficients A were obtained as 1.04E+08 for Group 1 and 6.58E+07 for Group 2, respectively.

The corrosion coefficient factors from ISO coefficients (ISO 9224, 1992) and following the proposed the corrosion factors by Aghoury and Galal (2014) were used to implementation of the SWT corrosion model. The number of cycles was set at 10 million cycles to achieve infinite fatigue life (Puckett et al. 2014). Figure 5.5 shows the S-N curves for Groups 1 and 2 with the corresponding CAFT values.
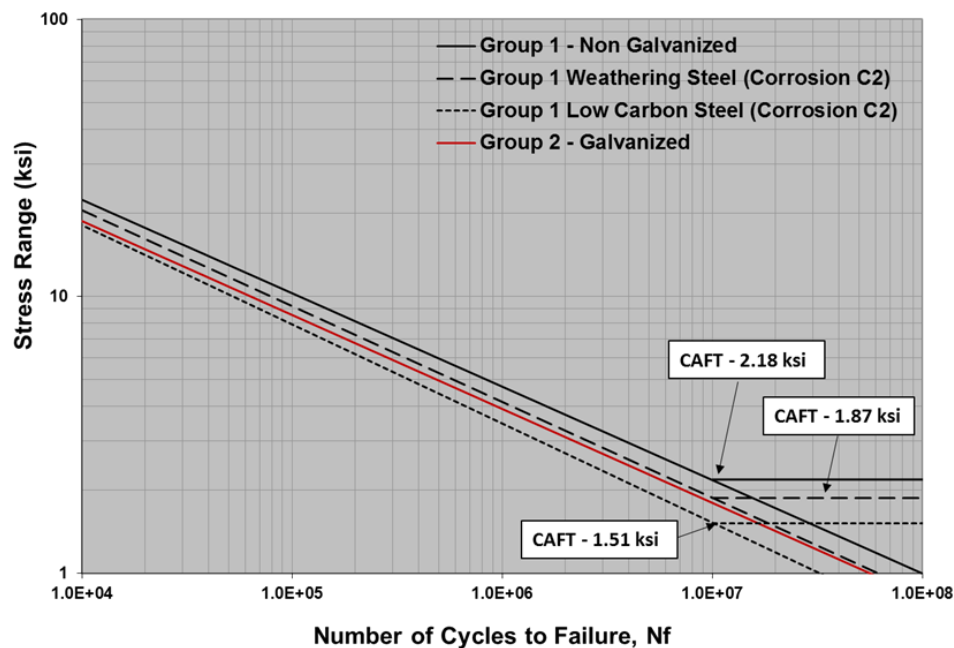
Figure 5.5 S-N curve for Group 1 and 2 with proposed CAFTs

The results for Group 1 test data which has non-galvanized socket connection shows CAFT value of 2.18 ksi. Under corrosion category C2, the CAFT values of the WS and LS decreased to 1.88 ksi and 1.52 ksi respectively. The results for Group 2 which has Galvanized, zinc coated specimens are also plotted to compare with the non-galvanized specimens exposed the corrosion environment. As obtained in Chapter 3, CAFT Group 2 is 1.88 ksi. As observed in Figure 5.5, a CAFT value of 1.87 ksi was obtained for the non-galvanized weathering steel under C2 corrosion conditions. Based on these observations and results, it seems that weathering steel is not recommended for locations with corrosion Categories from C3 to C5. For these situations, it may advised to have galvanization treatments for the steel components. Table 5.7 summarized the obtained CAFT values for Group 1.

Table 5.7 Proposed CAFTs for Group 1

Fatigue Category		Group 1
CAFT (No Corrosion)	WS	2.18
	LS	
Proposed CAFT (C1)	WS	2.16 – 2.17
	LS	2.14 – 2.16
Proposed CAFT (C2)	WS	1.88 – 1.96
	LS	1.52 – 1.68
Proposed CAFT (C3)	WS	0.94 – 1.10
	LS	0.63 – 0.79
Proposed CAFT (C4)	WS	0.35 – 0.46
	LS	0.06 – 0.10
Proposed CAFT (C5)	WS	0.00 – 0.00
	LS	0.00 – 0.00

5.3.3 Discussions

Experimental Validation Period

For the proposed SWT corrosion model proposed by Aghoury and Galal (2014), the experimental investigation results by Albrecht and Shabshab (1994) were used to validate the corrosion model. They performed experimental fatigue testing to evaluate the fatigue behavior of 24 corroded rolled beams made of A588 weathering steel. The beams were weathered for approximately five to six years under three different corrosion conditions.

Material Constant Coefficients

The proposed corrosion material constants for the proposed SWT model were adopted from the previous study by Aghoury and Galal (2014) as $\alpha_b = 0.182$ and $\alpha_b = 0.034$ respectively. It should be noted that these factors were derived from a 2-year JIS-JMS weathering steel fatigue testing data (Kunihiro et al., 1972). Hence, factor modifications may be possible with an additional future experimental work. In addition to weathering steel, testing results for both low-carbon steel and hot-dip galvanized steel may enhance an

accuracy of the SWT corrosion model.

Effect of Hot-dip Galvanization versus corrosion effects

In the light of fatigue resistance without any corrosion effect, a recent experimental result (Ocel, 2014) found that there is a reduction in the fatigue resistance of the hot-dip galvanized fillet-welded tube connection for support structures. However, formed zinc patina which provides cathodic protection to protect the specimens from corrosion attack and also weathering steel protects a corrosion by having the protective rust layers. It is important to investigate the fatigue resistance by utilizing synthetic data analysis results for the unstiffened socket connection details. Based on the results, it seems that weathering steel may not the best option for use in environments with corrosion categories C1 or C2 and better to have galvanization treatments.

CHAPTER VI

FATIGUE RELIABILITY ASSESSMENT OF POTENTIAL CRACK INITIATION OF TUBE-TO-TRANSVERSE PLATE CONNECTION

In highway transportation systems, sign structures play an important role in providing useful information to the public. Cantilever sign structures are typically long span structures with smaller cross sections and low mass. These structures are typically characterized by their flexibility, low damping, and low natural frequency. According to previous studies (Kaczinski et al. 1998; Gilani and Whittaker 2000, Fisher et al. 1991), the main cause of failure for cantilever sign structure is due to fatigue stresses due to wind. In a number of states, fatigue cracks at connection details of sign support structures have been observed and fatigue failures were also reported (Foley et al. 2004). Excessive vibrations of those structures and large amplitudes due to wind have been a major issue for several state DOT's (Foley et al. 2004).

Because of high amplitude of vibrations, the long-term fatigue performance of cantilever sign support structure under the non-constant amplitude wind load becomes

critical. However, fatigue stresses due to the altered wind loading component have not been fully investigated and experimental studies under the constant stress amplitude are limited. In addition there are no available field data on the fatigue behavior of support structures. Therefore, the reliability of these structures under the non-constant amplitude fatigue loading is an area that needs further study.

In New Jersey, the tube-to-transverse plate connection of cantilever sign structures with longitudinal stiffeners are common and are detailed following standard drawings (NJDOT, 2007) and extensively used for cantilevered and overhead sign structures. This stiffened fillet-welded connection was initially developed to achieve a lower stress level at the fillet weld toe at the base by decreasing out-of-plane distortion at the pole wall (Roy et al. 2009). However, the termination at the tip of stiffeners becomes a potential fatigue crack location (AASHTO 2015). Figure 6.1 shows standard details for NJDOT cantilever sign structures.
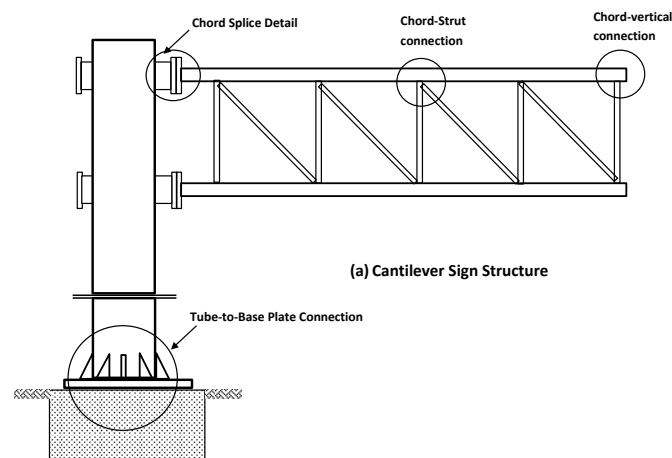
(a)
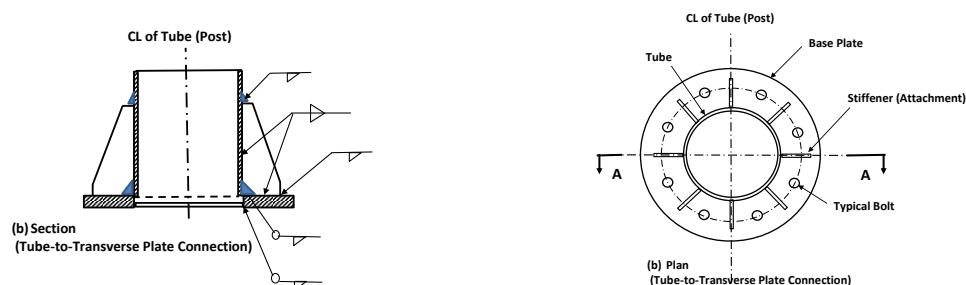
(b)

Figure 6.1 Typical cantilever sign structure in New Jersey, (a) Elevation, (b) Details for

tube-to-transverse plate connection with welded longitudinal stiffeners.

Previous editions of the AASHTO Standard Specifications for structural supports

for Highway Signs, Luminaires and Traffic Signals, (AASHTO 2001, AASHTO 2009),

specified the tube-to-transverse plate attachment detail in term of 'Fatigue Categories'.

However, the Load and Resistance Factored Design (LRFD) design specification

(AASHTO 2015) introduced the new Constant Amplitude Fatigue Threshold (CAFT) for

the tube-to-stiffener weld toe on the tube wall. The CAFT for this detail depends on the

stress concentration factor (SCF). The SCF in AASHTO is determined by empirical

equations based on experimental and analytical studies performed under NCHRP Project

10-70 (Roy et al. 2011).

Because of the revised CAFT values for the tube-to-transverse plate connection in

the LRFD AASHTO-LTS specifications, there is a need to perform further research on the

reliability of fatigue performance of this commonly used attachment detail. In the

reliability-based fatigue assessment, the main focus was assessing uncertainties in non-

constant wind loading components and fatigue resistance of these connection details.

6.1 Methodology for Fatigue Reliability Assessment
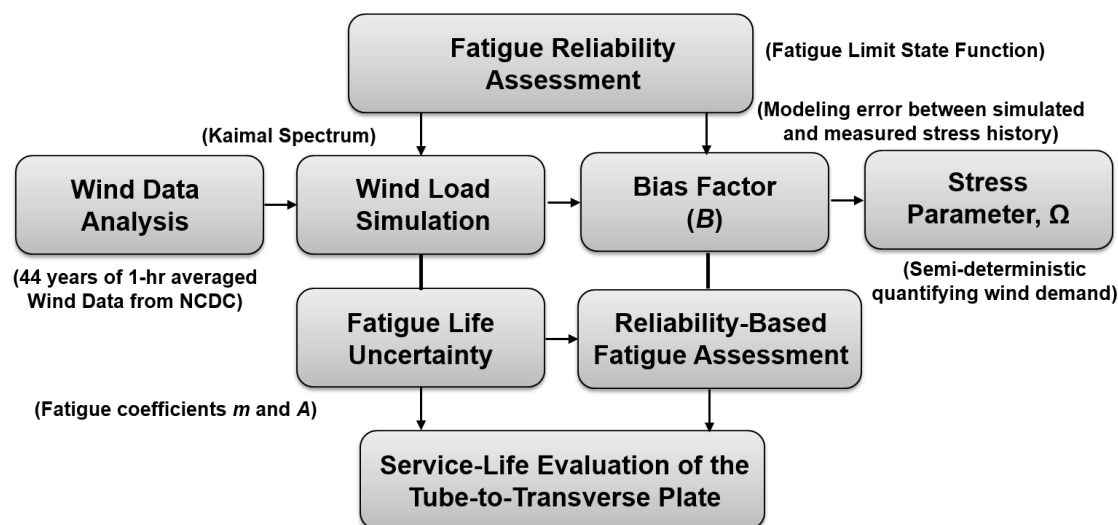
Figure 6.2 Flowchart showing methodology of Reliability-Based Fatigue Assessment.

The fatigue reliability assessment methodology is presented in the flow chart illustration in Figure 6.2. The long-term period of one hour averaged wind data was collected from the National Climatic Data Center (NCDC) Automated Surface Observation System (ASOS) for a comprehensive wind data analysis. Collected wind speeds were simulated using the Kaimal spectrum to represent the non-constant and fluctuating natural wind speeds. A bias factor, B which represents uncertainties in modeling error was determined as the ratio of the simulated and measured one hour stress histories.

To estimate the wind demand uncertainties, the stress parameter, Ω was defined as a semi-deterministic variable. Parameters such as stress-ranges, number of cycles, wind direction, and combined probability, were accounted for in calculating the stress parameter Ω. This procedure was performed for each year of wind data to obtain 44 years of stress parameters. For fatigue life uncertainties of the tube-to-transverse plate connection detail, fatigue coefficients m and A were determined by performing a least square regression analysis for stress range and number of cycle for fatigue crack-initiation.

Limit state function or performance function for reliability-based fatigue assessment was studied using the fatigue life cycle formulation approach (Ayyub et al. 2002). Using Miner's cumulative fatigue damage, a limit state function of fatigue reliability was investigated and used for many other structural applications such as offshore structures (Wirsching 1984), bridge structures (Kwon 2011), high-mast tower lights and others (Dawood et al 2014). Life cycle formulations for the fatigue reliability limit state function are defined by researchers (Foley and Diekfuss 2016; Ayyub et al) and by assuming parameters are statistically independent,

$$g(X) = N_c - N_T < 0 \ or \ g(X) = \frac{T_c}{T_T} \le 1 \qquad (6.1)$$

where N_c is the critical number of stress-range cycles resulting in crack initiation and N_T is the total number of applied stress-range cycles of any magnitude. The number of stress-range cycles can be also expressed in a form of service time intervals, T_c and T_T. A bias factor, B is introduced for wind demand uncertainties and prediction of stress-range magnitudes (Kwon 2011)

$$D = \frac{N_T(B^m \cdot S_{RE}{}^m)}{A} \ge \Delta \qquad (6.2)$$

where S_{RE} is stress range and m and A are constants corresponding to a specific connection detail. Δ defines the damage parameter (Miner 1945). The critical time, T_C needed for fatigue-induced crack initiation is defined as (Wirsching 1984),

$$T_C = \frac{\Delta \cdot A}{B^m \cdot \Omega} \qquad (6.3)$$

where Ω is the semi-deterministic stress parameter (Foley and Diekfuss 2016). Further discussion of parameter Ω will be addressed in a later section. By applying developed time interval function above, the limit state function, $g(X)$, can be rewritten,

$$g(X) = \frac{T_c}{T_T} = \frac{\Delta \cdot A}{B^m \cdot \Omega \cdot T_T} \leq 1 \qquad (6.4)$$

This function becomes a product of lognormal random variables and A, Δ and B, are assumed to be log-normally distributed random variables. The reliability index or safety index β is defined from the following equation from reference (Foley and Diekfuss 2016),

$$\beta = \frac{ln\left(\frac{u_A u_\Delta}{u_B \overline{m}}\right) - \frac{1}{2} ln\left[\frac{\left(1+CV_A{}^2\right)\left(1+CV_\Delta{}^2\right)}{(1+CV_B{}^2)^m}\right] - ln\Omega - lnT}{\sqrt{ln\left[\left(1+CV_A{}^2\right)(1+CV_\Delta{}^2)(1+CV_B{}^2)^{m^2}\right]}} \qquad (6.5)$$

It should be noted that if the limit state function is not a product of lognormal random variable, the limit state function becomes nonlinear function of random variables (Nowak and Collins 2000) and the equation for reliability index will not be applicable. Further, if the coefficients of variables are less than 0.2, the expression of the reliability index β in equation 6.5 can be simplified as shown below (Nowak and Collins 2000).

$$\beta = \frac{ln\left(\frac{u_A u_\Delta}{u_B \overline{m}}\right) - ln\Omega - lnT}{\sqrt{\left[\left(CV_A{}^2\right) + (CV_\Delta{}^2) + (CV_B{}^2)m^2\right]}} \qquad (6.6)$$

The cumulative distribution function (CDF) describing the probability of fatigue crack-initiation is defined (Foley and Diekfuss 2016),

$$P_f = P[g(X) \leq 1.0] = \phi\left[\frac{ln(1) - u_{lng(X)}}{\sigma_{lng(X)}}\right] = \phi\left[\frac{u_{lng(X)}}{\sigma_{lng(X)}}\right] = \phi[-\beta] \qquad (6.7)$$

It should be noted that if the limit state function is not a product of lognormal random variable, the limit state function becomes nonlinear function of random variables (Nowak and Collins 2000) and the equation for reliability index will not be applicable. Further, if the coefficients of variables are less than 0.2, the expression of the reliability index β in equation 6.5 can be simplified as shown below (Nowak and Collins 2000).

6.2 Synthetic Analysis of Wind Data

Wind Data Analysis Procedures

In order to evaluate wind demand uncertainties, synthetic analysis of wind data from New Jersey were collected from National Climatic Data Center (NCDC) Automated Surface Observation System (ASOS). For the wind data collecting procedure, two minutes averaged wind speeds are updated once every 5 seconds in the NCDC database once per hour (ASOS 1998). Two weather stations were selected where each provided 44 years of uninterrupted wind data from 1973 to 2015. Obtained wind data such as speed and direction were sorted out and then reorganized to perform wind data analysis.

(a)   (b)
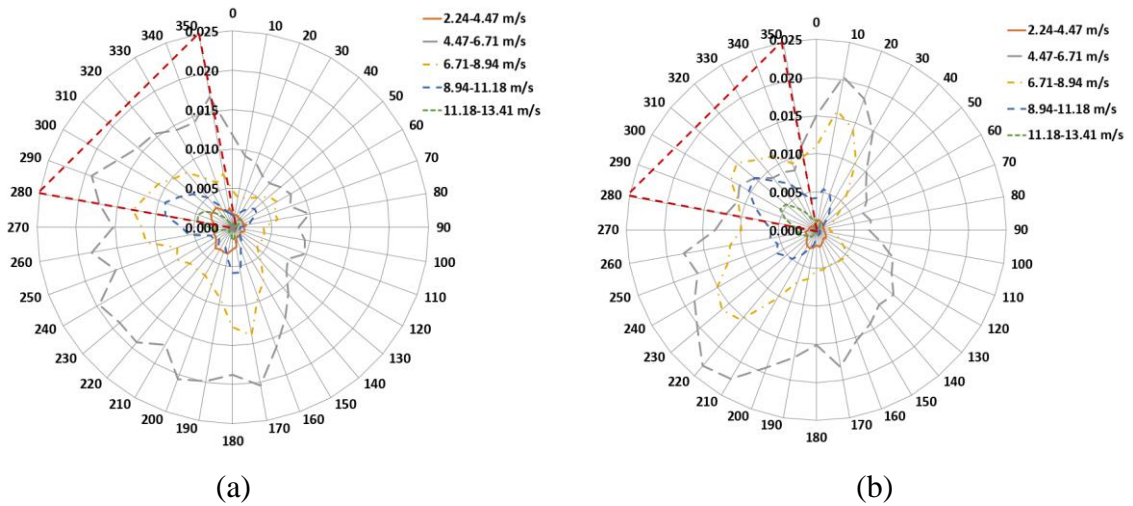
Figure 6.3 Wind Rose Histogram for (a) Atlantic City and (b) Newark

With collected wind data sets, wind rose histograms are constructed to observe wind speed and its corresponding direction. Figure 6.3 illustrates the wind rose diagram at two weather stations, Atlantic City and Newark. The dash lines represent the probability of occurrence at specified wind speed range for a given wind direction. The combined probability, $P(U = u_i \cap Dir = d_j)$ for a wind speed range i, and wind direction j, is calculated by assuming that the two random variables are statistically independent. The

probability of one hour averaged wind speeds and directions for Atlantic City with all wind data set is tabulated in Table 6.1. One hour averaged wind speeds are grouped into 2.24 m/s range and wind directions are sorted for eight different directions. Based on wind data analysis results, it was found that high wind speeds where the wind speed was greater than 8.94 m/s were observed in the northwest, north and west direction. Time-dependent service-life evaluation and the probability of fatigue crack-initiation were evaluated for additional wind load directions acting perpendicular to the sign panel.

Table 6.1 Probability of 1-hour Wind Speed and Direction for Atlantic City, New Jersey

1-hour average wind speed range (m/s)	1-hour average wind direction								
	NE	E	SE	S	SW	W	NW	N	Sum
0 – 2.24	0.0111	0.0149	0.0114	0.0256	0.0260	0.0248	0.0243	0.0214	0.1594
2.24 – 4.47	0.0304	0.0434	0.0369	0.0870	0.0685	0.0855	0.0653	0.0626	0.4796
4.47 – 6.71	0.0175	0.0210	0.0127	0.0445	0.0241	0.0444	0.0385	0.0233	0.2261
6.71 – 8.94	0.0088	0.0071	0.0030	0.0151	0.0075	0.0211	0.0228	0.0069	0.0922
8.94 – 11.18	0.0036	0.0020	0.0010	0.0040	0.0021	0.0100	0.0108	0.0016	0.0350
11.18 – 13.41	0.0006	0.0003	0.0001	0.0005	0.0002	0.0021	0.0021	0.0001	0.0061
13.41 – 15.64	0.0002	0.0001	0.0000	0.0001	0.0000	0.0005	0.0004	0.0000	0.0013
15.64 – 17.88	0.0000	0.0000	0.0000	0.0000	0.0000	0.0001	0.0001	0.0000	0.0002
17.88 – 20.12	0.0000	0.0000	0.0000	0.0000	0.0000	0.0000	0.0000	0.0000	0.0000
20.12 – 22.35	0.0000	0.0000	0.0000	0.0000	0.0000	0.0000	0.0000	0.0000	0.0000
Sum	0.0722	0.0888	0.0651	0.1768	0.1284	0.1883	0.1642	0.1159	1.0000

6.3 Wind Load Simulation Procedures and Wind Demand Uncertainty

Wind Load Simulation Procedures

Collected one hour averaged wind data was simulated to represent the fluctuating natural wind phenomena. Because of a reasonable agreement with field measured wind data (Foley and Diekfuss 2016; Diekfuss 2013), Kaimal spectrum was used to transform the averaged-wind speed to transient wind speed component (Kaimal et al. 1972). Wind

load simulation technique known as Kaimal spectrum generated power spectral density function (PSD) for the turbulent components of the natural wind speed. From simulated 1-hour wind speed history, the wind pressures, P_Z, was calculated by utilizing the equation 6.8 given in the AASHTO-LTS specifications (AASHTO 2015) and ASCE/SEI 7-10 (ASCE 2010):

$$P_Z = 0.613 K_Z K_d G V^2 C_d \text{ (Pa)} \quad\quad (6.8)$$

The drag coefficient, C_d, is a strong function of Reynold's number and it is determined by the ratio of length and width of sign panel (AASHTO 2015). The resultant wind pressure force is applied to perpendicular to the sign panel. The orientation of sign panel is represented by the degree angle of wind load directions. This orientation corresponds to a load direction of 300 degrees as shown in Figure 6.4.
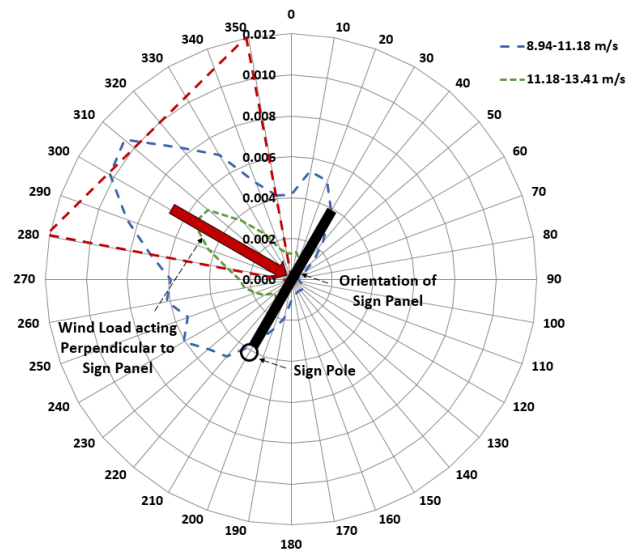
Figure 6.4 An example of wind load acting on sign panel under wind rose histogram in Newark

The bending moments and moment of inertia are obtained from the geometry of the tube-to transverse plate attachment and the time-dependent stress histories for both x and

y directions were determined. The sign design area used to calculate wind stresses is shown in Figure 6.5 (a). A photo of cantilever sign structure with flat panel is shown in Figure 6.5 (b).
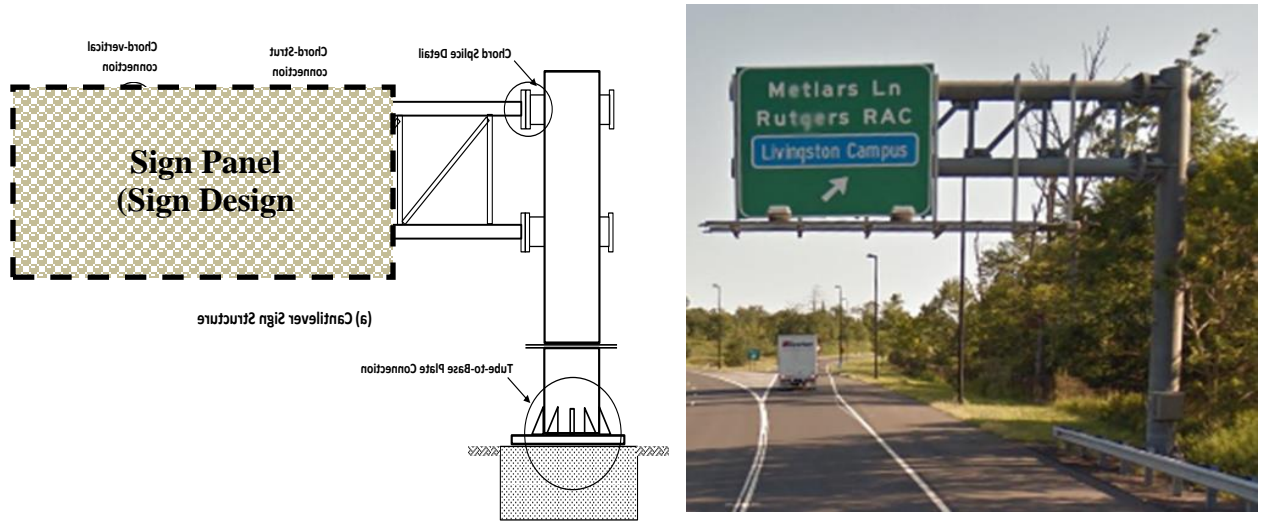
Fig. 6. (a) Sign design area for cantilever sign, (b) photo of cantilever sign structure with flat

Figure 6.5 (a) Sign design area for cantilever sign, (b) photo of cantilever sign structure with flat panel area

Then, expected stress range and the number of cycles of time-dependent stress histories were estimated by the Rainflow counting technique following ASTM Standard (ASTM E1049-85, 2011). To automate the calculations, scripts were programmed in MATLAB and the developed MATLAB algorithm was conjugated to perform the Rainflow counting procedure. The detail of the MATLAB script is at Appendix B.

Modeling Error Bias Factor, B

Diekfuss and Foley (Foley and Diekfuss 2016) introduced a modeling error induced by performing wind load simulation. The bias factor, B, is defined as the ratio between the simulated 1-hour stress history and the 1-hour measured stress history response.

$$B = \frac{S_{RE,s}}{S_{RE,m}} \qquad (6.9)$$

where $S_{RE,s}$ is the expected 1-hour stress range for the simulated stress histories and $S_{RE,m}$ is the expected 1-hour stress range for the measured stress histories. A previous study for the mast-arm sign support structures (Foley and Diekfuss 2016, Diekfuss 2013) obtained statistical values of the bias factor, B, from six month of measured wind stress data. Since no measured wind stress data are available for signs at the two for NJ locations, the bias factor B for the reliability-based fatigue assessment in this study was similar to the value obtained from previous studies (Foley and Diekfuss 2016). A mean, standard deviation, and coefficient of variation for B were determined as 1.288, 0.311, and 0.241, respectively.

It should be noted that parameters for the bias factor B were determined using a small sample size as noted in the previous studies (Foley and Diekfuss 2016, Diekfuss 2013). Because of the small sample size used for determining the modeling error bias factor B, the effect of coefficient of variation of the bias factor B on the probability of fatigue crack initiation was evaluated in this study. The analysis results showed that the variations of probability values were not significantly affected by the variation in B.

It is worth noting that the stress range and the number of cycles generated by the power density function are different for each run of the Kaimal spectrum simulation because of superimposed cosine waves of various frequencies and randomly generated

phase angles, ϕ_k (Ginal 2003). The variance induced by each simulation should be accounted within a bias factor. Statistical parameters of the error term from other structural applications are shown in Table 6.2. The proposed fatigue limit state function for this study is only applicable when the error term is log-normally distributed.

Table 6.2 Statistical parameters for error term

Error term	Mean	COV	Distribution	Structural Application	Reference
B	1.000	0.300	Lognormal	Offshore Structure	(Wirsching, 1984)
k_s	1.000	0.100	Normal	Ship Structure	(Ayyub, 2002)
e	1.000	0.040	Lognormal	Bridge	(Frangopol, 2008)
B	1.288	0.241	Lognormal	Mast-Arm Sign Support	(Diekfuss, 2016)

Stress Parameter, Ω

To account for wind demand uncertainties, the stress parameter Ω is determined as semi-deterministic variable and is then employed in this study. Because of the non-constant wind loading characteristic induced by variable magnitude and direction, a combined probabilistic model is adopted for wind demands (Foley and Diekfuss 2016, Diekfuss 2013). Stress parameter is Ω defined as follows:

$$\Omega = n_{1-h/year} \sum_i \sum_j \left[P\left(U = u_i \cap Dir = d_j \right) \right] n_{cycles/hr,i} (S_{RE}{}^m)_i cos\Theta_j] \quad (6.10)$$

where $n_{1-h/year}$ is the number of 1-hour intervals in a year and $P\left(U = u_i \cap Dir = d_j \right)$ is the combined probability of a 1-hour averaged wind speed i and wind direction j respectively. $n_{cycles/hr,i}$ is number of stress range cycles for a given 1-hour wind speed i, and by performing Rainflow counting for stress histories, an average value was used for the calculation. $(S_{RE}{}^m)_i$ is an equivalent stress range magnitude for a given 1-hour wind speed i, and it was obtained by performing a least square regression analysis developing a quadratic model between wind speed and stress range from the results of Kaimal spectrum

simulation (Kaimal et al. 1972). This polynomial regression model fits well and has an R-square value of 0.99.The angle θ_j is angle between a given wind direction, j and the perpendicular to the sign panel. The orientation of the cantilever sign structure is assumed to be facing wind acting perpendicular to sign face at 300° and the opposite side of wind loads are also considered for the fatigue performance of the tube-to-transverse basement connection. The angle of sign panel is varied from 280° to 350° to further evaluate the service-life of the stiffened plate connection detail.

6.4 Fatigue Life Uncertainty

Fatigue Test Results for the Tube-to-Transverse Plate Attachment

Longitudinal stiffeners (attachments) of the tube-to-transverse plate detail are added to increase the stiffness and reduce stresses as well as to minimize out-of-plane behavior and prevent distortion of tube wall. The fatigue test data used in this study were obtained from previous studies (Roy et al. 2011; Thompson 2012). The test specimens of the tube-to-transverse plate detail included eight stiffeners installed at alternating corners on the cross section between the transverse plates. The stiffeners were 18 inch long and 3/8 in thick with a 15 degree stiffener termination angle on the tube. The tube diameter and the plate thickness were 24 inch and 2 inch, respectively. Fatigue cracks were observed both at tube-to-stiffener weld toe and at the tube-to-end plate fillet weld toe (Roy et al. 2011; Thompson 2012). Based on those fatigue testing results, fatigue crack-initiation life and stress range at the top of stiffeners are selected for fatigue testing data analysis. It was noted that crack lengths at the first observation varied from 12.7 mm to 28.7 mm (Roy et al. 2011). This variation in crack length was attributed to the difficulty in observing the initial

crack while cyclic loadings are applied.

Fatigue Data Analysis
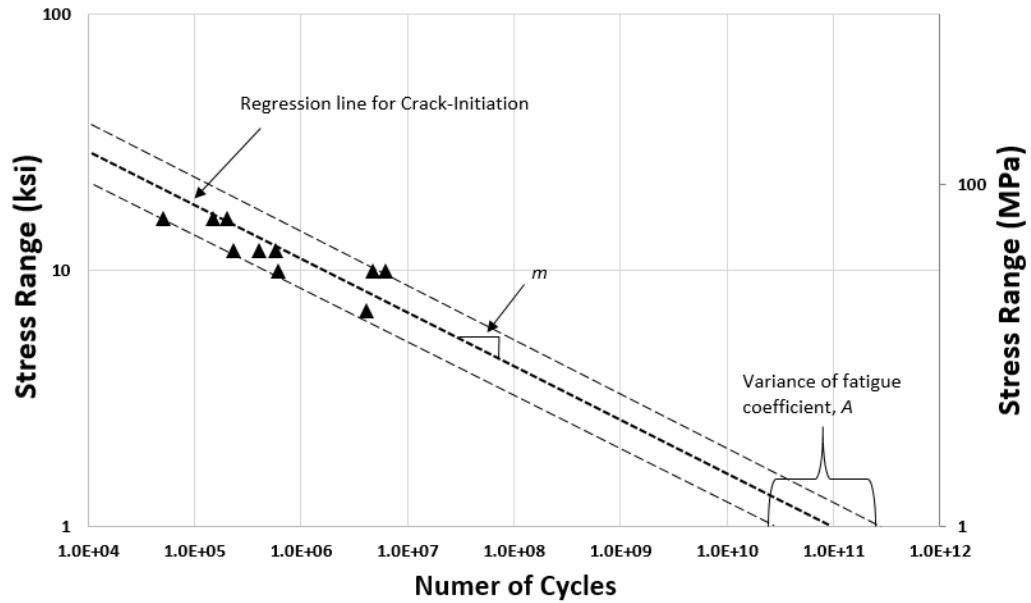
Figure 6.6 Fatigue test results on S-N curve and corresponding regression line

As can be seen in Figure 6.6, existing fatigue test data (Thompson 2012) is plotted on log-log scale with a least square regression line. Regression line for crack-initiation life, lower bound and upper bound are presented to demonstrate the variance of fatigue coefficient, *A* which is determined from each test results for a given slope, *m*. This statistical analysis was performed following the procedures in ASTM Standard E739-91. The linear regression line represents the relationship between stress-range and the number of cycles for crack-initiation. The fatigue life curve is generally expressed by Equation (6.11):

$$N \cdot S_R{}^m = A \qquad (6.1)$$

where m represents the slope of the linear line in log-log scale and A is the value

of the intercept on the x-axis. A is assumed to be a log-normal random variable according to the recommendation from previous study (Wirsching 1984). The variance is calculated as follows:

$$\sigma_A{}^2 = \frac{\sum_{i=1}^{k}(A_i - \bar{A}_i)^2}{k-2} \qquad (6.12)$$

where k is the number of test specimen and the *(k-2)* term in the denominator is used instead of k to make the variance of A an unbiased estimator of the normal population variance. Fatigue coefficients m and A are used in fatigue limit state function for reliability-based fatigue assessment. Parameters for this analysis is summarized in Table 6.3.

Table 6.3. Parameters for reliability-based fatigue assessment analysis

Variable	Notation	Mean	Coefficient of Variance	Distribution
Damage	Δ	1.0	0.3	Log-normal
Bias Factor	B	1.288	0.241	Log-normal
Stress parameter	Ω	-	-	Semi-Deterministic
Fatigue Coefficients	m	5.18	-	Deterministic
	A	$2.83(10^{11})$	1.048	Log-normal

6.5 Results and Discussion

6.5.1 Service Life Evaluation Results

In order to evaluate the service life of the stiffened tube-to-transverse plate connection details, a reliability-based fatigue assessment is investigated to estimate the probability of crack-initiation at the top of the longitudinal stiffeners. By utilizing proposed equation 6.7 and obtained parameters from this study, a probability of fatigue crack-initiation versus years in service curve is established for the stiffened tube-to-transverse plate attachment. Fatigue Reliability Index, B, is shown on a vertical axis to the right of the curves in Figure 6.7 and 6.8. A cumulative distribution function (CDF) represents the

probability of fatigue crack-initiation at the top of longitudinal stiffeners of the tube-to-transverse plate detail for the cantilever sign structures located in Atlantic City and facing perpendicular wind load direction of 300 degree.
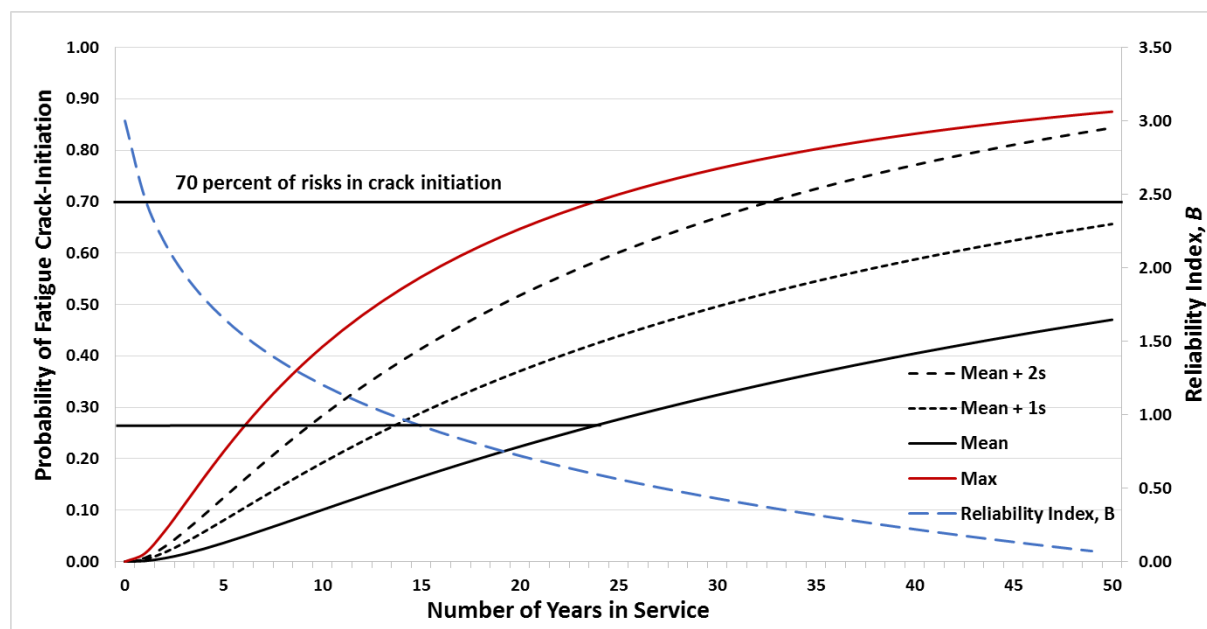
Figure 6.7 Time-dependent probability of fatigue crack-initiation in Atlantic City

A probability of fatigue crack-initiation versus time plot is developed for each year of wind demands which represents yearly stress parameters. The number of years in service was determined by wind load simulation results in which the number of cycles was correlated with the number of years in service using rain flow counting. Statistical parameters such as a mean, mean plus standard deviations and the maximum probability of crack-initiation are calculated and schematically illustrated in Figure 6.8. With the maximum probability, a 70 percent risk of crack-initiation is found in 24 years. In this year of stress parameter calculation, it is found that the highest risk in fatigue crack-initiation is caused by high probability of occurrence in wind speed and its direction.

The difference between the max and mean is about 43 percent which is a reflection

in the high variability of yearly wind data. This difference is due to the uncertainties in wind demand such as combined probability, wind direction and speed. With the mean plus two standard deviation of probability of fatigue-crack initiation, a 70 percent of risks reaches in 33 years.
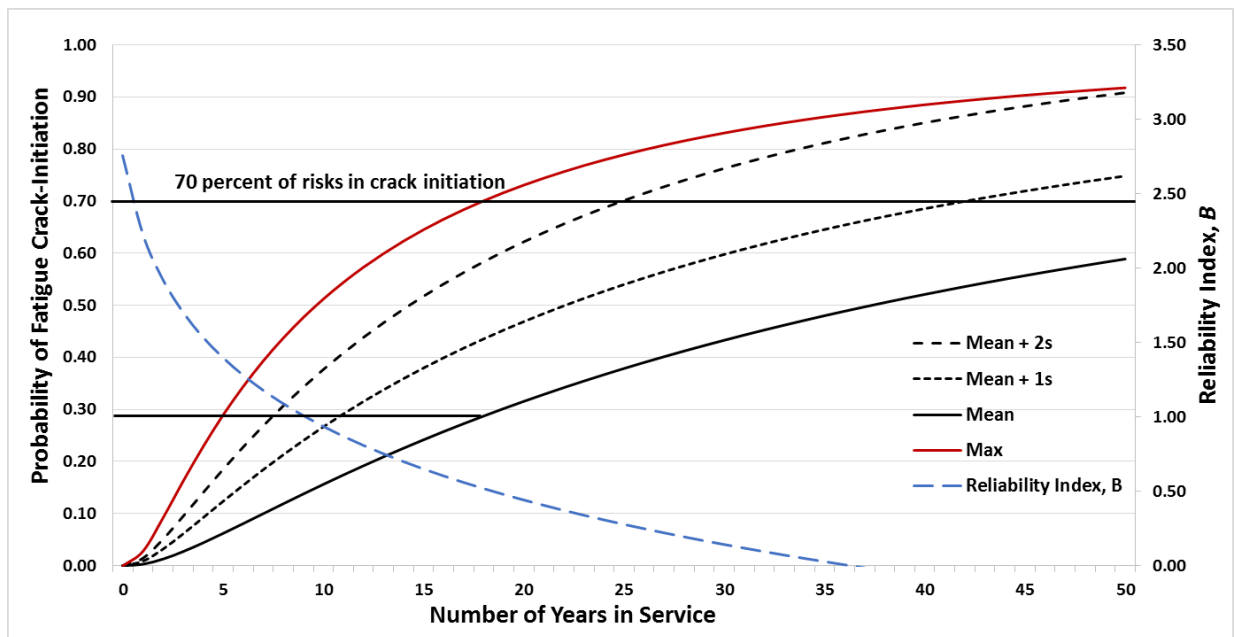
Figure 6.8 Time-dependent probability of fatigue crack-initiation in Newark

In similar manner, probability of fatigue crack-initiation at the top of the longitudinal stiffener of the tube-to-transverse plate detail of sign structures located in Newark is illustrated in Figure 6.8. Based on the wind data and wind directions available for the Newark locations, it is observed that at about 18 years of service, there is a 70 percent probability of crack initiation using the maximum possible probability prediction. Using the mean of the probability prediction, the probability of crack initiation over 18 years of service life is about 29 percent. According to the analysis results from two weather stations, the probability of fatigue crack-initiation in the tube-to-transverse plate connection of sign structures was higher in Newark than in Atlantic City. It is concluded

that higher risks in probability of crack initiation are caused by wind demands.

6.5.2 Fatigue crack-initiation curve for different wind load directions

In addition to previous results, the time-dependent probability of fatigue crack-initiation curves were developed for different wind load directions which represent the orientation of sign by utilizing the reliability-based fatigue assessment approach herein.

a. Atlantic City   b. Newark
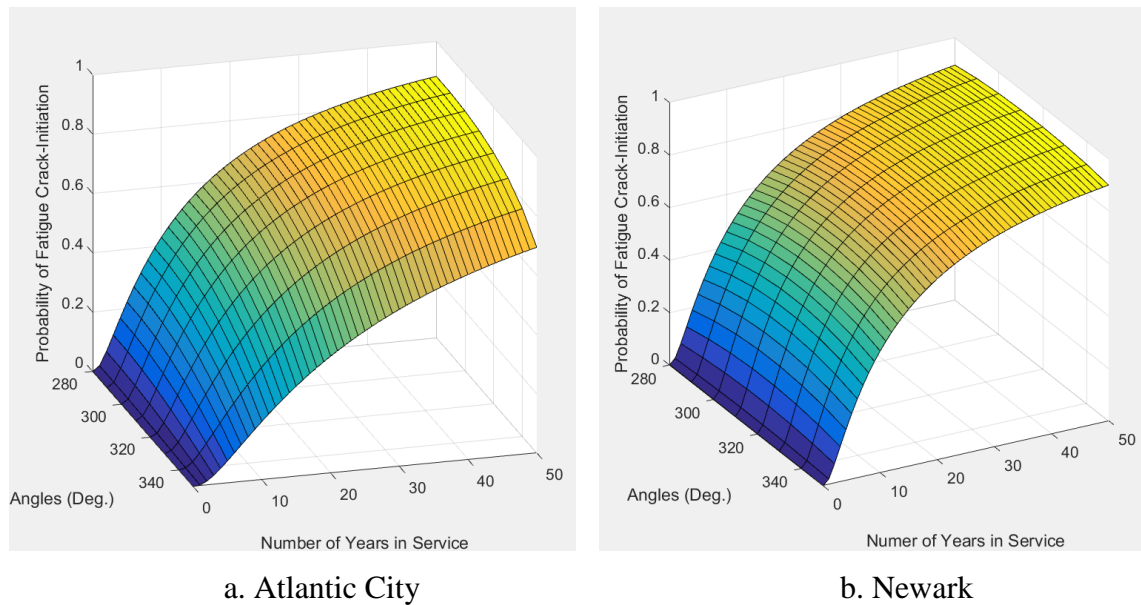
Figure 6.9 Time-dependent probability of fatigue crack-initiation for various wind load directions

Figure 6.9 shows a three dimensional surface plot for a probability of fatigue crack-initiation for both sites with varied wind load directions from 280° to 350° with respect to the sign. Figure 6.9 (a) also illustrates high variations in the probability of fatigue crack-initiation at the Atlantic City location compared to the Newark location. These variations can be attributed to the variations in wind loads and wind fluctuations.

6.5.3 Discussions

The AASHTO specification (AASHTO 2015) provides fatigue resistance limits for

the design of the stiffened tube-to-transverse plate fillet-welded connection for cantilever sign structures. In the light of remaining fatigue life of this detail, the specification has limitations based on the traditional methods of fatigue analysis. The utilized reliability approach of this study will provide a better understanding of the remaining fatigue life of existing sign structures. Furthermore, this approach can be used to evaluate other fatigue-susceptible connection details. However, it requires using the site-specific wind data and existing fatigue test results. The probability curves developed in this study such as mean, the maximum, and the mean plus two standard deviation probability curve can be used to determine the inspection frequencies or maintenance strategies. In addition to this, in situ inspection to validate the results from this research work is required as the future work. The methodology followed in this study for reliability-based fatigue assessment can be used for other sign connection details provided that experimental fatigue data are available for the stress range experienced by those details. There is a need for site-specific field level of wind measurements to enhance the accuracy of modeling error parameter B as well as the stress parameter Ω.

CHAPTER VII

CONCLUSIONS AND RECOMMENDATIONS

In this study, the fatigue resistance of stiffened and unstiffened tube-to- base plate fillet-welded connection details was investigated. The study included a synthetic fatigue data analysis of existing fatigue test results, development of FE model using the fatigue module platform in ANSYS Workbench, development of a modified strain-life SWT corrosion model, and a fatigue reliability assessment and probability of crack initiation of stiffened tube-to-base plate connection. Based on the results of this study, the following conclusions can be drawn:

Synthetic Fatigue Data Analysis of Existing Test Data

1. The fatigue resistance of specimens with thinner base plates were lower compared to those with thicker plates except those of Group 4 specimens which had 1.5 inch plate thickness.

2. The fatigue resistance of galvanized test specimens were lower than those without galvanization. For test specimens with peening treatment, it seems that

the peened surfaces improve the fatigue resistance compared to specimens with no peening.

3. For the socket connection with stiffeners, the existing fatigue test data showed significant differences in the fatigue resistance which can be attributed to the geometric variations and the associated weld geometries of stiffeners. It seems that because of the variations in the geometric parameters, some stiffeners' configurations may cause higher stress concentrations at the toe.

4. The Constant Amplitude Fatigue Threshold (CAFT) values from the AASHTO specifications seem to be conservative for connections with eight stiffeners (Group 3). However, for connections with four stiffeners (Group 2) and for those specimens where failure occurred at the base, the synthetic data analysis shows that the AASHTO fatigue limit may not be conservative.

FE Model Analysis Results

1. Results from the static FE model analysis showed that the local principal stress decreases with the increase in the base plate thickness. As expected, adding stiffeners near the bottom of the tube reduced the stress level compared to unstiffened connection.

2. The FE analysis showed that the fatigue resistance represented by fatigue design life and fatigue damage was lower with galvanization while the fatigue safety factor was higher. On the contrary, the FE analysis showed that the peening surface treatment enhanced the fatigue resistance of socket connections.

3. For all test groups evaluated in this study, a higher fatigue resistance was observed when a lower local stress range was applied using fully fixed boundary conditions.

4. The fully fixed boundary condition reduced the local principal stress at the base toe compared to partially fixed conditions. This is due to completely restrained bottom side of base plate which enables to make the base plate more rigid.

Modified Strain-Life Corrosion Model

1. A modified Strain-Life Smith-Watson-Topper (SWT) corrosion model was developed to evaluate corrosion effects on fatigue resistance. The modified model was used to establish a range of Constant Amplitude Fatigue Thresholds (CAFT's) for various corrosion categories for infinite fatigue life design.

2. Hot-Galvanized Steel (HGS) that has a zinc coating layer showed the best corrosion protection by achieving the highest CAFT values for all AASHTO fatigue categories.

3. Very low values for the CAFT were observed for weathering steel for locations with corrosion Categories from C3 to C5. For these conditions, hot-galvanization treatments or other surface treatment of the steel components may be needed to achieve higher values of CAFT.

Fatigue Reliability Assessment

1. The probability of fatigue crack initiation versus years in service of the tube-to-transverse plate connection detail of cantilever sign structures was developed using site-specific wind data. The wind load uncertainties are accounted for in the stress parameter Ω as a semi-deterministic variable.

2. The probability of fatigue crack initiation near the top of the longitudinal stiffeners of the tube-to-transverse plate connection can be obtained for different levels of wind speed spectra and for the orientation of sign panel.

3. The probability of fatigue crack initiation versus time developed in this study can be used by state engineers and state officials for establishing maintenance criteria and inspection frequencies of cantilever sign structures having these details.

4. The methodology followed in this study for reliability-based fatigue assessment can be used for other sign connection details provided that experimental fatigue data are available for the stress range experienced by those details.

5. There is a need for site-specific field level of wind measurements to enhance the accuracy of modeling error parameter B as well as the stress parameter Ω for better prediction of potential crack initiation.

RECOMMENDATIONS FOR FUTURE RESEARCH

1. There is a need for additional fatigue testing of stiffened and unstiffened connections to investigate the effects of various weld and stiffener geometries, galvanizations, and surface treatments on the fatigue performance of these connections.

2. There is a need for further testing of stiffened and unstiffened connections to validate a proposed SWT corrosion model with respect to different types of steel such as low carbon, weathering steel and HGS under moderate and severe corrosion conditions to determine their fatigue resistance.

3. The fatigue reliability assessment from this study can be utilized to establish probabilities of fatigue crack initiation for various tube-to-base plate connection geometries. Site-specific wind data is required to enhance accuracy of the reliability assessment.

Appendix A. Literature summary of previous fatigue study for structural supports

Authors	Title	Publication Type	Year
Azzam, D	Fatigue Behavior of Highway Welded Aluminum Light Pole Support Structures	PhD Dissertation at University of Akron	2006
Azzam,D and Menzemer C.	Numerical Study of Stiffened Socket Connections for Highway Signs, Traffic Signals, and Luminaires Structures	ASCE Journal of Structural Engineering	2008
Chen, G. et al.	Signal Mast Arm Failure Investigation	Missouri DOT Report	2003
Diekfuss, J	Reliability-Based Fatigue Assessment of Mast-Arm Sign Support Structures	PhD Dissertation at Marquette University	2013
Fisher et al.	Steel Through Plate Socket Connection Tests	California DOT Report	1981
Foley et al.	Fatigue Risks in the Connections of Sign Support Structure	Wisconsin DOT Report	2008
Hall and Connor	Influence of Base Plate Flexibility on the Fatigue Performance of Welded Socket Connections	ASCE Journal of Structural Eng.	2008
Hosseini, M	Parametric Study of Fatigue In Light Pole Structures	MS Thesis at University of Arkon	2011
Hosch, I	Design of Highway overhead cantilever-type sign support structures for fatigue loads	PhD Dissertations at University of Alabama at Birmingham	2009
Johns and Dexter	Fatigue Testing and Failure Analysis of Aluminum Luminaire Support Structures	New Jersey DOT Report	1998
Kaczinski	Fatigue-Resistant Design of Cantilevered Signal, Sign, and Light Supports	NCHRP Report 412	1998
Koenigs, M et al.	Fatigue Strength of Signal Mast Arm Connections	Texas DOT Report	2003
Li, Z and Zhang, Y	Fatigue Life Prognosis Study of Welded Tubular Joints in Signal Support Structures	International Journal of Steel Structures	2014
Li et al.	Fatigue Strength and Evaluation of Double-Mast Arm Cantilevered Sign Structures	Transportation Research Record	2005
Macchietto	Valmont Fatigue Testing Presentation	Presentation AASHTO T-12 Commiittee	2001
Ocel, J. et.al.	Fatigue-Resistant Design for Overhead Signs, Mast-Arm Signal Poles, and Lighting Standards	Minnesota DOT Report	2006
Ocel, J	Fatigue Testing of Galvanized and Ungalvanized Socket Connections	FHWA Project Report	2014
Pool, C	Effect of Galvanization on the Fatigue Strength of High Mast Illumination Pole	MS Thesis at University of Texas at Austin	2010

Roy et al.	Cost-effective Connection Details for Highway Sign, Luminarie, and Traffic Signal Structures	NCHRP Project 10-70	2011
Roy et al.	Fatigue Performance of Stiffened Pole-to-Base Plate Socket Connections in High-Mast Structures	ASCE Journal of Structural Engineering	2012
Stam et al.	Fatigue Life of Steel Base Plate to Pole Connections for Traffic Structures	Texas DOT Report	2011
Tomptson	Evaluation of High-Level Lighting Poles Subjected to Fatigue Load	MS Thesis at Lehigh University	2012
Warpinski, M. et al.	Influence of Base Plate Flexibility on the Fatigue Performance of Base Plate Connection in High-Mast Lighting Towers	ASCE Journal of Structural Engineering	2010

Appendix B1. – Summary Synthetic Fatigue Data – Unstiffened Socket Connections

Research Institute/ Reference	Specimen Number	Specimen Name	Connection location	Galv.	Peened.	Manufacturer	Stress Range (ksi)	Number of Cycles
University of Taxas/	1	VAL U A	Mast-Arm	No	No	Valmont - TX	11.9	2.49E+05
Koenigs 2003	2	VAL U B	Mast-Arm	No	No	Valmont - TX	11.9	4.54E+05
	3	VAL U C	Mast-Arm	No	No	Valmont - TX	6.3	2.07E+06
	4	VAL U D	Mast-Arm	No	No	Valmont - TX	6.2	6.86E+06
	5	VAL U E-P	Mast-Arm	No	Yes	Valmont - TX	11.4	3.94E+05
	6	VAL U F-P	Mast-Arm	No	Yes	Valmont - TX	11.5	3.53E+05
	7	TX U A	Mast-Arm	No	No	TX	6.0	2.20E+06
	8	TX U B	Mast-Arm	No	No	TX	6.1	2.82E+06
	9	TX U C	Mast-Arm	No	No	TX	11.8	1.78E+05
	10	TX U D	Mast-Arm	No	No	TX	12.0	1.95E+05
	11	TX U E-P	Mast-Arm	No	Yes	TX	11.8	3.21E+05
	12	TX U F-P	Mast-Arm	No	Yes	TX	11.7	1.41E+05
Phase 2	13	VALN U A	Mast-Arm	No	No	Valmont - Neb	11.9	3.89E+05
	14	VALN U B	Mast-Arm	No	No	Valmont - Neb	11.8	2.66E+05
	15	VALN U G A	Mast-Arm	Yes	No	Valmont - Neb	11.6	1.83E+05
	16	VALN U G B	Mast-Arm	Yes	No	Valmont - Neb	11.5	1.52E+05
	17	VALN U 2 A	Mast-Arm	No	No	Valmont - Neb	11.9	5.14E+06
	18	VALN U 2 B	Mast-Arm	No	No	Valmont - Neb	11.8	1.68E+06
Valmont Inc/	1	Socket 1	High-Mast	NA	NA	Valmont	13.4	4.81E+06
Machietto 2002	2	Socket 2	High-Mast	NA	NA	Valmont	17.6	1.24E+06
	3	Socket 3	High-Mast	NA	NA	Valmont	17.6	5.32E+06
	4	Socket 4	High-Mast	NA	NA	Valmont	17.6	1.98E+06
	5	Socket 5	High-Mast	NA	NA	Valmont	24.1	Discarded
	6	Socket 6	High-Mast	NA	NA	Valmont	24.1	1.48E+05
	7	Socket 7	High-Mast	NA	NA	Valmont	24.1	3.03E+05

	8	Socket 8	High-Mast	NA	NA	Valmont	24.1	1.11E+05
University of Taxas/	1	10-1.75-S-B	Mast-Arm	Yes	No	Valmont	12.0	1.43E+05
Stam 2011	2	10-1.75-S-B (flip)	Mast-Arm	Yes	No	Valmont	12.0	1.34E+05
	3	10-2-S-B	Mast-Arm	Yes	No	Valmont	12.0	1.66E+05
	4	10-2-S-A	Mast-Arm	Yes	No	Valmont	12.0	2.36E+05
	5	10-2-S-A (2)	Mast-Arm	Yes	No	Valmont	12.0	2.11E+05
	6	10-2-S-A (2) (flip)	Mast-Arm	Yes	No	Valmont	12.0	2.61E+05
	7	10-2-S-B (2)	Mast-Arm	Yes	No	Valmont	12.0	6.23E+05
	8	10-2-CA-A	Mast-Arm	Yes	No	Valmont	12.0	2.54E+05
	9	10-2-CA-B	Mast-Arm	Yes	No	Valmont	12.0	3.10E+05
	10	10-3-S-B	Mast-Arm	Yes	No	Valmont	12.0	7.93E+05
	11	10-3-S-B (flip)	Mast-Arm	Yes	No	Valmont	12.0	3.76E+05
	12	24-1.5-8-S-A	High-Mast	Yes	No	Valmont	12.0	1.32E+04
	13	24-1.5-8-S-B	High-Mast	Yes	No	Valmont	12.0	1.32E+04
	14	24-1.5-12-S-A	High-Mast	Yes	No	Valmont	12.0	2.80E+04
	15	24-1.5-12-S-B	High-Mast	Yes	No	Valmont	12.0	2.80E+04
	16	24-2-8-S-A	High-Mast	Yes	No	Valmont	12.0	4.68E+04
	17	24-2-8-S-B	High-Mast	Yes	No	Valmont	12.0	4.67E+04
	18	24-2-12-S-A	High-Mast	Yes	No	Valmont	12.0	1.43E+05
	19	24-2-12-S-B	High-Mast	Yes	No	Valmont	12.0	1.43E+05
	20	24-3-8-S-A	High-Mast	Yes	No	Valmont	12.0	1.48E+05
	21	24-3-8-S-B	High-Mast	Yes	No	Valmont	12.0	1.48E+05
Mn DOT / Ocel 2006	1	1A-IP-FR1	Mast-Arm	No	No	-	8.25	8.38E+04
(Multi side)	2	2A-IP-FR1	Mast-Arm	No	No	-	3.43	9.81E+05
	3	3A-IP-FR1	Mast-Arm	No	No	-	3.80	6.10E+05
	4	5A-OP-FR1	Mast-Arm	No	No	-	5.41	1.71E+05
	5	6A-OP-FR1	Mast-Arm	No	No	-	5.41	3.01E+05
	6	7A-OP-FR1	Mast-Arm	No	No	-	5.41	2.29E+06
	7	1A-IP-FR2	Mast-Arm	No	No	-	4.26	5.92E+05
	8	2A-IP-FR2	Mast-Arm	No	No	-	3.65	8.68E+05

	9	3A-IP-FR3	Mast-Arm	No	No	-	4.10	1.66E+06
Hammer Peening	10	3HPR-IP-FR1	Mast-Arm	No	Yes	-	4.55	4.13E+06
	11	1HPR-IP-FR2	Mast-Arm	No	Yes	-	6.99	1.11E+06
	12	2HP-IP-FR2	Mast-Arm	No	Yes	-	5.82	8.50E+06
	13	4HP-IP-FR2	Mast-Arm	No	Yes	-	7.10	2.56E+06
	14	5HP-IP-FR2	Mast-Arm	No	Yes	-	10.00	1.24E+05
	15	6HP-IP-FR2	Mast-Arm	No	Yes	-	6.00	5.57E+06
	16	7HPR-IP-FR2	Mast-Arm	No	Yes	-	7.91	1.13E+06
	17	8HP-IP-FR2	Mast-Arm	No	Yes	-	7.91	5.37E+06
	18	1T-IP-FR2	Mast-Arm	No	No	-	11.17	4.22E+06
	19	2T-IP-FR2	Mast-Arm	No	No	-	14.90	8.19E+04
	20	3HP-IP-FR2	Mast-Arm	No	Yes	-	14.90	9.78E+05
	21	4T-IP-FR2	Mast-Arm	No	No	-	14.90	5.66E+05
	22	5T-IP-FR2	Mast-Arm	No	No	-	14.90	1.02E+05
	23	6T-IP-FR2	Mast-Arm	No	No	-	15.00	3.30E+05
	24	7T-IP-FR2	Mast-Arm	No	No	-	15.00	1.41E+05
	25	8T-IP-FR2	Mast-Arm	No	No	-	15.00	1.84E+05
	26	9T-IP-FR2	Mast-Arm	No	No	-	15.00	8.69E+04
FHWA / Ocel 2014	1	1U1	High-Mast	No	No	Fabricator 1	5.85	2.17E+06
(Fabricator 1)	2	1U2	High-Mast	No	No	Fabricator 1	5.85	1.60E+06
	3	1U3	High-Mast	No	No	Fabricator 1	5.85	3.85E+06
	4	1U4	High-Mast	No	No	Fabricator 1	5.85	8.56E+06
	5	1U5	High-Mast	No	No	Fabricator 1	5.85	9.25E+05
	6	1U6	High-Mast	No	No	Fabricator 1	5.85	Discarded
	7	1G1	High-Mast	Yes	No	Fabricator 1	5.85	Run-out
	8	1G2	High-Mast	Yes	No	Fabricator 1	5.85	4.46E+06
	9	1G3	High-Mast	Yes	No	Fabricator 1	5.85	3.07E+06
	10	1G4	High-Mast	Yes	No	Fabricator 1	5.85	1.23E+06
	11	1G5	High-Mast	Yes	No	Fabricator 1	5.85	1.36E+06
	12	1G6	High-Mast	Yes	No	Fabricator 1	5.85	2.93E+06
Fabricator 2	13	2U1	High-Mast	No	No	Fabricator 2	5.73	3.74E+06

	14	2U2	High-Mast	No	No	Fabricator 2	5.73	4.87E+06
	15	2U3	High-Mast	No	No	Fabricator 2	5.73	7.00E+06
	16	2U4	High-Mast	No	No	Fabricator 2	5.73	4.41E+06
	17	2U5	High-Mast	No	No	Fabricator 2	5.73	3.41E+06
	18	2U6	High-Mast	No	No	Fabricator 2	5.73	5.63E+06
	19	2G1	High-Mast	Yes	No	Fabricator 2	5.73	1.17E+06
	20	2G2	High-Mast	Yes	No	Fabricator 2	5.73	8.78E+05
	21	2G3	High-Mast	Yes	No	Fabricator 2	5.73	6.40E+05
	22	2G4	High-Mast	Yes	No	Fabricator 2	5.73	1.86E+06
	23	2G5	High-Mast	Yes	No	Fabricator 2	5.73	7.00E+05
	24	2G6	High-Mast	Yes	No	Fabricator 2	5.73	7.48E+05
Lehigh Univ./	1	X1	High-Mast	Yes	No	-	10.00	1.78E+06
Roy 2011	2	X2	High-Mast	Yes	No	-	8.00	2.39E+06
	3	X3	High-Mast	Yes	No	-	8.00	1.02E+06

Appendix B2. – Summary Synthetic Fatigue Data – Stiffened Socket Connections

Research Institute/ Reference	Specimen Number	Specimen Name	Connection location	Galv.	Peened.	Manufacturer	Stress Range (ksi)	Number of Cycles
University of Taxas/	1	VAL 3x1/4 A	Mast-Arm-Wall	No	No	Valmont - Neb	11.10	4.76E+05
Koenigs 2003	2	VAL 3x1/4 B	Mast-Arm-Wall	No	No	Valmont - Neb	11.40	6.96E+05
	3	VAL 3x1/4 C	Mast-Arm-Wall	No	No	Valmont - Neb	6.10	3.59E+06
	4	VAL 3x3/8 A	Mast-Arm-Wall	No	No	Valmont - Neb	11.70	3.86E+05
	5	VAL 3x3/8 B	Mast-Arm-Wall	No	No	Valmont - Neb	11.60	4.10E+05
	6	VAL 3x3/8 C P (1)	Mast-Arm-Wall	No	Yes	Valmont - Neb	11.50	3.94E+05
	7	VAL 3x3/8 C P (2)	Mast-Arm-Wall	No	Yes	Valmont - Neb	11.50	3.53E+05
	8	VAL 6x3/8 A	Mast-Arm-Wall	No	No	Valmont - Neb	11.20	2.43E+05
	9	VAL 6x3/8 B	Mast-Arm-Wall	No	No	Valmont - Neb	11.30	6.53E+05
	10	VAL 6x3/8 C	Mast-Arm-Wall	No	No	Valmont - Neb	5.90	3.59E+06
	11	TX 3x1/4 A	Mast-Arm-Wall	No	No	TX	11.70	6.16E+05
	12	TX 3x1/4 B	Mast-Arm-Wall	No	No	TX	11.80	4.16E+05
	13	TX 3x1/4 C LMS	Mast-Arm-Wall	No	No	TX	11.90	5.23E+05
	14	TX 3x3/8 A	Mast-Arm-Wall	No	No	TX	11.70	4.74E+05
	15	TX 3x3/8 B	Mast-Arm-Wall	No	No	TX	11.60	6.58E+05
	16	TX 3x3/8 C P LMS	Mast-Arm-Wall	No	Yes	TX	12.10	1.71E+06
	17	TX 6x3/8 A	Mast-Arm-Wall	No	No	TX	11.20	7.84E+05
	18	TX 6x3/8 B	Mast-Arm-Wall	No	No	TX	11.30	7.84E+05
	19	TX 6x3/8 C	Mast-Arm-Wall	No	No	TX	5.76	7.50E+06
Phase 2	20	VALN 6x3/8@45 A	Mast-Arm-Wall	No	No	TX	11.96	2.39E+05
	21	VALN 6x3/8@45 B	Mast-Arm-Wall	No	No	TX	11.98	1.62E+05
	22	VALN 6x3/8@45 C	Mast-Arm-Wall	No	No	TX	4.30	6.07E+06
	23	VALN 6x3/8@45 D	Mast-Arm-Wall	No	No	TX	4.30	6.07E+06
Mn DOT / Ocel 2006	1	1G-IP-FR1	Mast-Arm-Wall	No	No	-	4.15	1.64E+06

(Multi side)	2	2G-IP-FR1	Mast-Arm-Wall	No	No	-	11.3	1.30E+06
	3	3G-IP-FR1	Mast-Arm-Wall	No	No	-	10.38	1.72E+05
	4	4G-IP-FR1	Mast-Arm-Wall	No	No	-	13.0	1.23E+06
Valmont Inc/	1	Gusset	-	-	-	Valmont	13.40	5.75E+05
Machietto 2002	2	Gusset	-	-	-	Valmont	13.40	3.77E+05
Lehigh / Roy 2011	1	XII-1	Base Plate	Yes	No	-	12	7.90E+05
	2	XII-2	Base Plate	Yes	No	-	12	9.10E+05
	3	XII-3	Base Plate	Yes	No	-	12	1.06E+06
	4	XII-4	Base Plate	Yes	No	-	10	2.31E+06
	5	XII-5	Base Plate	Yes	No	-	10	6.12E+06
	6	XII-6	Base Plate	Yes	No	-	7	5.94E+06
	7	XII-7	Base Plate	Yes	No	-	10	7.98E+06
	8	XII-8	Base Plate	Yes	No	-	16	4.90E+05
	9	XII-9	Base Plate	Yes	No	-	16	4.30E+05
	10	XII-10	Base Plate	Yes	No	-	16	4.70E+05

REFERENCES

AASHTO. (2001). AASHTO Standard Specifications for Structural Supports for Highway Signs, Luminaires, and Traffic Signals, *American Association of State Highway and Transportation Officials*, Washington, DC.

AASHTO. (2009). AASHTO Standard Specifications for Structural Supports for Highway Signs, Luminaires, and Traffic Signals, *American Association of State Highway and Transportation Officials, Washington*, DC.

AASHTO. (2015). AASHTO LRFD Specifications for Structural Supports for Highway Signs, Luminaires, and Traffic Signals, *American Association of State Highway and Transportation Officials, Washington*, DC.

AASHTO. (2017). AASHTO LRFD Specifications for Structural Supports for Highway Signs, Luminaires, and Traffic Signals, *American Association of State Highway and Transportation Officials, Washington*, DC.

Al-Obaid, Y. F. (1995). Shot peening mechanics: experimental and theoretical analysis. *Mechanics of Materials*, 19(2-3), 251-260.

Al-Obaid, Y. F. (1991). The automated simulation of dynamic non-linearity to shot-peening mechanics. *Computers & structures*, 40(6), 1451-1460.

American Galvanizers Association. (2012). Hot-Dip Galvanizing for Corrosion Protection, a specifier's guide.

ASCE. (2010). Minimum design loads for buildings and other structures, Reston, VA.

ASOS. (Automated Surface Observation System). (1998). "Automated Surface Observation System users guide*." 〈http://www.nws.noaa.gov/asos/pdfs/aum-toc.pdf〉* (Dec. 6, 2017).

ASTM. (2004). "Estimating the Atmospheric Corrosion Resistance of Low-Alloy Steels", *ASTM Standard G101*, ASTM, Philadelphia, PA.

ASTM. (2007). "Standard Practice of Statistical Analysis of Linear or Linearized Stress-Life (s-n) AND Strain-Life (e-N) Fatigue Data, *Annual Book of ASTM Standards." E739-91*, ASTM, West Conshohocken, PA.

ASTM. (2012). "Standard Test Method for Strain-Controlled Fatigue Testing." ASTM E606/E606M, West Conshohocken, PA.

ASTM. (2012). "Estimating the Atmospheric Corrosion Resistance of Low-Alloy Steels", *ASTM Standard G101*, ASTM, Philadelphia, PA.

ASTM. (2014). "Standard Specification for Steel Tubes, Low-Carbon or High-Strength Low-Alloy, Tapered for Structural Use1", *ASTM Standard A595/A595M*, ASTM, Philadelphia, PA

ASTM. (2015). "Standard Specification for High-Strength Low-Alloy Columbium-Vanadium Structural Stee1", *ASTM Standard A572/A572M*, ASTM, Philadelphia, PA

ASTM. (2015). "A588 standard specification for high strength low alloy structural steel with 345 MPa (50 ksi) minimum yield point", *ASTM Standard A588/A588M*, ASTM, Philadelphia, PA

Ayyub, B. M., Assakkaf, I. A., Kihl, D. P., and Siev, M. W. (2002). "Reliability-based design guidelines for fatigue of ship structures." Nav. Eng. J., 114(2), 113–138.

Azzam, D. (2006). Fatigue Behavior of Highway Welded Aluminum Light Poe Support Structures, *PhD Dissertation*, the University of Akron

Baumel, A., Jr., and Seeger, T. (1990). Materials data for cyclic loading, supplement 1*, Elsevier Science*, Amsterdam, Netherlands.

Chen, G., Barker, M., Dharani, L. R., and Ramsay, C., (2003). Signal Mast Arm Fatigue Failure Investigation, Missouri Department of Transportation, RI 97-019

Dawood, M., Goyal, R., Dhonde, H., and Bradberry, T. (2014). "Fatigue life assessment of cracked high-mast illumination poles." *J. Perform. Constr. Facil*., 10.1061/(ASCE)CF.1943-5509.0000438, 311.

Dexter, R. J., Ricker, M. J., (2002). "Fatigue-Resistant Design of Cantilevered Signal, Sign, and Light Supports", *NCHRP Report 469*

Diekfuss, A. J. (2013), Reliability-Based Fatigue Assessment of Mast-Arm Sign Support Structures, *PhD Dissertation*, Marquette University

El Aghoury, I. M., & Galal, K. (2014). Corrosion-fatigue strain-life model for steel bridge girders under various weathering conditions. *Journal of Structural Engineering*, 140(6), 04014026.

Fisher, J. W., Slutter, R. G., and Miki, C. (1981). "Fatigue Behavior of Steel Light Poles." *FHWA/CA/SD - 81/82, California Department of Transportation*, Sacramento, CA.

Fisher, J. W., E. J. Kaufmann, and J. D. Culp. (1991). Fatigue Cracking in Highway Sign Anchor Rods. *Proc., Ninth Structures Congress,* Indianapolis, pp. 319–322.

Foley, C. M., and Diekfuss, J. A. (2016). "Reliability-based inspection protocols for mast-arm sign support structures." *J. Struct. Eng*., 10.1061/(ASCE)ST.1943-541X.0001497, 04016043.

Foley, C. M., Fournelle, R. A., Ginal, S. J., and Peronto, J. L. (2004). "Structural analysis of sign bridge structures and luminaire supports." *Rep. No. 04-03*, Wisconsin DOT, Madison, WI.

Frangopol, D., Strauss, A., and Kim, S. (2008). "Bridge reliability assessment based on monitoring." *J. Bridge Eng.,* 10.1061/(ASCE)1084-0702 (2008)13:3(258), 258–270.

Gerber, W. (1874). Bestimmung der zulossigenin eisen construcionen. *Z. Bayer Arch. Ing Ver*. 6, pp. 101–110.

Gilani, A., and Whittaker, A. (2000). "Fatigue-life evaluation of steel post structures. I: Background and analysis." *J. Struct. Eng.,* 10.1061 /(ASCE)0733-9445(2000)126:3(322), 322–330.

Ginal, S. J. (2003). "Fatigue performance of full-span sign support structures considering truck-induced gust and natural wind pressures." *M.S. thesis*, Marquette Univ., Milwaukee.

Goodman, J. (1930). *Mechanics Applied to Engineering, Vol. 1*, 9th edition. Longmans Green and Co., London.

Gray, B. D. (1999). "Fatigue effects on traffic signal structures". *University of Wyoming*, M.S. Thesis.

Hall III, J. (2004). "The effect of baseplate flexibility on the fatigue performance of welded socket

connections in cantilevered sign structures*", Lehigh University*, M.S. Thesis

Hall, J. and Connor, J. R. (2008). "Influence of base plate flexibility on the fatigue performance of welded socket connections, *ASCE Journal of Structural Engineering,* 134(6): 911-918

Hosseini (2013). Parametric Study of Fatigue Light Pole Structures, *the University of Akron,* MS Thesis.

ISO. (1992a). "Corrosion of metals and alloys Corrosivity of atmospheres Classification." ISO-9223, Geneva.

ISO. (1992b). "Corrosion of metals and alloys Corrosivity of atmospheres Guiding for the corrosivity categories." ISO-9224, Geneva.

ISO. (2009). "Zinc coating – Guidelines and recommendations for the protection against corrosion of iron and steel in structures – part 2: Hot dip galvanizing" ISO-14713-2, Geneva.

ISO. (2012). "Corrosion of metals and alloys Corrosivity of atmospheres Classification." ISO-9223, Geneva.

Johns. K. W., and Dexter, R. J. (1998). "Fatigue testing and failure analysis of aluminum luminaire support structure", *Advanced Technology for Large Structural Systems Report No.98-06.* Bethlehem, PA.

Kaczinski, M. R., R. J. Dexter, and J. P. Van Dien, J.P. (1998). NCHRP Report 412:Fatigue-Resistant Design of Cantilevered Signal, Sign and Light Supports. TRB, *National Research Council*, Washington, D.C.

Kaimal, J. C.,Wyngaard, J. C., Izumi, Y., and Coté, O. R. (1972). "Spectral characteristics of surface-layer turbulence." *Q, J. R. Meteorolog. Soc.,* 98(417), 563–589.

Kayser, J. R., & Nowak, A. S. (1989). Capacity loss due to corrosion in steel-girder bridges. *Journal of Structural Engineering*, 115(6), 1525-1537.

Koenigs, M.T., Botros, T.A., Freytag, D. and Frank K. H., (2003). Fatigue Strength of Signal Mast Arm Connections, *TX DOT Report*

Komp, M. E. (1987). Atmospheric corrosion ratings of weathering steels―calculation and significance. *Materials performance*, 26(7), 42-44.

Kunihiro, T., Inove, K., and Fukuda, T. (1972). "Atmospheric exposure study of weathering steel." Public Works of Research Laboratory Rep. Br, 71–08, *Ministry of Construction*, Tokyo, Japan (in Japanese).

Kwon, K. (2011). "Reliability assessment, performance prediction and life cycle management of fatigue sensitive structures based on field test data." Ph.D. dissertation, Lehigh Univ., Bethlehem, PA.

Lee, Y. L. (2005). Fatigue testing and analysis: theory and practice (Vol. 13). *Butterworth-Heinemann*.

Legault, R. A., and Leckie, H. P., (1974). "Effect of Composition on the Atmospheric Corrosion Behavior of Steels Based on a Statistical Analysis of the Larrabee-Coburn Data Set," *Corrosion in Natural Environments*, ASTM STP 558, ASTM, pp. 334–347.

Larrabee, C. P., and Coburn, S. K., (1962). "The Atmospheric Corrosion of Steels as Influenced

by Changes in Chemical Composition," *First International Congress on Metallic Corrosion, Butterworths*, London, pp. 276–285.

Macchietto, C. (2002). "Valmont Fatigue Testing Presentation' Presentation *AASHTO T-12 Committee, November*, Las Vegas, NV (Electronic Presentation - Unpublished)

MATLAB [Computer software]. MathWorks, Natick, MA.

Miner, M. A., (1945). "Cumulative Damage in Fatigue", *Trans. ASME, 67, Journal of Applied Mechanics*, Vol. 12, 154-164.

Morrow JD. (1965). Cyclic plastic strain energy and fatigue of metals. *In: Internal friction, damping, and cyclic plasticity*. ASTM .p. 45–86.

Morrow, J. (1968). Fatigue properties of metals, section 3.2. *In: Fatigue Design Handbook, Pub*. No. AE-4. SAE, Warrendale, PA.

NCDC (National Climatic Data Center). (2014). "National weather service automated surface observing system." ⟨*http://www.nws.noaa.gov/asos/*⟩ (Dec. 6, 2017).

NJDOT (New Jersey Dept. of Transportation). (2007). General design criteria and standard drawings for overhead and cantilever sign support structures, Ewing Township, NJ.

Nowak, A. S., and Collins, K. R., (2000). Reliability of Structures, *McGraw-Hill,* New York, NY.

Ocel, J. M. (2006). "The Behavior of Thin Hollow Structural Section (HSS) to Plate Connections," *PhD Thesis*, University of Minnesota, Minneapolis, MN.

Ocel, J. M., Dexter, R. J., and Hajjar, J. F. (2006). "Fatigue-Resistant Design for Overhead Signs, Mast-Arm Signal Poles, and Lighting Standards." *Report No. MN/RC-2006-07*, Minnesota Department of Transportation, St. Paul, MN.

Ocel, J. M. (2014). "Fatigue testing of galvanized and ungalvanized socket connections, *FHWA-HRT-14-066*

Puckett, J. A., Garlich, M. G., Nowak, A. and Barker, M, (2014). Development and Calibration of AASHTO LRFD Specifications for Structural Supports for Highway Signs, Luminaires, and Traffic Signals, *NCHRP Report 796*

Ramberg, W., & Osgood, W. R. (1943). Description of stress-strain curves by three parameters.

Raymond Browell and Al Hancq, (2006). Calculating and Displaying Fatigue Results, *ANSYS Inc*.

Roy, S., Y. C. Park, R. Sause, and J. W. Fisher, (2009). "Fatigue Performance of Stiffened Tube-to-End Plate Socket Connections in High-mast Structures." *In Proc. 2nd Int. Conf. on Fatigue and Fracture in the Infrastructure*, July 26-29, Philadelphia, PA.

Roy, S., Y. C. Park, R. Sause, J. W. Fisher, and E.K. Kaufmann, (2011). "Cost Effective Details for Sign, Luminaires and Signal Structure." *NCHRP Report 10-70, Transportation Research Board*, *National Research Council*, Washington, DC.

Roy, S., Park, Y. C., Sause, R., and Fisher, J. W. (2012). "Fatigue Performance of Stiffened Tube-to-End Plate Socket Connections in High-mast Structures", *Journal of Structural Engineering, ASCE* 138(10)

Schneider, C. R. A., Maddox, S. J. (2003). Best practice guide on statistical analysis of fatigue data. *Doc. IIW-XIIIWG1-114-03*.

Smith, K., Topper, T. H., and Watson, P. (1970). "A stress-strain function for the fatigue of metals." *J. Mater.*, 5(4), 767–778.

Soderberg, C. R. (1930). *ASME Transactions 52*, APM-52–2, pp. 13–28.

Stam, A., Richman, N., Pool, C., Rios, C., Anderson, T., & Frank, K. (2011). Fatigue life of steel base plate to pole connections for traffic structures, *No. FHWA/TX-11/9-1526-1*.

Stephens, R. I., Fatemi, A., Stephens, R. R., & Fuchs, H. O. (2000). *Metal fatigue in engineering*. John Wiley & Sons.

Stresstech, (2018). https://www.stresstech.com/en-fi/know-how/articles/stresstech-bulletin-14-shot-peening-residual-stresses/

Thompson, R. W. (2012). "Evaluation of High-Level Lighting Poles Subjected to Fatigue Loading." *M.S. Thesis*, *Lehigh University*, Bethlehem, PA

Townsend, H. E. (1999). "The Effects of Alloying Elements on the Corrosion of Steel in Industrial Atmospheres," *Proceedings of the 14th International Corrosion Congress*, Corrosion Institute of Southern Africa, Kelvin.

Vaynman, S., Guico, R. S., Fine, M. E., & Manganello, S. J. (1997). Estimation of atmospheric corrosion of high-strength, low-alloy steels. *Metallurgical and Materials Transactions* A, 28(5), 1274-1276.

Wirsching P. H., (1984). "Fatigue Reliability for Offshore Structure, *Journal of Structural Engineering*. ASCE 110(10)

Zhang, P., & Lindemann, J. (2005). Influence of shot peening on high cycle fatigue properties of the high-strength wrought magnesium alloy AZ80. *Scripta materialia*, 52(6), 485-490.

Zhang, W., & Yuan, H. (2014). Corrosion fatigue effects on life estimation of deteriorated bridges under vehicle impacts. *Engineering Structures*, 71, 128-136.